Formgedächtnislegierungsdrähte in Hochleistungsanwendungen

DISSERTATION

Zur Erlangung des Grades
des Doktors der Ingenieurswissenschaften
der Naturwissenschaftlichen-Technischen Fakultät
der Universität des Saarlandes

VON

ROUVEN BRITZ

SAARBRÜCKEN

2022

Tag des Kolloquiums:	12. Juni 2023
Dekan:	Prof. Dr. Ludger Santen
Berichterstatter:	Prof. Dr.-Ing. Stefan Seelecke
	Prof. Dr.-Ing. Matthias Nienhaus
Vorsitz:	Prof. Dr.-Ing. Rainer Müller
Akad. Mitarbeiter:	Dr. Michael Roland

Tu es oder tu es nicht. Es gibt kein Versuchen.

- Meister Yoda -

VORWORT

Die vorliegende Dissertation entstand im Rahmen meiner Tätigkeit als wissenschaftlicher Mitarbeiter am Lehrstuhl für intelligente Materialsysteme und ist das Ergebnis meiner Promotion im Fachbereich Systems Engineering an der Universität des Saarlandes.

Der Lehrstuhl für intelligente Materialsysteme der Universität des Saarlandes forscht an Aktor- und Sensorlösungen mit intelligenten Materialien. Das Spektrum der Arbeiten des Lehrstuhls reicht dabei von Grundlagenuntersuchungen bis hin zu anwendungsnahen Prototypen. Mir wurde die Möglichkeit geboten innerhalb dieses vollständigen Spektrums des Lehrstuhls zu arbeiten, wodurch ich vielfältige Erfahrungen sammeln konnte, was letztlich zu dieser Arbeit führte.

Für die Möglichkeit dafür möchte ich an erster Stelle Prof. Dr.-Ing. habil. Stefan Seelecke und Prof. Dr.-Ing. Paul Motzki danken. Neben der Möglichkeit der Promotion gilt den beiden auch ein besonderer Dank für die stets gute Zusammenarbeit, den Freiraum, der mir geboten wurde, und dem Vertrauen, das mir fortwährend entgegengebracht wurde.

Ebenfalls möchte ich mich bei allen ehemaligen und aktuellen Mitarbeitern des Lehrstuhls für intelligente Materialsysteme für die vielen fachlichen sowie persönlichen Diskussionen und Gespräche, ob in oder außerhalb der Arbeitszeit, und das allgemein außergewöhnlich gute Arbeitsklima bedanken. Dies gilt besonders für Yannik Goergen, Dominik Scholtes und Lukas Zimmer sowie für Philipp Molitor, dem zusätzlich noch mein Dank für das Mitwirken an dieser Arbeit gilt.

Ich danke in gleicher Weise meinem gesamten Freundeskreis, insbesondere Yves Valentin und Johannes Birk, die immer für den nötigen Ausgleich zur Arbeit sorgten.

Abschließend bedanke ich mich bei meinen Eltern Bärbel und Joachim, meiner Schwester Sarah und meinen Großeltern Christel und Helmut, auf deren Unterstützung ich jederzeit zählen konnte.

KURZZUSAMMENFASSUNG

Die vorliegende Arbeit beschäftigt sich mit der Untersuchung von Formgedächtnislegierungsdrähten (FGL-Drähten) in Hochleistungsanwendungen sowie der Entwicklung erster funktionaler Prototypen für entsprechende Applikationsbeispiele. In den gezeigten Fällen ist unter der Definition von Hochleistung die Bündelung von FGL-Drähten zur Erzeugung hoher Kräfte, die schnelle Aktivierung von FGL-Drähten mit erhöhten elektrischen Leistungen oder die Kombination aus beidem zu verstehen. Bei den untersuchten Bündeln handelt es sich um eine spezielle Bauform, die sich dadurch kennzeichnet, dass ein definierter Abstand zwischen den einzelnen Drähten innerhalb des Bündels besteht. Die Möglichkeit der schnellen Aktivierung von FGL-Drähten wird anhand einer praxisrelevanten Entwicklung eines Prototyps aufgezeigt. Dabei handelt es sich um ein Ventil zur Entlüftung von Spritzgusskavitäten. Der Prototyp zeigt neben der Fähigkeit der schnellen Aktivierung, wie durch innovative konstruktive Lösungen die prominenten Schwachstellen der FGL-Technologie umgangen oder kompensiert werden können. Die Arbeit eröffnet somit neue Einsatzgebiete für Anwendungen von FGL-Aktoren. Zum Abschluss wird die Entwicklung eines Technologiedemonstrators vorgestellt, der eine Kombination aus beiden Hochleistungsgebieten darstellt und das Potenzial von FGL anschaulich aufzeigt. Dazu werden FGL-Bündel mit hoher elektrischer Leistung aktiviert, um eine Bowlingkugel senkrecht in die Luft zu katapultieren.

ABSTRACT

The present work deals with initial investigations of shape memory alloy (SMA) wires in high-power applications as well as the development of first functional prototypes for this field. In the regarded cases, the definition of high-power is described as the bundling of SMA wires to generate high forces, the fast activation of SMA wires with increased electrical power, or the combination of both. The SMA wire bundles shown in this work are special actuator elements characterized by having a defined space between the individual wires within the bundle. The behavior of such SMA bundles is investigated and discussed in the first part of this work. The potential for fast activation of SMA wires is demonstrated in this dissertation by the development and validation of a functional prototype. The prototype is a valve, which is used for venting cavities in injection molding. The prototype demonstrates the possibilities of fast activation and how prominent drawbacks of the SMA technology can be compensated or erased by innovative system design. Thus, this work expands the field of use for future applications. Finally, this work presents the development of a technology demonstrator, which constitutes the combination of both high-power areas and vividly showcases the potential of the SMA technology. For this purpose, SMA bundles are used in the demonstrator to catapult a bowling ball vertically into the air by high electrical power.

INHALTSVERZEICHNIS

1 EINLEITUNG

Formgedächtnislegierungen (FGL) auf der Basis von Nickel-Titan (NiTi) verzeichnen seit ihrer Entdeckung in den Fünfzigerjahren [1]–[3] einen stetig steigenden Anteil an Anwendungen [4]–[7]. Zu den prominenten Anwendungsfeldern für FGL gehören industrielle Anlagen [7]–[11], Medizintechnik [12]–[18], Robotik [19]–[25], Automotive [26]–[29] sowie Luft- und Raumfahrt [30]–[33]. Der Vormarsch der FGL-Technologie lässt sich mit in den besonderen Eigenschaften der FGL begründen. Besonders hervorzuheben ist dabei die hohe Energiedichte [34], [35], die es erlaubt, kompakte und leichtgewichtige Aktoren mit hohen Kräften zu entwickeln [36], [37]. Des Weiteren sind die Biokompatibilität [38] und die Möglichkeit des so genannten „self-sensings“ zu nennen. „Self-sensing“ beschreibt die Eigenschaft, mittels des elektrischen Widerstandes von FGL-Drähten auf deren Länge zu schließen [39]–[44], wodurch auf zusätzliche Sensoren verzichtet werden kann. Die größten Nachteile wie der technologiebedingte geringe Wirkungsgrad oder die thermisch limitierte Zykluszeit lassen sich durch verschiedenste konstruktive und ansteuerungstechnische Maßnahmen für spezielle Anwendungen eliminieren [45]–[53]. Um die FGL-Technologie in weitere noch anspruchsvollere Anwendungsfelder zu bringen und den daraus resultierenden steigenden Anforderungen gerecht zu werden, bedarf es an neuen Ansätzen zur Lösung der dadurch entstehenden technischen Herausforderungen. Differenziert betrachtet, handelt es sich dabei um zwei vorherrschende Anforderungen an die FGL-Technologie: Erstens die Erzeugung hoher Kräfte mittels FGL-Drähte und zweitens die schnelle Aktivierung von FGL-Drähten. Die Kraft eines FGL-Drahtes ist abhängig von dessen Querschnittsfläche. Die Erzeugung höherer Kräfte erfolgt deshalb in der Regel durch die Verwendung von FGL-Drähten mit größerem Durchmesser [54]–[56]. Eine Erhöhung des Durchmessers wirkt sich jedoch nachteilig auf das Abkühlverhalten des Drahtes aus, wodurch der Nachteil der limitierten Schaltzeiten weiter verstärkt wird. Um dem entgegenzuwirken, wird ein Ansatz der

Bündelung von mehreren dünnen FGL-Drähten verfolgt. Ein solches Bündel, in dem die einzelnen Drähte mit definiertem Abstand zueinander angeordnet sind, hat den Vorteil eines größeren Oberflächen-Volumen-Verhältnisses, das sich positiv auf das Abkühlverhalten und damit die erreichbare Schaltfrequenz von FGL-Aktuatoren auswirkt. Dadurch können höhere Kräfte bei deutlich geringeren Auswirkungen auf die Zykluszeit erzeugt werden [57]–[59]. Die zweite Hochleistungsanforderung, die in der Praxis immer öfter an die FGL-Technologie gestellt wird und in Anwendungen wie z.B. Ventilen oder Schaltschützen benötigt wird, ist die schnelle Aktivierung von FGL-Drähten. Grundlegende Versuche mit anschließender Diskussion wurden bereits in [60]–[63] gezeigt. Neben dem aus der Praxis aufgezeigten Bedarf an schnellen Aktoren ist der Vorteil der Energieeinsparung bei schnell aktivierten FGL-Drähten hervorzuheben [64]–[66].

In dieser Arbeit erfolgen eine erste Analyse und Evaluation von FGL-Bündeln, um in entsprechenden Anwendungen einen korrekten und funktionierenden Einsatz zu gewährleisten. Es wird der Einfluss und die Bedeutung der elektrischen Kontaktierung auf ein FGL-Bündel sowie das Verhalten von FGL-Bündeln in zwei unterschiedlichen Grenzbelastungsfällen aufgezeigt [67], [68].

Da die FGL-Technologie mit dem Vorurteil behaftet ist, lediglich langsam zu funktionieren und aus diesem Grund für viele praktische Anwendungen nicht in Betracht gezogen wird, wird in dieser Arbeit die Entwicklung eines Prototyps eines schnellschaltenden Ventiles für die Anwendung in Spritzgussanlagen zur Entlüftung der Kavität vorgestellt. Der entwickelte Ventilprototyp zeigt die Vorteile der FGL-Technologie hinsichtlich Bauraums und wie durch geschickte Konstruktion einige der genannten Nachteile gemindert werden können. Zusätzlich zeigt dieser Anwendungsfall, dass der Einsatz von FGL mit entsprechenden Maßnahmen auch bei erhöhten Umgebungstemperaturen möglich ist [69]–[71].

Zuletzt gewährt diese Arbeit einen Einblick in das Leistungspotenzial der FGL-Technologie, wenn beide Hochleistungsanforderungen kombiniert werden. Dazu wurde ein Demonstrator entwickelt, der es ermöglicht, eine Bowlingkugel auf eine Höhe von $45\ cm$ senkrecht in die Luft zu katapultieren. Die zur Beschleunigung benötigte Kraft von annähernd $1000\ N$ wird dabei von drei FGL-Bündeln innerhalb von $11\ ms$ erzeugt.

2 ZUSAMMENFASSENDE DISKUSSION DER VERÖFFENTLICHUNGEN

Im folgenden Kapitel wird eine Zusammenfassung über die für diese Arbeit relevanten Veröffentlichungen gegeben. Zusätzlich wird der Zusammenhang der Veröffentlichungen zu dem übergeordneten Thema von FGL-Drähten in Hochleistungsanwendungen aufgezeigt. Grundsätzlich lassen sich Hochleistungsanwendungen mit FGL-Drähten in zwei Gebiete unterteilen: die Erzeugung hoher Kräfte und die schnelle Aktivierung. Eine Kombination von beiden Gebieten ist ebenfalls möglich. Zu unterscheiden davon sind Anwendungen, die umgebungsbedingt hohe Leistung von FGL-Drähten fordern wie beispielsweise der Einsatz bei hohen Umgebungstemperaturen. Da die Relevanz solcher Anwendungsgebiete mit den steigenden Anforderungen, die an die FGL-Technologie gestellt werden, unbestreitbar ist, wird auch dies in der vorliegenden Arbeit anhand einer Prototypentwicklung und -validierung exemplarisch thematisiert und erste Möglichkeiten aufgezeigt.

Für die Erzeugung hoher Kräfte eignen sich besonders Bündel aus FGL-Drähten. Diese haben im Gegensatz zu dickeren FGL-Drähten den Vorteil eines größeren Oberflächen-Volumen-Verhältnisses, das sich positiv auf das Abkühlverhalten auswirkt. FGL-Bündel lassen sich in zwei Varianten unterteilen: Erstens als geschlagenes Seil, vergleichbar mit konventionellen Stahlseilen, in dem die einzelnen Drähte zu einem Strang verdreht werden [72]–[75] oder zweitens als Bündel mit Abstand zwischen den einzelnen Drähten. Die letztere Variante hat dabei den größten Effekt auf das Oberflächen-Volumen-Verhältnis, da jeder Draht rundum mit einem Medium umschlossen ist, das die Wärme abführen kann.

In der in dieser Arbeit inkludierten ersten Veröffentlichung findet eine erste systematische Untersuchung von FGL-Bündel der zweiten Art statt. Dazu startet sie mit einer Einführung in die FGL-Thematik und erklärt die Unterschiede bezüglich einer elektrischen Serien- oder

Parallelschaltung der einzelnen Drähte innerhalb eines Bündels. Aufgrund der praxisrelevanten höheren Ausfallsicherheit durch die entstehende Redundanz wird sich für die Untersuchung von Bündeln mit elektrisch parallelen Drähten entschieden. Zur besseren Nachvollziehbarkeit der Experimente wird der verwendete Prüfstand erläutert. Dieser besteht im Wesentlichen aus einem steuerbaren Linearantrieb, einer Messeinrichtung zur Erfassung der relevanten mechanischen und elektrischen Größen sowie einer Infrarotkamera zur Temperaturmessung der Bündel.

Als erstes Ergebnis führt der Artikel das thermische Verhalten von den untersuchten FGL-Bündeln auf. Dabei zeigen die Untersuchungen in dem aufgebauten Prüfstand eine unterschiedliche Temperaturverteilung innerhalb der Bündel. Dies ist für die zu erwartende Lebensdauer der Bündel ungünstig, da einige Drähte wärmer werden und daraus eine höhere erzeugte Kraft und somit mechanische Spannung resultiert. Zurückzuführen ist diese inhomogene Temperaturverteilung auf die Klemmung der Drähte und unterschiedliche Übergangswiderstände innerhalb der Klemmen. Nach einer Anpassung der Klemmen und Verbesserung des Übergangswiderstandes zeigt die Veröffentlichung eine deutliche Verbesserung in der Temperaturverteilung des Bündels. Außerdem zeigen die thermischen Untersuchungen, dass sich eine isolierende Luftschicht zwischen den einzelnen Drähten abhängig von der Anzahl der Drähte im Bündel bilden kann. Es zeigt sich eine Relevanz im Verhalten von FGL-Bündel in späteren Versuchen, bei denen unter bestimmten Bedingungen keine isolierende Luftschicht vorhanden ist und somit ein Wärmeaustausch zwischen den Drähten möglich ist.

Um Erkenntnisse über das elektro-mechanische Verhalten von FGL-Bündel zu erhalten, werden zwei unterschiedliche Experimente, die jeweils einen Grenzbelastungsfall darstellen, durchgeführt. Konkret handelt es sich dabei um Versuche, bei denen entweder der Hub oder die Kraft der FGL-Bündel konstant gehalten wird.

Im ersten Experiment kann das FGL-Bündel eine größtmögliche Kontraktion bei konstant gehaltener Kraft durchführen, wobei die mechanischen, elektrischen und thermischen Kenngrößen gemessen werden. Erreicht wird ein maximaler Hub von 4 – 4,5 %. Auffällig dabei ist, dass mit sinkender Drahtanzahl bei gleichbleibendem Strom pro Draht der erzeugte Hub abnimmt, bis nur noch 1 % an Hub bei dem Bündel mit 4 FGL-Drähten erreicht wird. Zurückzuführen ist dieses Verhalten auf einen Temperaturaustausch, der abhängig von der vorhandenen oder nicht vorhandenen isolierenden Luftschicht zwischen den Drähten innerhalb eines Bündels stattfindet. In der Veröffentlichung wird gezeigt, dass durch dieses

passive Heizen von umliegenden Drähten innerhalb eines Bündels bis zu 60 % Energie eingespart werden kann.

Bei konstant gehaltenem Hub (Blockierkraft-Versuch) entwickeln sich durch die Phasenumwandlung und die Blockierung der Möglichkeit einer Kontraktion hohe innere Materialspannungen, die sich in einer messbaren Kraft äußern. Erzeugt werden so Kräfte von bis zu $1200\ N$ in Abhängigkeit der Drahtanzahl innerhalb eines Bündels. Unabhängig der Drahtanzahl und somit der entsprechenden Absolutkraft wird eine mechanische Spannung von $850 - 900\ MPa$ pro Draht generiert mit Ausnahme des Bündels mit vier FGL-Drähten. Wie in dem Experiment davor liegt dies an dem besseren Wärmeaustausch bei weniger Drähten an die Umgebung. Es wird wieder gezeigt, dass sich dies mit dem Einbringen einer höheren elektrischen Leistung kompensieren lässt.

Zusätzlich zu den bereits erwähnten Erkenntnissen ist das unterschiedliche Verhalten der elektrischen Widerstände der Bündel in den beiden Experimenten zu nennen. In dem ersten Experiment zeigt sich das typische und in der Literatur gängige Widerstandsverhalten [76] von FGL-Drähten, das sich aus dem Verhältnis der Phasenanteile von Martensit und Austenit, der Temperatur des Drahtes und der Geometrie (Länge, Durchmesser) der FGL-Drähte zusammensetzt. Im zweiten Experiment hingegen kann ein anderes Verhalten des elektrischen Widerstands beobachtet werden. In diesem ist der thermische Anteil der Widerstandsänderung der dominierende Anteil, was voraussichtlich auf die fehlende Kontraktion und somit nicht stattfindende Geometrieänderung der FGL-Drähte zurückzuführen ist.

In zukünftigen Versuchen sollte der Einfluss des Abstandes der einzelnen Drähte zueinander untersucht werden, um den Effekt der möglichen Energieeinsparung zu optimieren. Dies steht außerdem in Konflikt mit dem Anspruch, eine höhere Dynamik mit FGL-Bündeln zu erreichen, und sollte zusätzlich im Vergleich zu einem dicken FGL-Draht, untersucht werden. Da in den meisten FGL-Anwendungen wiederholbare Aktivierungen gefordert sind, sollten ebenfalls Untersuchungen des Verhaltens von FGL-Bündeln bzgl. dieser Anforderung angestellt werden. Die hier gewonnen Erkenntnisse über das Widerstandsverhalten von FGL-Drähten bilden ebenfalls die Grundlage für ein besseres Verständnis von FGL und sollten vertieft werden. Diese Veröffentlichung und die genannten weiteren Experimente legen den Grundstein für das Design zukünftiger FGL-Aktoren mit hoher Kraft und Dynamik.

Das zweite Gebiet der Hochleistungsanwendung, die schnelle Aktivierung von FGL-Drähten, umfasst in dieser Dissertation die beispielhafte Entwicklung eines Entlüftungsventils für Anwendungen im Spritzguss. Durch die bereits geschaffenen Grundlagen in [60]–[62], [65] stellt die hier gezeigte praxisnahe Umsetzung und die daraus gewonnenen Erkenntnisse den nächsten Schritt auf der Entwicklung neuer FGL-Aktoren und die damit einhergehende Erschließung neuer Anwendungsgebiete dar. Nach der Einleitung startet die Veröffentlichung mit einer Erläuterung, wieso die Entlüftung von Kavitäten im Spritzguss notwendig ist, wie sie normalerweise umgesetzt wird und bringt dies in den Zusammenhang mit den Vorteilen, die durch eine Realisierung mittels FGL-Technologie entstehen. Die Vorteile liegen darin, eine Entlüftung einfacher umzusetzen und den Anforderungen komplexer Spritzgussteile somit leichter gerecht zu werden. Die durch die FGL-Technologie gegebene Möglichkeit eines kompakten Designs steht hierbei im Fokus. Die wichtigste Kenngröße des zu entwickelnden Aktors für den genannten Anwendungsfall ist die Schließzeit des Ventils. Da der Kunststoff mit hohem Druck eingespritzt wird, füllt sich die Kavität entsprechend schnell. Ziel ist es, dass so wenig Luft wie möglich in der Kavität verbleibt, was durch ein möglichst spätes Schließen des Ventils erreicht wird. Als Anforderung an das entwickelte FGL basierte Entlüftungsventil wird deshalb eine Schließzeit von $100\ ms$ gefordert. Eine weitere für die FGL-Technologie nicht alltägliche Herausforderung bei der Entwicklung dieses Ventils ist die durch das Einsatzgebiet in Spritzgussanlagen gegebene erhöhte Umgebungstemperatur. Als Ziel wurde sich eine maximale Einsatztemperatur von 65°C gesetzt, bei der das Ventil voll funktionsfähig bleiben soll.

Im Anschluss an die Motivation wird in der Veröffentlichung das Konzept des entwickelten FGL-Aktors vorgestellt. Vereinfacht ausgedrückt, handelt es sich bei dem Aktorkonzept um zwei gegeneinander arbeitende FGL-Feder-Mechanismen. Dabei ist ein Mechanismus stärker ausgelegt und gibt somit die Ruheposition des Aktors vor. Dies ist die geschlossene Position des Ventils. Das Aktivieren des entsprechenden FGL-Drahtes resultiert in einer Bewegung in eine Richtung, die dem Öffnen des Ventils gleichkommt. Durch die entwickelte Mechanik und das zweite FGL-Feder-System stehen zwei Möglichkeiten zum erneuten Schließen zur Verfügung: Zum einen durch Deaktivieren des zuvor Aktivierten FGL-Drahtes, was abhängig von dem Abkühlverhalten zu einer langsamen Schließbewegung führt. Zum anderen durch den zweiten FGL-Draht, der in Kombination mit der Mechanik eine vom Abkühlverhalten des ersten FGL-Drahtes unabhängige und

somit schnelle Schließbewegung erlaubt. Zur Bestimmung des Schließzeitpunktes, der möglichst kurz vor dem Zeitpunkt, an dem der flüssige Kunststoff das Ventil erreicht, liegen soll, stehen in der Praxis zwei Verfahren zur Möglichkeit: Durch Flusssimulationen lassen sich Zeiten und Positionen des eingespritzten Kunststoffes ausreichend genau bestimmen, sodass ein Schließen des Ventils zeitversetzt zum Einspritzstart vorgenommen werden kann. Die zweite Variante sind zusätzliche Sensoren, die die Position des flüssigen Kunststoffs in der Kavität vor dem Ventil erkennen und das Schließen initiieren [77].

Um eine entsprechende Ansteuerung des Aktors zu gewährleisten, wird eine Elektronik entwickelt, die es erlaubt, über ein Auslösesignal direkt oder zeitabhängig das Ventil zu steuern. Die Elektronik ermöglicht, die zwei sich auf ihr befindenden Stromquellen in den Parametern Stromamplitude und Bestromungsdauer via USB zu programmieren. Zur Validierung der Elektronik findet eine für die Praxis realitätsnahe Programmierung mit einer Stromhöhe von $300\ mA$ und der Dauer von $1\ s$ für die erste Stromquelle und $400\ mA$ bzw. $100\ ms$ für die zweite Stromquelle statt. Die entwickelte Elektronik setzt die entsprechenden Werte nach dem Eintreffen eines Auslösesignals korrekt um.

Die Entwicklung des Aktors ist in zwei Bereiche unterteilt: Den Nachweis, dass das Konzept der zwei antagonistischen FGL-Feder-Systeme und der zugehörigen Mechanik funktioniert, und die Optimierung des Prototyps für den Einsatz in erhöhten Umgebungstemperaturen. Im Kapitel zum Nachweis der Funktionalität des Aktors wird auf die Auslegung und den Aufbau eingegangen, um im Anschluss eine Validierung in einem speziell für diesen Zweck aufgebauten Prüfstand vorzunehmen. Ausgelegt ist der Aktor auf $1\ mm$ Hub mit $2\ \%$ Dehnung der FGL-Drähte. Dies ist wichtig, um eine möglichst hohe Lebensdauer der Drähte zu gewährleisten. Um den Einbau der inneren Mechanik zu gewährleisten, ist der Aktor in zwei Halbschalen aufgebaut, die im Anschluss in ein Gehäuse geschoben werden. Das Gehäuse hält die Halbschalen zusammen und schützt den inneren Aufbau vor äußeren Einflüssen. Fertig zusammengebaut hat der Aktor einen Durchmesser von $8\ mm$ und eine Länge von $130\ mm$.

Bei der Validierung des ersten aufgebauten Prototyps im dafür vorgesehenen Prüfstand, der auch einen Einsatz in erhöhten Umgebungstemperaturen darstellen kann, zeigt sich die grundsätzliche Funktion des Aktors. Mit entsprechend eingestellten Stromhöhen und -zeiten kann die geforderte Schließzeit von $100\ m$ erreicht werden. Bei erhöhter Umgebungstemperatur zeigt der Prototyp eine Abnahme in seiner Öffnungs- und Schließbewegung, weshalb die nächste Iteration des Aktors speziell auf die

Funktionsfähigkeit bei erhöhten Umgebungstemperaturen ausgelegt wird. Zusätzlich werden kleinere Verbesserungen der Mechanik und der elektrischen Kontaktierung vorgenommen.
Bei dem zweiten Prototyp wird die Auslegung der beiden FGL-Feder-Systeme für hohe Temperaturen mittels eines am Lehrstuhl entwickelten Simulationstools vorgenommen. Dieses erlaubt, das Verhalten der FGL-Feder-Systeme bei erhöhten Umgebungstemperaturen vorherzusagen und verschiedene Konfigurationen im Vorfeld zu untersuchen. Als Konsequenz für den Einsatz in höheren Umgebungstemperaturen wird die mechanische Spannung, bei der die Aktordrähte arbeiten, drastisch erhöht. Nach Anpassung der Einzelteile und erneutem Aufbau des Aktors wird dieser im Prüfstand validiert. Es zeigt sich ein identisches Verhalten der Öffnungs- und Schließbewegung bei Raumtemperatur und erhöhter Umgebungstemperatur. Um die Funktion des entwickelten Ventils in der Praxis zu verifizieren, wird es in eine Demospritzgussform eingebaut und auf einer Versuchsanlage getestet. Als Ergebnis zeigt sich bei aktivem Ventil ein Spritzgussteil ohne Gussfehler.
Es kann ein Fazit gezogen werden, dass der hier entwickelte Aktor praxisnah die Möglichkeiten der schnellen Aktivierung von FGL-Drähten aufzeigt. Außerdem wird dargelegt, wie durch geschicktes Mechanikdesign weitere Schwachstellen der FGL-Technologie, wie das langsame Abkühlen oder der durch die Temperaturabhängigkeit begrenzte Einsatz in widrigen Umgebungen, weitestgehend eliminiert werden können. Bei zukünftigen Untersuchungen sollte der Schwerpunkt auf Lebensdauerversuchen liegen, da die durch den aufgezeigten Anwendungsfall auftretenden Belastungen außerhalb des bekannten dauerfesten Bereiches für die FGL-Technologie liegen.

Zum Abschluss dieser Arbeit wird in einer dritten Veröffentlichung die Entwicklung eines Demonstrators vorgestellt, der die beiden Gebiete in einer Hochleistungsanwendung vereint. Ziel des Demonstrators ist es, eine Bowlingkugel einen halben Meter in die Luft zu katapultieren, wofür eine hohe Kraft sowie eine schnelle Aktivierung der FGL-Drähte nötig ist. Nach der Einleitung startet die Veröffentlichung mit der theoretischen Berechnung der benötigten kinetischen Parameter, um eine $3\ kg$ schwere Bowlingkugel $500\ mm$ senkrecht in die Luft zu katapultieren und erläutert die Anzahl und Anordnung der verwendeten FGL-Bündel. Ebenfalls wird die benötigte Aktivierungsenergie für ein Bündel berechnet. Eine Herausforderung für das anvisierte Katapultieren der Bowlingkugel besteht darin, diese Energie schnell genug in die FGL-Bündel einzubringen. Bevor auf die dafür nötige

Entwicklung einer Elektronik eingegangen wird, geht die Veröffentlichung auf den mechanischen Aufbau des Demonstrators, einzelner funktioneller Bauteile wie die Drahtklemmen und die Auslegung der FGL-Drähte ein. Die entwickelten Drahtklemmen erlauben es, bis zu fünf $500\ \mu m$ dicke FGL-Drähte zu klemmen und somit zu einem Bündel zusammenzufassen. Das komplette System ist so ausgelegt, dass bei der Verwendung von vier FGL-Drähten ein Draht zum Beschleunigen der Kugel eine Spitzenlast von $76{,}5\ N$ aufbringen muss. Dies entspricht pro $500\ \mu m$ Draht einer mechanischen Spannung von $390\ MPa$. Im Wesentlichen besteht der Demonstrator aus den drei benötigten FGL-Bündeln, drei kugelgelagerten Linearführungen, einer Trägerplattform für die Kugel und einer Acrylglasröhre. Durch die Aktivierung der FGL-Bündel kontrahieren diese und ein Hub von $16\ mm$ wird generiert. Um eine Trennung von Plattform und Bowlingkugel nach der Beschleunigung zu gewährleisten, sind Endanschläge an den Linearführungen angebracht. Nach dem Flug und dem erneuten Aufliegen der Bowlingkugel auf der Plattform können die FGL-Bündel erneut gelängt und der Vorgang wiederholt werden.

Um die benötigte Energie zur Umwandlung in entsprechend kurzer Zeit in die Bündel einzubringen, wurde eine entsprechende Hochleistungselektronik zur Ansteuerung konzipiert und entwickelt. Die Elektronik besteht aus insgesamt vier Platinen. Drei Platinen, jeweils eine pro Bündel, um die benötigte Energie in Kondensatorbänken zwischenzuspeichern und bei Bedarf mittels Hochleistungsschaltern, aufgebaut aus IGBTs (Insulated-Gate Bipolar Transistor), an die Bündel abzugeben. Bestückt werden können diese mit bis zu zwölf Kondensatoren und es kann ein Strom von maximal $960\ A$ geschaltet werden. Die vierte Platine ist für die Gleichrichtung der Versorgungsspannung und das Lademanagement der drei Kondensatorbankplatinen zuständig.

Zur Validierung der Bündel und der Elektronik wird ein Versuchsaufbau realisiert. Die Veröffentlichung erläutert den Ablauf der Vorexperimente und diskutiert diese. Es zeigt sich, dass die zuvor berechneten und im Idealfall benötigten $230\ V$ Aktivierungsspannung und der daraus resultierende Stromfluss zu niedrig ist, um die geforderte Abfluggeschwindigkeit zu erreichen. Ein zufriedenstellendes Ergebnis erbringt eine Erhöhung der Ladespannung auf $280\ V$, was in einem Stromfluss von $560\ A$ pro FGL-Bündel resultiert.

Final wird in der Veröffentlichung der Komplettaufbau des Demonstrators erläutert, um im Anschluss dessen Funktionalität zu überprüfen. Der fertige Demonstrator umfasst den mechanischen Aufbau inklusive der drei FGL-Bündel und die komplette Elektronik. Um den

Demonstrator zu testen, werden die Kondensatoren mit der zuvor ermittelten Ladespannung von $280\,V$ aufgeladen, was zu einer Flughöhe der Kugel von $41\,cm$ führt. Die umgesetzte Energie pro Bündel beträgt dabei $145{,}1\,J$. Somit ergibt sich für den gesamten Demonstrator eine Gesamtenergie von $435\,J$. Um das Maximum an Flughöhe auszureizen, wird im Anschluss die Ladespannung auf $300\,V$ erhöht. Die umgesetzte Gesamtenergie beträgt damit $495\,J$ und resultiert in einer Flughöhe von $45\,cm$. Nach erfolgreichem Aufbau und Test des Demonstrators endet die Veröffentlichung mit einem Ausblick, der weitere Untersuchungen im Hinblick auf die Lebensdauer von FGL-Drähten in solchen Hochleistungsanwendungen aufzeigt. Besonders der Einfluss der durch die kurze Aktivierungszeit benötigten erhöhten Leistung und der damit resultierenden dynamischen Belastungen sind hier zu erwähnen.

3 PUBLIKATIONEN FORMGEDÄCHTNISLEGIERUNGSDRÄHTE IN HOCHLEISTUNGSANWENDUNGEN

Artikel	Journal	Verlag	Erst-veröffentlichung	Impact Factor (2021)
Analysis and Evaluation of Bundled SMA Actuator Wires	Sensors and Actuators A: Physical	Elsevier	23.11.2021	4,291
High-Speed Antagonistic Shape Memory Actuator for High Ambient Temperatures	Advanced Engineering Materials	Wiley	05.04.2022	4,122
High-Power Shape Memory Alloy Catapult Actuator for High-Speed and High-Force Applications	IEEE Access	IEEE	26.08.2022	3,476

3.1 Analysis and Evaluation of Bundled SMA Actuator Wires

Rouven Britz[1], Paul Motzki[1,2]

[1] Lehrstuhl für Intelligente Materialsysteme, Fachrichtung Systems Engineering, Fachrichtung Materialwissenschaft und Werkstofftechnik, Universität des Saarlandes, Saarbrücken

[2] AG Intelligente Materialsysteme, Zentrum für Mechatronik und Automatisierungstechnik, ZeMA gGmbH, Saarbrücken

Veröffentlicht in Sensors and Actuators: A. Physical.
DOI: 10.1016/J.SNA.2021.113233

Sensors and Actuators: A. Physical 333 (2022) 113233

Contents lists available at ScienceDirect

Sensors and Actuators: A. Physical

journal homepage: www.elsevier.com/locate/sna

Analysis and evaluation of bundled SMA actuator wires

Rouven Britz[a,*], Paul Motzki[b]

[a] Department of Systems Engineering, Department of Materials Science and Engineering, Saarland University, Saarbrücken, Germany
[b] Center for Mechatronics and Automation Technologies (ZeMA gGmbH), Saarbrücken, Germany

ARTICLE INFO

Article history:
Received 25 June 2021
Received in revised form 29 October 2021
Accepted 16 November 2021
Available online 23 November 2021

Keywords:
Shape Memory Alloys
SMA
Bundle
Ni-Ti
NiTi
Nitinol
High Force
Actuator

ABSTRACT

The attractive properties of shape memory alloys (SMA), especially their high energy density, steadily expand the range of applications in which SMA wires represent attractive alternative actuator components. Industrial applications in particular, oftentimes require large forces, which scale with the diameter of SMA actuator wires. The higher the required actuator force, the larger the total effective cross-sectional area of the SMA wires is needed. Increasing the SMA wire diameter results in worse actuator dynamics due to a decreasing surface-to-volume ratio and thus slower convective cooling. Instead of simply increasing the wire diameter, the bundling of several thin wires offers a suitable alternative to generate higher forces. This results in an increased surface-to-volume ratio and thus permits higher dynamic system performance.

This paper discusses the mechanical and thermal behavior of SMA wire bundles and shows the influence of contact resistance inside the clamps, which is important to optimize for a long-lasting functionality of SMA bundles. In addition, the experiments show an indirect heating between single SMA wires inside a bundle, which leads to an energy saving capability up to 60%. Two electro-mechanical experiments show the behavior of SMA bundles in a constant force and a constant strain measurement. The experimental results show a maximum stroke of 4–4.5% and a generated maximum force of 1200 N. The results are discussed to provide an understanding of the mechanical characteristics of SMA bundles. In addition, an infrared (IR)-Camera provides an insight into the thermal behavior.

1. Introduction

Shape memory alloys (SMAs) are well known for bio-medical applications like stents or guide wires [1–6]. Recently, SMA research is focusing on the high potential as lightweight integrated actuator systems [7–19], as well as the strongly emerging field of elastocaloric cooling [20–23]. Due to their high energy density and multi-functional properties [24], they are suitable for the design of compact actuator-sensor-systems. In the automotive sector and consumer electronics, SMA based actuator systems have already established in several applications [25–29]. Typically, nickel-titanium (NiTi) actuator wires with a diameter between 0.025 mm and 0.5 mm are used [30,31] as SMA actuators. The thermal shape memory effect as underlying effect of shape memory actuators is based on a reversible phase transformation of the material crystal lattice between the low temperature martensitic phase and the high temperature austenitic phase. The cold wire elongates when a tensile stress is applied. Joule heating by an electric current lead to a temperature increase of the wire, which results in a macroscopic contraction. Microscopically, the length change is based on a first order phase transformation from the martensitic lattice structure to the austenitic lattice [24], [32]. After the wire is cooled down, an external force can return the wire to its original length. This process is thus repeatable. The contraction of the wire can be correlated with the electrical resistance of the wire, referred to as “self-sensing” effect [33].

Actuator systems using SMA technology usually consist of an SMA element and a biasing mechanism like a spring or a mass. The diameter of the SMA wire is determined by the required force. A higher force means a larger diameter accompanied by reduced system dynamics. Using multiple SMA wires in parallel allows for generating high forces without decreasing the dynamic performance, as shown in a bistable SMA vacuum suction cup [34]. In contrast to an SMA bundle in form of a twisted cable, which makes a convective cooling of the single wires almost impossible, a bundle of separated wires allows an airflow through the bundle and therefore improved convective cooling for better dynamic behavior.

Since an SMA bundle consists of several SMA wires arranged mechanically parallel, the actuator can compensate the breakdown of a single wire. Thus, bundling SMA wires not only allows for a high

* Corresponding author.
E-mail address: rouven.britz@imsl.uni-saarland.de (R. Britz).

https://doi.org/10.1016/j.sna.2021.113233
0924-4247/

output force system with a high dynamic performance, but also provides an increased reliability and redundancy. A major challenge when using SMA wires as actuators is the electrical integration and contacting. There are basically two ways to contact the SMA wires electrically within a bundle - in series or in parallel configuration. The following example is intended to briefly illustrate the advantages and disadvantages of the two electrical configuration options and their effects on the mechanical properties.

An exemplary NiTi SMA wire with a diameter of 0.25 mm and a length of 100 mm has a resistance of approximately 1.85 Ω. To heat the wire up to the austenite finish temperature of 90 °C, a current of 1050 mA for 1 s at 172 MPa mechanical tensile stress is needed [30]. A voltage of 1.94 V is required to generate this current flow through the wire. Contacting five wires in series, the voltage increases to 9.7 V, because of the resistance increase by a factor of five. The failure of a single SMA wire in a serially contacted bundle would result in an overall actuator system failure. The insulation of the wires to each other and inside the clamps is also critical in the serial case since short circuits lead to inactive areas of the bundle. Contacting the SMA electrically in parallel, a current of 5.25 A is required, since the resistance is reduced by a factor of five, while the voltage drop remains at 1.94 V. The disadvantage of the high current flow using this topology can be compensated by the mechanical advantages. The system is mechanically redundant. Contrarily to the arrangement of the SMA wires in series, the failure of a single wire does not lead to an actuator failure. Such a defect can be easily detected by a resistance measurement and the actuator bundle can be replaced during planned maintenance. Additionally, a lower design effort is required since no electrical insulation in between the SMA wires is required.

In this paper, SMA bundles in electrical parallel configuration are investigated. First, the experimental setup to characterize SMA bundles in different power and load conditions will be presented. The setup includes an IR-Camera to determine the thermal characteristics of the SMA bundles, including the temperature distribution of an SMA bundle in general as well as the influence of the clamps on it. Also, a possible thermal influence of a wire to each other wires in the bundle can be observed by the IR-Camera. After outlining the thermal measurements, the experiments to characterize the mechanical and electrical behavior of parallel SMA bundles are discussed. The results show a significant mutual influence of the wires in a bundle, which can help save energy. The findings of the possibilities of an SMA bundle in terms of force, stroke, electrical properties and energy saving will subsequently serve as a basis for the design of future actuator-sensor systems based on bundled SMA actuator wires.

2. Materials and methods

The measurement setup is based on components from National Instruments and uses LabVIEW to control the experiments and record the data. A load cell KS25 from GTM is attached to measure the generated force of the SMA bundle, while a linear drive – in combination with a control algorithm – allows either holding a constant stress level of the SMA bundle during activation for constant force measurements or a constant position for constant strain measurements. In both cases, the SMA bundle voltage and current are measured with a NI CompactRIO data acquisition system. The voltage is measured by a NI 9229 voltage measuring module, the current by a NI 9227 current measuring module. Additionally, an IR-Camera IR 8380 from Infratec is equipped, enabling for the measurement of the temperature distribution of the bundles. Fig. 1, right shows the vertically arranged final experimental setup including an SMA bundle.

The SMA bundles are made of commercially available SMA wires. Due to a standardized manufacturing process, reproducible properties of the SMA material are given and documented by the manufacturer in [36]. Fig. 2 shows a DSC measurement of the used SMA material.

3. Results

3.1. Thermal investigations

In this section, the results of the thermal investigations of SMA wire bundles are presented and discussed. In this study, two bundles of different sizes are compared. The first bundle consists of four wires mechanically in parallel and the second bundle analogously of 28 wires. In general, heating an SMA wire yields a phase transformation and thus a force can be generated. The force that can be

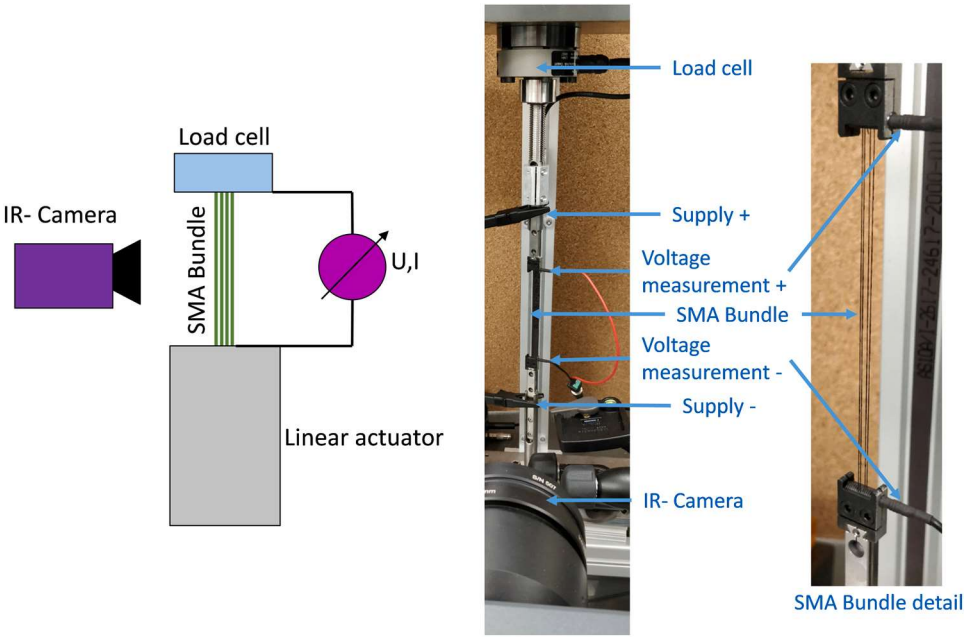

Fig. 1. Schematic view of the test rig (left) and final experimental setup with SMA bundle (right) [35].

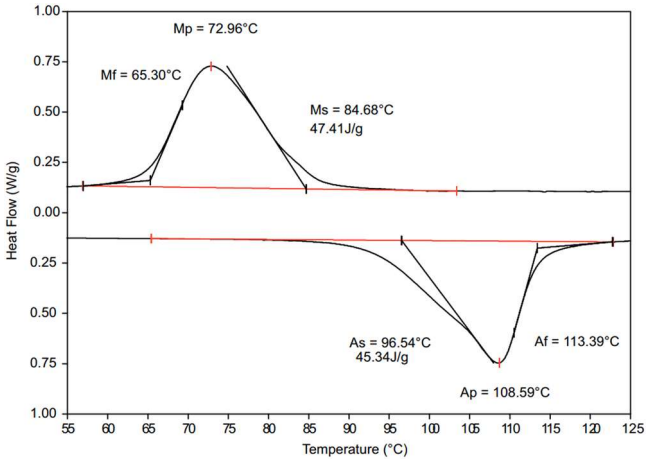

Fig. 2. DSC measurement of the used SMA material [36].

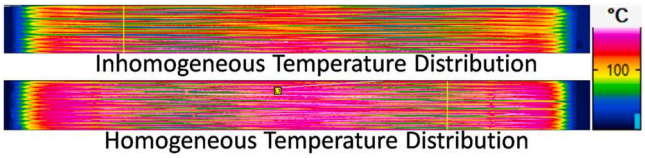

Fig. 3. Inhomogeneous (upper part) and homogeneous (lower part) temperature distribution of an SMA bundle.

generated by one wire and thus the mechanical stress in the material depends on the temperature of the wire. Therefore, a homogeneous temperature distribution and hence equal temperatures in all wires is inevitable for an actuation using SMA bundles to ensure an equal load distribution over all wires and to avoid an overload of single wires. The upper part in Fig. 3 shows an IR-Camera recording, where an inhomogeneous temperature distribution can be observed. The bundle is divided into two temperature areas, a hotter section at the bottom (pink) and a colder section at the top (red and yellow, respectively). Such an inhomogeneous temperature distribution suggests different Joule heating of the single wires. The Joule heating depends on the electrical power, which is influenced by the current through the wires and their electrical resistance. But since all SMA wires have through a semi-automatic winding process, which keeps the pretension constant, initially the same dimensions, phase configuration and temperature, their resistance is also identical. This leads to the conclusion that the contact resistance inside the clamps has an important influence on the current flow. By adding copper foil and silver paste inside the clamps a better contact resistance could be ensured and thus a homogeneous temperature distribution is achieved (Fig. 3, lower part).

Looking at the temperature of individual wires in the bundle over time using a measurement line at one position on the x-axis (Fig. 4), a temperature gradient from the inner wires to the outer wires can be observed. The pictures of the IR-Camera show only one half of the SMA wires of a bundle, since the bundles are arranged in two layers (see Fig. 1: SMA Bundle detail). As a consequence, only the front layer of the bundle is observed, for example 14 SMA wires while investigating a bundle of 28 SMA wires.

The temperature distribution in Fig. 4 has two reasons: On the one hand, there is a better heat exchange of the outer wires with the environment, on the other hand, there is reduced indirect heating of these outer wires by less adjacent wires. Indirect heating means a heat exchange from one wire to another through the air gap between them. The measurement shows a significant heating of the air between the wires, in contrast to Fig. 5 with an insulating layer of air between the wires. In both experiments, the energy per wire is identical. The two bundles with four and 28 wires respectively, differ regarding the resulting maximum temperature. Figs. 4 and 5 show the two measurements and a lower maximum temperature in the wires of the bundle with four wires can be observed. This indicates a higher heat transfer to the environment and therefore a decrease in the temperature of the bundles. With increasing temperature between the single wires, the temperature gradient between a wire and the surrounding air decreases, which in turn helps heating up the wires. The influences of this effect regarding actuation properties are described in the experiments in Section 4.

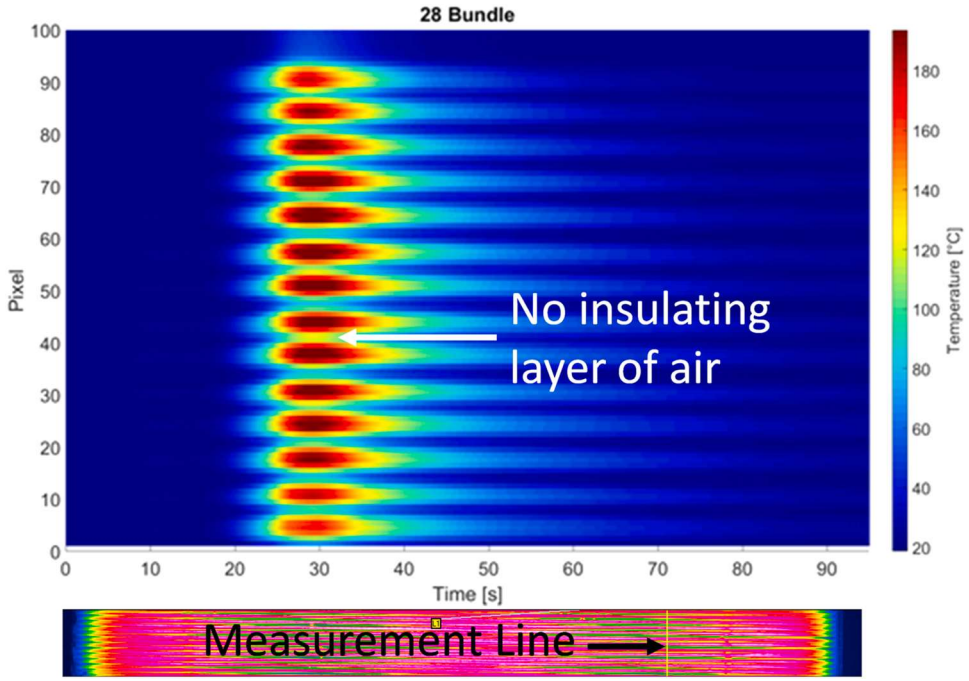

Fig. 4. Temperature distribution inside a bundle of 28 wires [35].

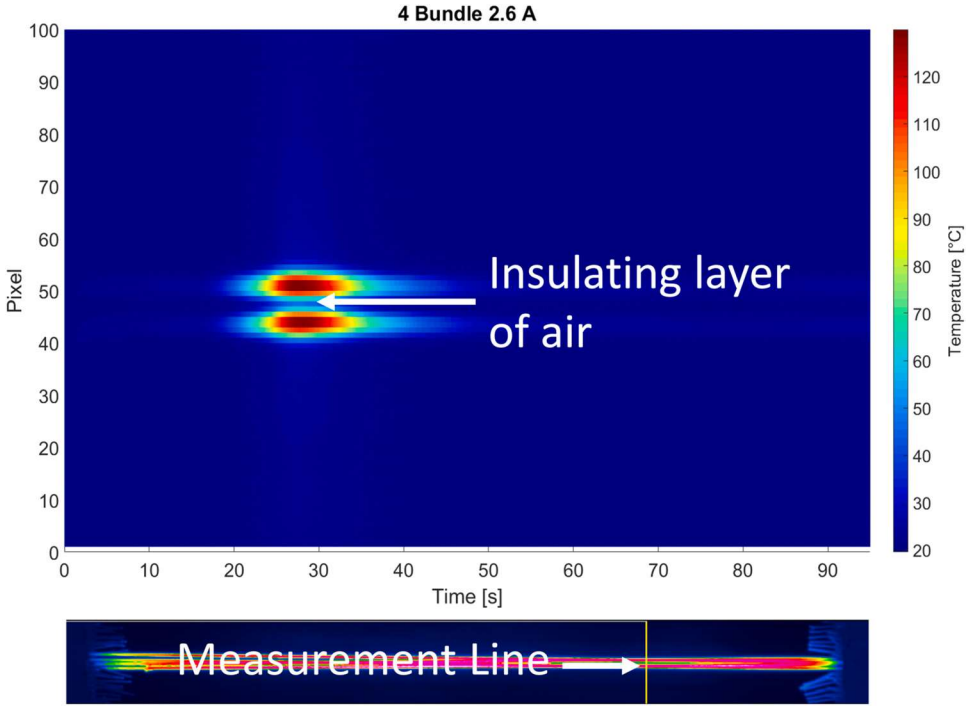

Fig. 5. Temperature distribution inside a bundle of 4 wires [35].

3.2. Constant force and constant stroke measurements

This section discusses the electro-mechanical measurements of SMA bundles using SMA wires with a diameter of 250 µm and a length of 100 mm. The total dimensions of the bundles including the clamps are 130 mm of length and 16 mm of width (Fig. 6).

To characterize their mechanical behavior by an electrical activation, two experiments are conducted, representing two extreme stress types (maximum stroke and maximum force) of SMA wires. In the first experimental series, the bundles are loaded with a constant force while being activated. As a result of these experiments the maximum stroke of the SMA bundle is obtained. In the second series of experiments, the bundle is pre-strained to a defined stress level. After reaching this stress level, the position is fixed, while the SMA wires are activated. As a result, the maximum (blocking) force of the SMA bundle is obtained.

Seven different bundle types with SMA wire numbers between four and 28 are used for the following measurements.

3.2.1. Constant force experiment results

The constant force experiments show the maximum stroke of the SMA bundles. Each bundle is loaded with a force equivalent to a mechanical pre-stress of 200 MPa per wire (Fig. 7a) and this load is kept constant during the experiment. An electrical current in triangle signal form with a rising and falling time of 90 s each is applied to activate the wires. The peak of each current triangle is predetermined and corresponds to a peak current of 0.39 A per wire, assuming a homogeneous current distribution (Fig. 7d). A homogeneous current distribution leads to a homogeneous temperature distribution, which leads to a homogeneous load distribution and prevents overloads.

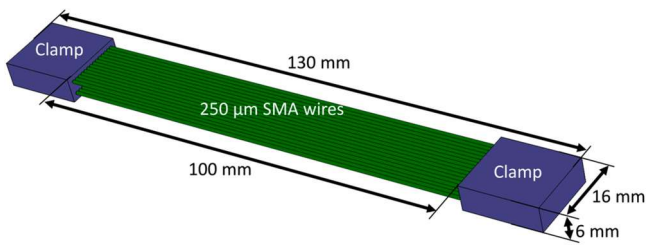

Fig. 6. Sketch of the SMA bundle dimensions.

The wires contract up to a maximum value of 4 mm, which corresponds to a stroke of 4% (Fig. 7b,c). The voltage signals in Fig. 7e show significant changes in the voltage rise rate at 80 – 90 s with the exception of the bundle of 4 wires, which shows an almost constant voltage rise rate. The voltage drop over the wires is influenced by the electrical resistance of the wires, which is described by the equation [37]:

$$R_{SMA}(T, x_A, x_+, x_-) = \rho_{SMA}(T)\frac{L}{A} \tag{1}$$

with

$$\rho_{SMA}(T) = x_+\rho_+(T) + x_-\rho_-(T) + x_A\rho_A(T) \tag{2}$$

The equation shows that three factors contribute to the resistance of SMA wires: The temperature T, the phase fractions x_A, x_+, x_- and the wire geometry, where L is length of the wire and A is the cross-sectional area. Fig. 8 (left upper part) shows the bundle resistance as a function of time calculated with the measured voltage and current. Fig. 8 (right upper part) shows the bundle resistance as a function of temperature. The resistance of the bundles decreases according to the equation for parallel connection of resistors:

$$\frac{1}{R_{Total}} = \sum_{i=1}^{n}\frac{1}{R_i} \tag{3}$$

For example, with a resistance of 18.5Ω/m [30] for a 250 µm wire and a length of 100 mm, one wire has a theoretical resistance of 1.85Ω. A bundle of 4 wires has a total resistance of 0.46Ω (Eq. 3).

For better comparison of the resistance behavior, the specific resistance is calculated and shown in Fig. 8 (lower part). It is shown

that the resistance drop decreases with a decreasing number of wires. The lower resistance change correlates with the lower stroke shown in Fig. 7b.

The reason for this lower resistance change is shown in Fig. 9, illustrating the temperature of the bundles over time. To measure the temperature of the wires, again the IR-Camera is used. The maximum temperature of the bundle with four wires is less than 90 °C, thus below the austenite finish temperature. Due to this low temperature, there is only little phase transformation and therefore low wire contraction. Although the current per wire is equivalent in all experiments, the heating rate decreases with a decreasing number of wires in the bundle. This indicates a lower indirect heating by the adjacent wires and results in the lower maximum temperature. The plateaus in the temperature measurement at 75 and 175 s indicate the latent heat that is absorbed or released during the phase transformation. The maximum temperature of the wires in the bundle with four wires and in the bundle of eight wires is too low to develop such a plateau, indicating only a small amount of phase transformation.

To compensate the low indirect heating, more active heating is required to achieve the same stroke of 4–4.5%. For this purpose, a second experiment with the bundle of 4 wires is conducted by increasing the current peak in 0.5 A steps, from 1.6 A to 2.6 A. The result of the stroke measurement at different peak currents is shown in Fig. 10 (upper part). After an increase of 1 A the stroke reaches 4–4.5%. The delta of the resistance (Fig. 10, lower part) increases as well, which indicates a near full phase transformation.

The calculation of the energy input per wire shows nearly the same energy levels in the first experiment for all bundles (see Fig. 11, green lines). As shown, the bundle of four wires only contracts about 1% at this energy level. The performance of such a bundle can be improved using a higher energy input (Fig. 11, red and orange lines). A bundle of 28 SMA wires saves more than 60% of the energy in contrast to the bundle with four wires assuming a complete

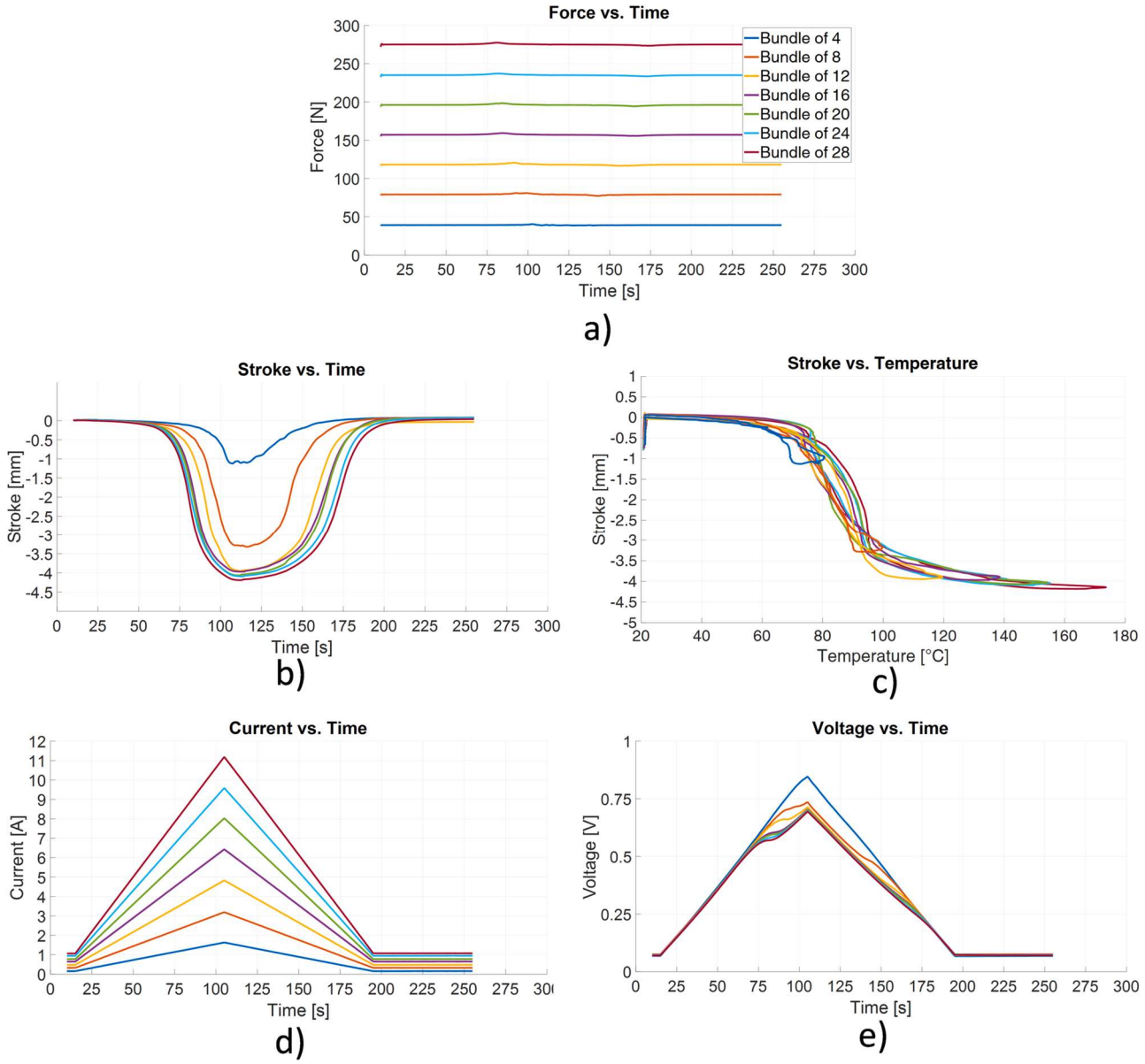

Fig. 7. Measured data from the constant force experiment – a) constant force of each bundle equivalent to a mechanical pre-stress of 200 MPa per wire, b) resulting stroke of each bundle due to activation over time, c) resulting stroke of each bundle due to activation over temperature, d) current triangle for activation, e) voltage drop over each bundle.

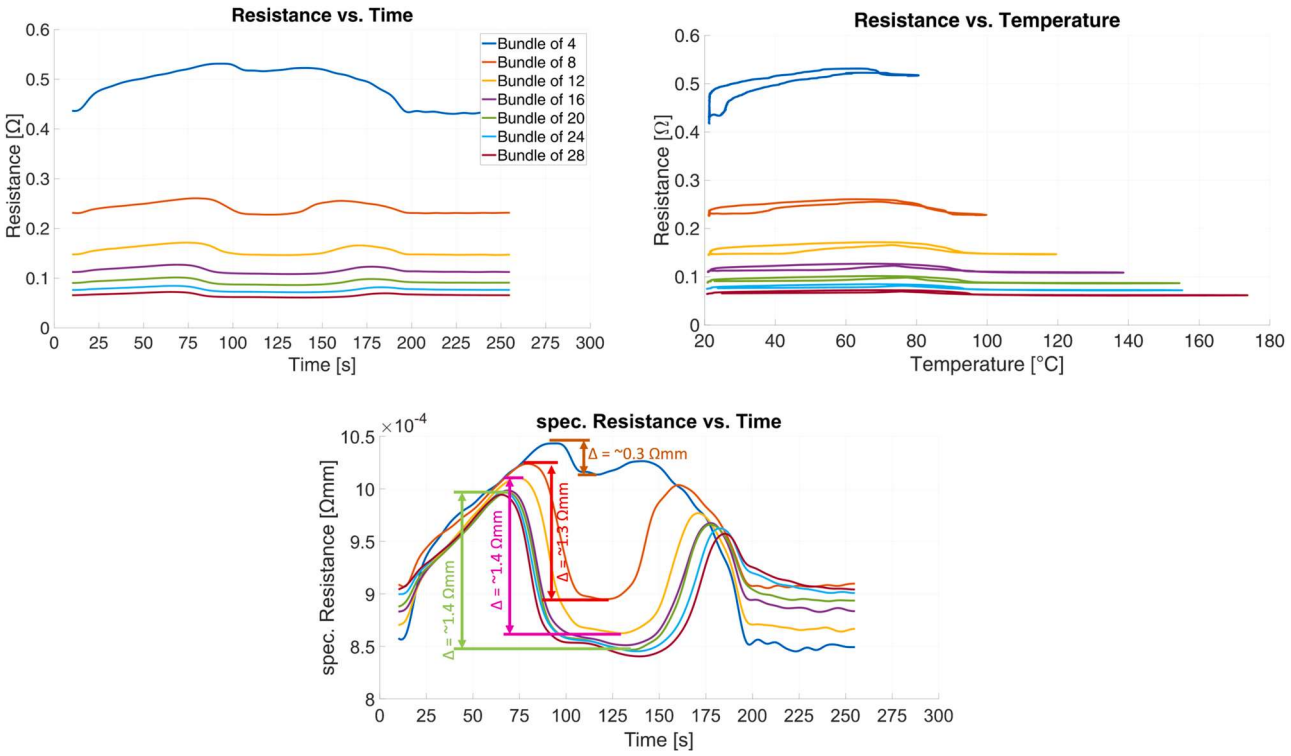

Fig. 8. Calculated resistance over time (left upper part), calculated resistance over temperature (right upper part) and specific resistance (lower part) of the SMA bundles in the constant force series of experiments.

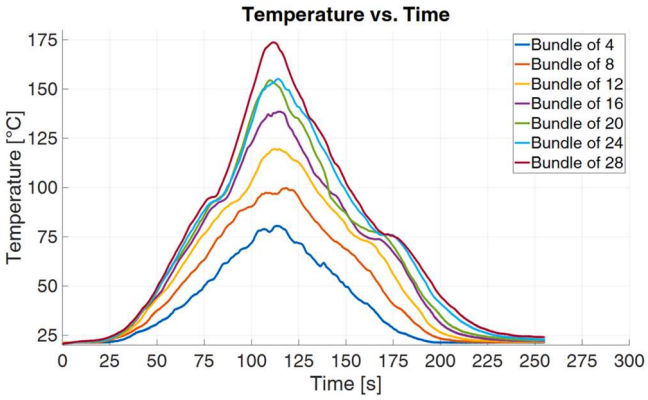

Fig. 9. Maximum temperature of SMA bundles in constant force experiment.

contraction of both bundles (Fig. 11). A bundle of multiple SMA wires not only brings the advantages mentioned, e.g. redundancy and high forces combined with increased dynamics, but it also helps to realize more energy-efficient activation.

3.2.2. Constant stroke experiment results

To complete the mechanical and electrical investigations of bundled SMA wires, a further series of experiments is conducted, pointing out the forces, which can be generated while using compact SMA bundle actuators. Each bundle is loaded to a force equivalent to a pre-stress of 200 MPa per wire. In contrast to the first experiment, the stroke is kept constant during the experiment (Fig. 12a). A current triangle with a rising and falling time of 10 s is applied to activate the wires. The peak of each current triangle is predetermined and corresponds to a peak current of 0.65 A per wire, assuming a homogeneous current distribution (Fig. 12d).

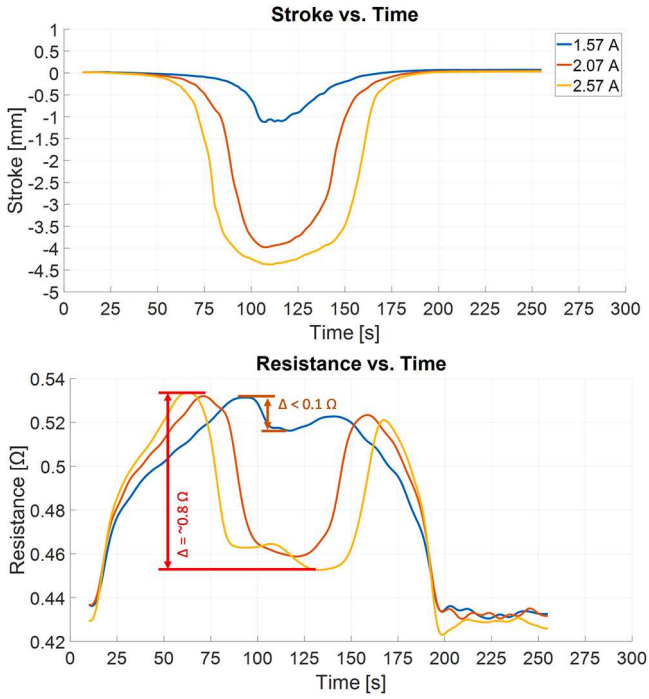

Fig. 10. Stroke (upper part) and resistance (lower part) change of a bundle of 4 wires by different currents.

Fig. 12b shows the resulting force due to the heating as a function of time. Each force maximum represents a stress maximum of about 850–900 MPa per wire, except the bundle of four wires with 700 MPa. Fig. 12c shows the resulting force due to the heating as a function of temperature. In this experiment, no voltage drops are visible in Fig. 12e, indicating less phase transformations. Plotting the

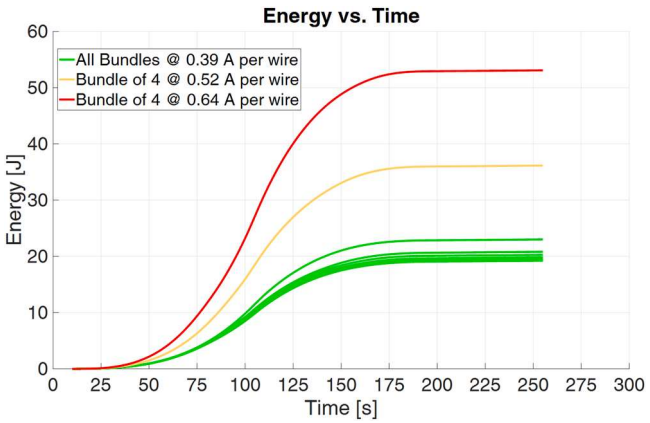

Fig. 11. Energy input for each wire in different experiments.

resistance as a function of time (Fig. 13, left upper part), and for a better comparison the specific resistance (Fig. 13, lower part), shows an equivalent behavior of the resistance like the temperature. Fig. 13 (right upper part) shoes the resistance as a function of temperature. First, the electrical resistance increases with increasing temperature, as it is typical for metal. First a sharp rise and after 16 s the resistance change rate changes until the temperature maximum at 28 s. This change indicates the phase transformations and generating the force, in contrast to the first experiment, the wire cannot transform to austenite completely. The constant increase of the mechanical stress results in an increase of the transformation temperature, so the transformation can only happen bit by bit.

The low generation of force of the bundle with four wires results from the low maximum temperature (Fig. 14). As already seen in the constant force experiments, this lower maximum temperature results from increased heat exchange to the environment compared to the heat exchange between the SMA wire themselves. Increasing the

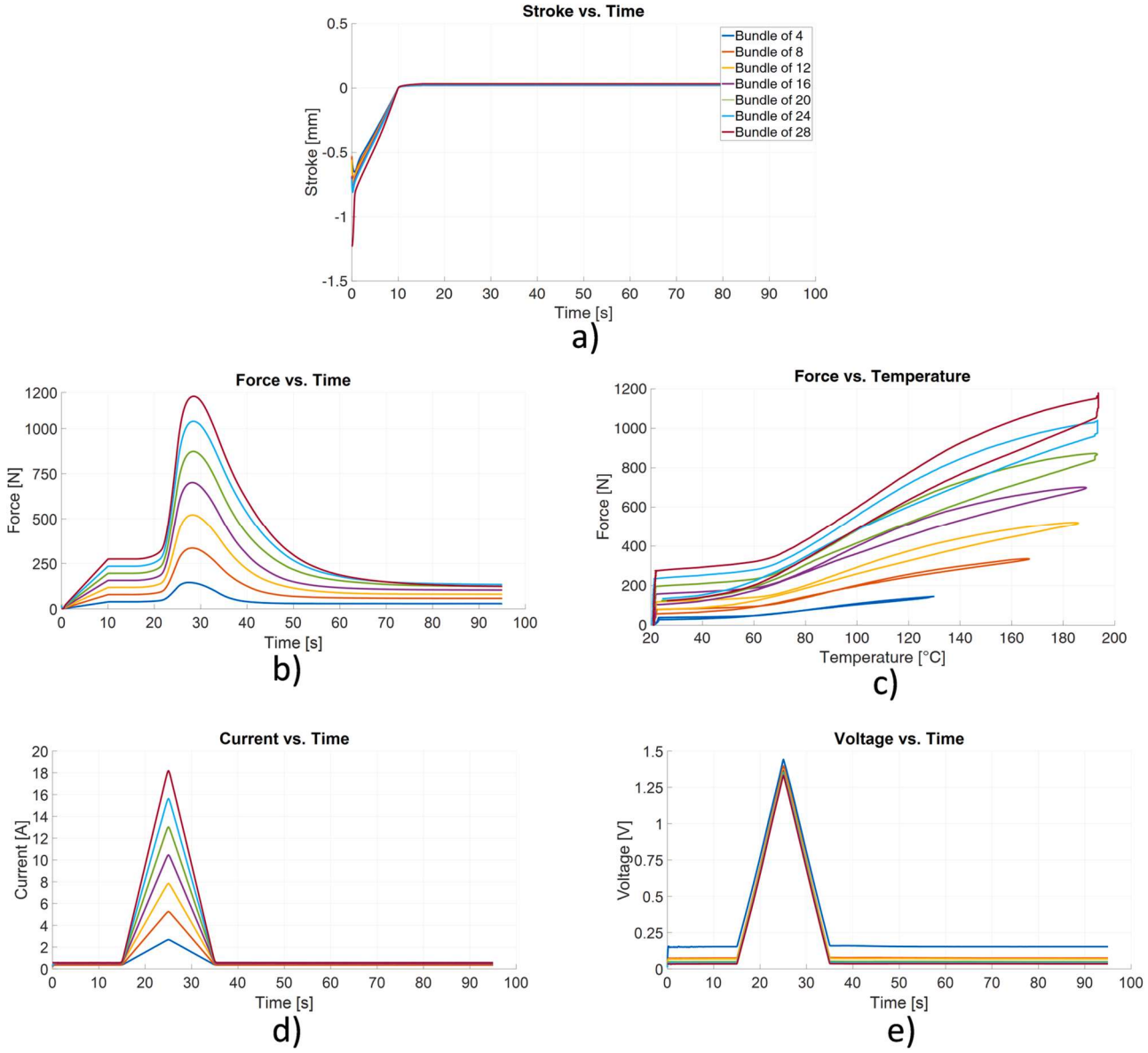

Fig. 12. Measured data from the constant stroke experiment – a) constant stroke of each bundle loaded to a mechanical pre-stress of 200 MPa per wire, b) resulting force of each bundle due to activation over time, c) resulting force of each bundle due to activation over temperature, d) current triangle for activation, e) voltage drop over each bundle.

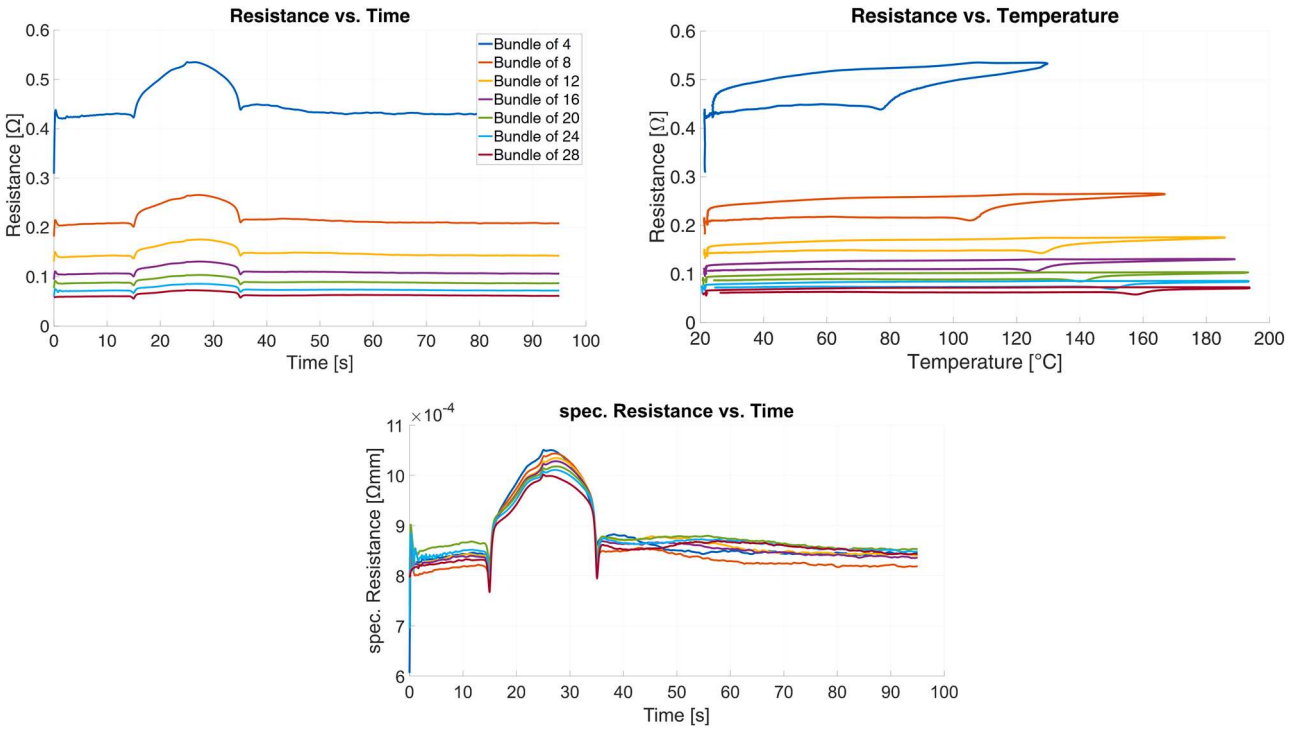

Fig. 13. Calculated resistance over time (left upper part), calculated resistance over temperature (right upper part) and spec. resistance (lower part) of SMA bundles in constant stroke experiments.

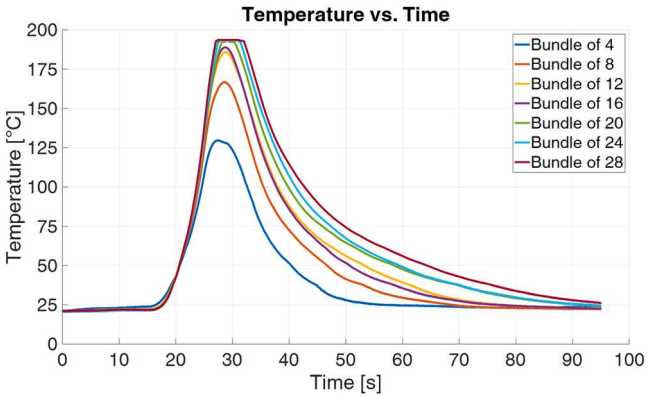

Fig. 14. Maximum temperature of SMA bundles in constant stroke experiments.

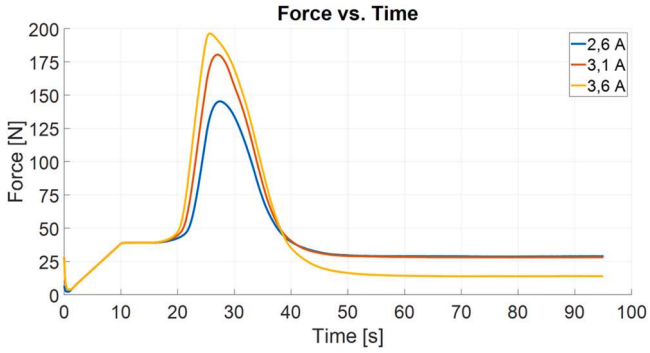

Fig. 15. Force change of a bundle of 4 wires by different currents.

current through the SMA wires can compensate for this behavior (Fig. 15).

4. Conclusion and outlook

First results of experiments with electrical and mechanical parallel SMA bundles have been presented. An overview of the advantages and disadvantages in contrast to an electrical series configuration has been outlined first. Subsequently, the test rig, enabling temperature measurements, as well as electrical-mechanical measurements, has been introduced. Section three discusses the thermal measurements of different SMA bundles, pointing out the importance of a low-ohmic contact resistance as well as the influence of the indirect heating between single SMA wires inside a bundle. Because of this indirect heating, up to 60% of the energy can be saved during activation. In section four, two series of experiments are presented, characterizing the mechanical and electrical behavior of SMA bundles. In the first series of experiments, the SMA bundles are loaded with a constant force. The experiment shows the resulting stroke of SMA bundles at constant loads. A maximum stroke of 4–4.5% can be obtained. In the second series of experiments, the stroke is kept constant. These experiments show the ability of generating high forces with compact SMA bundle actuators. A bundle of 28 SMA wires with a diameter of 250 µm is able to generate a maximum force of 1200 N.

In future work the influence of the distance between the wires will be investigated in order to optimize the energy savings due to indirect heating effects, which is in conflict with the cooling behavior and thus the desired high dynamics of SMA bundles. Due to the better surface-to-volume ratio, SMA bundling should results in an improved cooling behavior in comparison to one comparable thick SMA wire. Further investigations will show whether, in order to exploit this effect, the convection of the air is sufficient or whether an additional air flow is indispensable to get the warm air out of the bundle. In addition, effects like cumulative heating at repeated activation and the effects of mechanical pre-load and environmental conditions are important studies for future work. With these findings about SMA bundles, compact SMA actuators generating high forces at high frequencies can be specifically designed.

Declaration of Competing Interest

The authors declare that they have no known competing financial interests or personal relationships that could have appeared to influence the work reported in this paper.

References

[1] J. Mohd Jani, M. Leary, A. Subic, M.A. Gibson, A review of shape memory alloy research, applications and opportunities, Mater. Des. 56 (2014) 1078–1113, https://doi.org/10.1016/j.matdes.2013.11.084

[2] N.B. Morgan, Medical shape memory alloy applications - The market and its products, Mater. Sci. Eng. A 378 (1–2 SPEC. ISS) (2004) 16–23, https://doi.org/10.1016/j.msea.2003.10.326

[3] R. Pfeifer, C.W. Müller, C. Hurschler, S. Kaierle, V. Wesling, H. Haferkamp, Adaptable orthopedic shape memory implants, Procedia CIRP 5 (2013) 253–258, https://doi.org/10.1016/j.procir.2013.01.050

[4] S. Pittaccio, L. Garavaglia, C. Ceriotti, F. Passaretti, Applications of shape memory alloys for neurology and neuromuscular rehabilitation, J. Funct. Biomater. 6 (2) (2015) 328–344, https://doi.org/10.3390/jfb6020328

[5] K. Yanagihara, H. Mizuno, H. Wada, S. Hitomi, Tracheal stenosis treated with self-expanding nitinol stent, Ann. Thorac. Surg. 63 (6) (1997) 1786–1789, https://doi.org/10.1016/S0003-4975(97)00369-X

[6] I. Vinograd, B. Klin, T. Brosh, M. Weinberg, Y. Flomenblit, Z. Nevo, A new intratracheal stent made from nitinol, an alloy with 'shape memory effect, J. Thorac. Cardiovasc. Surg. 107 (5) (1994) 1255–1261, https://doi.org/10.1016/S0022-5223(94)70046-X

[7] P. Motzki and S. Seelecke, Bistable actuator device having a shape memory element, WO 2017/194591 A1, 2016.

[8] P. Motzki, F. Khelfa, L. Zimmer, M. Schmidt, S. Seelecke, Design and validation of a reconfigurable robotic end-effector based on shape memory alloys, ASME Trans. Mechatron. 24 (1) (2019) 293–303, https://doi.org/10.1109/TMECH.2019.2891348

[9] D.J. Hartl, D.C. Lagoudas, Aerospace applications of shape memory alloys, Proc. Inst. Mech. Eng. Part G J. Aerosp. Eng. 221 (4) (2007) 535–552, https://doi.org/10.1243/09544100JAERO211

[10] M. Kohl, Shape Memory Microactuators, Springer Verlag, Berlin Heidelberg, 2004.

[11] C. Lexcellent, Shape-memory Alloys Handbook. 2013.

[12] F. Simone, G. Rizzello, S. Seelecke, P. Motzki, A soft five-fingered hand actuated by shape memory alloy wires: design, manufacturing, and evaluation, Front. Robot. AI 7 (608841) (2020) 608841, https://doi.org/10.3389/frobt.2020.608841

[13] P. Motzki, S. Seelecke, Industrial applications for shape memory alloys, Reference Module in Materials Science and Materials Engineering, Elsevier, 2019.

[14] G.S. Mammano, E. Dragoni, Design and characterization of a continuous rotary minimotor based on shape-memory wires and overrunning clutches1, J. Mech. Des. 139 (1) (2016) 15001–15009, https://doi.org/10.1115/1.4034401

[15] O. Benafan, J. Brown, F.T. Calkins, P. Kumar, A.P. Stebner, T.L. Turner, R. Vaidyanathan, J. Webster, M.L. Young, Shape memory alloy actuator design: CASMART collaborative best practices and case studies, Int. J. Mech. Mater. Des. 10 (1) (2014) 1–42, https://doi.org/10.1007/s10999-013-9227-9

[16] J. Luntz, B. Barnes, D. Brei, P.W. Alexander, A. Browne, N.L. Johnson, SMA Wire Actuator Modular Design Framework, Proc. SPIE - Int. Soc. Opt. Eng. (2009), https://doi.org/10.1117/12.816752

[17] S.D. Oehler, D.J. Hartl, R. Lopez, R.J. Malak, D.C. Lagoudas, Design optimization and uncertainty analysis of SMA morphing structures, Smart Mater. Struct. 21 (2012) 094016, https://doi.org/10.1088/0964-1726/21/9/094016

[18] Y. Fu, H. Du, W. Huang, S. Zhang, M. Hu, TiNi-based thin films in MEMS applications: a review, Sens. Actuators A Phys. 112 (2–3) (2004) 395–408, https://doi.org/10.1016/j.sna.2004.02.019

[19] Y. Furuya, H. Shimada, Shape memory actuators for robotic applications, Mater. Des. (1991), https://doi.org/10.1016/0261-3069(91)90088-L

[20] M. Schmidt, S.-M. Kirsch, S. Seelecke, A. Schütze, Elastocaloric cooling: from fundamental thermodynamics to solid state air conditioning, Sci. Technol. Built Environ. 22 (5) (2016) 475–488, https://doi.org/10.1080/23744731.2016.1186423

[21] M. Schmidt, A. Schütze, S. Seelecke, Scientific test setup for investigation of shape memory alloy based elastocaloric cooling processes, Int. J. Refrig. 54 (2015) 88–97, https://doi.org/10.1016/j.ijrefrig.2015.03.001

[22] S. Qian, Y. Geng, Y. Wang, J. Ling, Y. Hwang, R. Radermacher, I. Takeuchi, J. Cui, A review of elastocaloric cooling: materials, cycles and system integrations, Int. J. Refrig. 64 (2016) 1–19, https://doi.org/10.1016/j.ijrefrig.2015.12.001

[23] J. Frenzel, G. Eggeler, E. Quandt, S. Seelecke, M. Kohl, High-performance elastocaloric materials for the engineering of bulk- and micro-cooling devices, MRS Bull. 43 (4) (2018) 280–284, https://doi.org/10.1557/mrs.2018.67

[24] H. Janocha, Unkonventionelle Aktoren - Eine Einführung, Oldenburg Verlag, München, 2010.

[25] D. Stoeckel, Shape Memory Actuators for Automotive Applications, 1990.

[26] J.B. Gault et al., Locking Mechanism, US 10,331,175 B2, 2019.

[27] "Ingpuls GmbH - Produktportfolio, 2020.

[28] M. Köpfer, Industrialisierung der FGL-Technologie in hochvolumigen Serienprodukt, VDI-Expertenforum: Smart Materials – aus der Forschung in die industrielle Anwendung. Karlsruhe, 2017.

[29] Actuator Solutions GmbH and A. S. GmbH, Actuator Solutions SMA Products, 2018.

[30] Dynalloy Inc, Technical Characteristics of Flexinol Actuator Wires, Dynalloy Inc., 2016, ⟨http://www.dynalloy.com/pdfs/TCF1140.pdf⟩.

[31] SAES Getters, SmartFlex Brochure, 2017.

[32] J. Van Humbeeck, M. Chandrasekaran, L. Delaey, Shape memory alloys: materials in action, Endeavour 15 (4) (1991), https://doi.org/10.1016/0160-9327(91)90119-V

[33] N. Lewis, A. York, S. Seelecke, Experimental characterization of self-sensing SMA actuators under controlled convective cooling, Smart Mater. Struct. 22 (9) (2013) 094012, https://doi.org/10.1088/0964-1726/22/9/094012

[34] S.-M. Kirsch, F. Welsch, M. Schmidt, P. Motzki, and S. Seelecke, Bistable SMA Vacuum Suction Cup, 2018.

[35] R. Britz et al., SMA wire bundles - Mechanical and electrical concepts, in ACTUATOR 2018 - 16th International Conference and Exhibition on New Actuators and Drive Systems, Conference Proceedings, 2018, pp. 514–517.

[36] SAES Smart Materials ®. SAES Getters Group, 2008, [Online]. Available: ⟨https://www.saesgetters.com/brochure-saes-smart-materials⟩.

[37] M.E. Pausley, S.J. Furst, V. Talla, S. Seelecke, Electro-mechanical behavior of a shape memory alloy actuator, Proc. SPIE - Int. Soc. Opt. Eng. 23 (2009) 783–789, https://doi.org/10.1117/12.817010

Rouven Britz completed his master's degree in mechatronics at Saarland University in 2016. Since August 2016, he has been pursuing a PhD in Systems Engineering at Saarland University, Saarbrücken, Germany. His current research focuses on shape memory wires as actuator-sensor systems in industrial applications.

Dr. Paul Motzki is the head of the research division "sensors and actuators" at the Center for Mechatronics and Automation Technology (ZeMA gGmbH) in Saarbruecken, Germany. He received his B.Sc., M.Sc. and Ph.D. degrees in Mechatronics and Systems Engineering from Saarland University, Germany. His research interests cover the design and development of multifunctional actuator-sensor-systems based on smart materials like shape memory alloys, electroactive polymers, piezo materials or magnetorheological fluids.

3.2 High-Speed Antagonistic Shape Memory Actuator for High Ambient Temperatures

Rouven Britz[1], Gianluca Rizzello[1], Paul Motzki[1,2]

[1] Lehrstuhl für Intelligente Materialsysteme, Fachrichtung Systems Engineering, Fachrichtung Materialwissenschaft und Werkstofftechnik, Universität des Saarlandes, Saarbrücken

[2] AG Intelligente Materialsysteme, Zentrum für Mechatronik und Automatisierungstechnik, ZeMA gGmbH, Saarbrücken

Veröffentlicht in Advanced Engineering Materials.

DOI: 10.1002/adem.202200205

RESEARCH ARTICLE

ADVANCED ENGINEERING MATERIALS

www.aem-journal.com

High-Speed Antagonistic Shape Memory Actuator for High Ambient Temperatures

Rouven Britz, Gianluca Rizzello, and Paul Motzki*

This work presents the development of an innovative shape memory alloy (SMA) actuator principle, which allows high-speed switching cycles through the decoupling of antagonistically arranged SMA wires. Being optimized for the use at high ambient temperatures up to 65 °C, a possible application area is the active venting of injection molds where it can be used to expel air, which is trapped during the injection mold process. The patented actuator principle is based on a decoupled agonist–antagonist SMA-spring system and allows a high-speed closing movement by a compact and lightweight design. Another innovation compared to conventional antagonistic SMA actuator systems is the integrated fail-safe mechanism, which guarantees a defined closed state in case of power failure. Subsequently, in the motivation the need for active venting valves for injection molding is first described. Second, the novel actuator principle is introduced, and the development of an electronics concept is discussed. Finally, the design process, assembly, and validation of two iterations of the actuator prototype are presented. The final prototype validation measurements showcase high performance by valve strokes of 1 mm within 100 ms at ambient temperature of 65 °C.

1. Introduction

In industrial applications, conventional nonelectric actuators such as pneumatics will increasingly be replaced in the near future by more energy-efficient electrically actuated drive systems. State-of-the-art electrical solutions are usually built with different kinds of electric motors or electromagnets. As an electric alternative, shape memory alloys (SMAs) can play an important role in this ongoing electrification process. SMA wires are already widely used in various commercially available products, for example, in industry,[1–3] the automotive and aerospace sector,[4–7] the medical field[8–10] and consumer electronics,[11–13] and offer the possibility of constructing lightweight, compact, and energy-efficient actuator systems.[14–20] The underlying mechanism for the use of SMA wires as actuators is their ability to perform a reversible phase transformation at the crystal lattice level.[20,21] This phase transformation is macroscopically visible in a change of the length (contraction) of the SMA wire up to 4%.[22,23] Initially at room temperature, the crystal lattice is in a martensitic phase and can undergo a phase transformation to an austenitic crystal structure by applying energy in the form of heat. The technically simplest way to heat a wire is applying an electric voltage, which generates a current flow through the SMA wire. For the use of this effect in an actuator system, which can generate repeated output motion, the SMA wire needs to be restored to its initial length using a biasing system (e.g., a linear spring).[24–27]

Due to their high energy density in the range of $10^7\,\mathrm{J\,m^{-3}}$, SMA wires excel as actuators in compact systems.[28] This advantage opens up application areas, which are hardly feasible or even not possible with conventional actuators.[29] The field of valves certainly contains a lot of possible applications that would profit from a more compact and lightweight design but the limited switching frequency and temperature range of SMA technology are still major obstacles on the way to widely spread commercial products. In some of these areas, the environmental conditions, especially high ambient temperatures, are challenging for SMA technology, because of the thermomechanical dependency. An exemplary application area for the latter is injection molding, which motivates this illustration of the capabilities of SMA wires in combination with a suitable mechanical design. In injection molding machines, various valves with different functions are represented. To take full advantage of the compact design possibilities, a venting valve for injection molds was selected for this cases study. Venting of an injection mold is needed to prevent air from being trapped in the cavity, which will lead to a casting failure. Therefore, the vent needs to be closed in a well-defined time slot to prevent the valve tappet from being back injected and simultaneously allow the air sufficient time to leave the cavity. Back-injection means that liquid plastic gets behind the valve

R. Britz, G. Rizzello, P. Motzki
Department of Systems Engineering
Department of Materials Science and Engineering
Saarland University
Saarbrücken 66123, Germany
E-mail: rouven.britz@imsl.uni-saarland.de

P. Motzki
Center for Mechatronics and Automation Technology (ZeMA gGmbH)
Saarbrücken 66121, Germany

The ORCID identification number(s) for the author(s) of this article can be found under https://doi.org/10.1002/adem.202200205.

DOI: 10.1002/adem.202200205

tappet and blocks this in movement and makes the ejection of the injection molded part impossible.

In this article, a patented novel actuator principle based on SMA wires is presented. Unlike current SMA systems, this originative actuator approach enables high-speed back and forth switching in an antagonistic configuration of SMA actuators. Additionally, this innovative SMA actuator system can be tuned to perform at high ambient temperatures, which is the most common restriction of state-of-the-art SMA-based drives. To illustrate the principle and capabilities of the actuator system, an example application in the field of injection molding is chosen. As an active venting valve in injection molds, the actuator faces the challenges of compact design, high ambient temperatures, and high-speed activation. The developed antagonistic actuator system is based on two actuators, each consisting of an SMA wire, which works against a mechanical bias spring. These two SMA-wire-spring configurations work against each other in only one direction. Specifically, one of these configurations is able to open and close the valve, the opening due to the activation of the SMA wire, the closing is due to the cooling of the SMA wire and the force of the biased spring. Because of the slow cooling behavior of SMA wires, preventing a back injection cannot be ensured. The timing and accurate triggering of opening and closing the valve is necessary for the chosen application. Therefore, the second SMA-wire-spring system can be activated independently from the first and ensures a high-speed closing at the right moment. This is possible due to the decoupling of the two antagonistic working SMA-wire-spring systems in the closing direction.

The subsequent chapters first illustrate the motivation of using SMA wires as actuators in a venting valve in injection molding. Afterward, the actuator concept is explained at the example of a venting valve. Furthermore, the developed control electronics is presented, including the validation of the electronics. The remaining chapters of the article describe the design process, assembly, and validation of two developed prototypes. Starting with the prototype for the proof-of-concept of the mechanism and ending with the second prototype optimized for high-ambient temperatures. Finally, the results of a trial injection mold process with the developed prototype are presented and a conclusion and outlook are given.

2. Motivation

When looking for alternative actuator technologies with the intention of replacing state-of-the-art drives in applications, SMA technology is oftentimes overlooked because they are known for their limited actuation frequency and feasible temperature range. While this holds true for the shape memory material itself, these drawbacks can be attacked and overcome by smart system design and control strategies.[18,19] The need for fast switching frequencies as well as functionality in higher ambient temperatures in a wide range of possible applications for SMA-based drives has led to the invention of this novel SMA system design approach. The field of injection molding was chosen to exemplary showcase the ability to overcome the commonly mentioned drawbacks of SMA technology while still maintaining the advantage of their unreached energy-density and ultra-compact system design and integration.

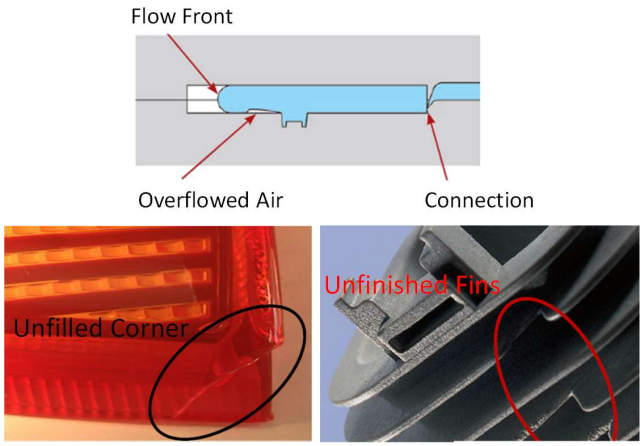

Figure 1. Effects of trapped air in injection molds. Reproduced with permission.[31] Copyright 2020, ASME.

Injection molding is a widely used technology for mass production of plastic parts. During the injection mold process, when the liquid plastic flows in the cavity, trapped air can prevent a complete filling.[30] **Figure 1** shows various examples of unfinished injection molded parts because of trapped air. Typically, an injection mold is separated in multiple parts but at least two halves. The state-of-the-art solution to release trapped air in cavities is a passive venting based on small gaps, which are ground between the halves. **Figure 2** explains the passive venting standard solution. Typically, the gaps are designed to generate either no edge or if not possible otherwise, a defined, small edge. Therefore, this method requires high planning effort and precision in production. Furthermore, the separation of the injection mold into at least two halves is essential to place the previously described gaps to release the air.

Additionally, to passive venting, active venting of injection molds represents an alternative approach, where an actuator is used as a valve, which opens a ventilation duct and is closed when the air in the cavity is ejected. **Figure 3**a shows an uncomplete

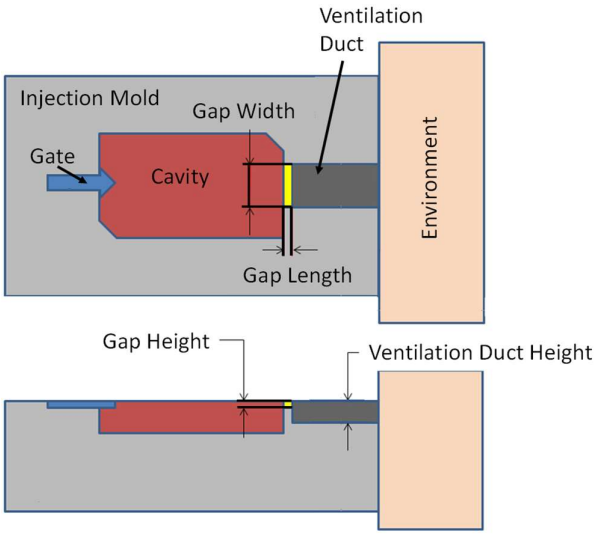

Figure 2. Standard passive venting solution.[31]

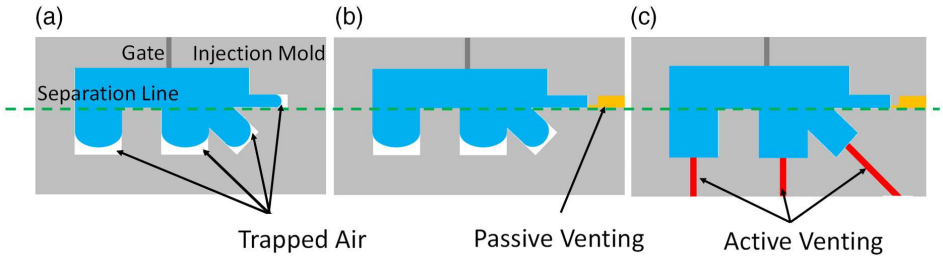

Figure 3. Advantage of an active venting valve.[31]

filled cavity due to trapped air when not using a venting system. The liquid plastic flows through the gate into the injection mold. While the plastic is shown in blue, the separation line in green indicates the two mold halves which are needed to be able to remove the injection molded part. In Figure 3b, a passive venting gap is positioned at the separation line of the two mold halves. On this position, the air can be expelled and makes a complete fill of the cavity possible if the liquid plastic flows in. Because of the missing separation lines at the other three locations, passive venting gaps cannot be easily implemented. In these cases, a separation of the mold to grind the gaps with a following reassembling would be required. Figure 3c, in contrast, shows the result using active venting valves and illustrates that there is no air left in the mold. By implementing an active venting valve, the advantage is that only drilled holes are needed for the positioning of the valves. This is easily possible at all positions and angles and reduces the effort for the overall venting of the molding process.

The motivation to use an SMA actuator instead of conventional actuators (commonly used electromagnetic systems) is the significantly reduced radial construction space they need (**Figure 4**). SMA wires can be highly integrated and allow for a compact active venting valve design. This fact leads to an advantage in case of complex injection mold geometries, for example, Figure 1, bottom right. This level of needed vents might be hard, or even impossible, to obtain with conventional, typically electromagnet-driven valves.

3. SMA Actuator Concept

The realized SMA actuator is based on two antagonistically working SMA-wire-spring configurations. As a result of this setup, one SMA-wire-spring-system is depending on the movement of the second system to open the actuator. For an active closing of the actuator, the second SMA-wire-spring-system can operate independently. This special kind of mechanical coupling allows for a fast closing without the need of waiting for the first activated SMA wire to cool down. The mechanical setup also allows for a slow passive closing after deactivating the first SMA wire, which is responsible for opening the valve. In this case, the system response time depends on the cooling rate of the first SMA wire. The advantage is given by a normally closed system, which is necessary to meet the security standards while working with injection molds. This SMA actuator concept is, therefore, different from a standard antagonistic SMA system, in which two wires are working directly against each other.[32–36]

An example of an injection molding process with a built-in valve is shown in **Figure 5**, explaining the patented operating principle in a more detailed way.[37] On the left-hand side, a simplified injection mold cavity with a drilled valve seat is shown. In dark blue and yellow the movable inner parts of the actuator system are shown. They are relatively movable to each other. The grey parts are representing the housing and show the fixed bearings of the springs and SMA wires, which additionally allow

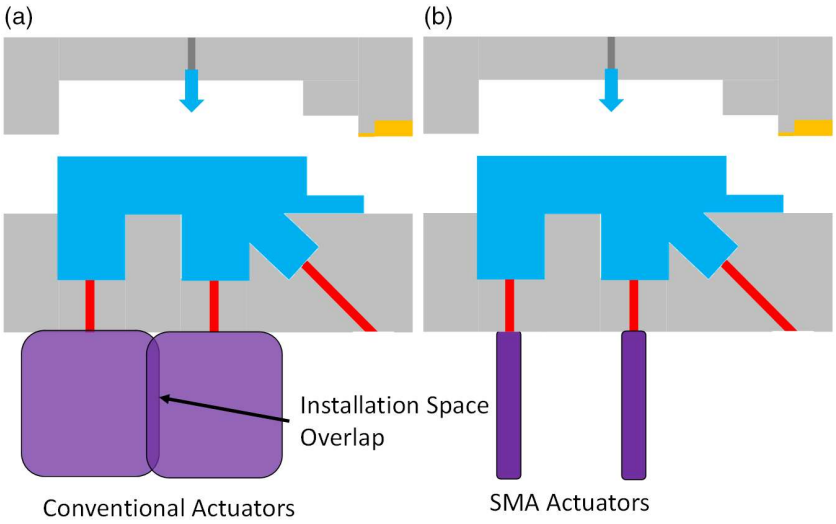

Figure 4. Installation space comparison of conventional and shape memory alloy (SMA) actuators.[31]

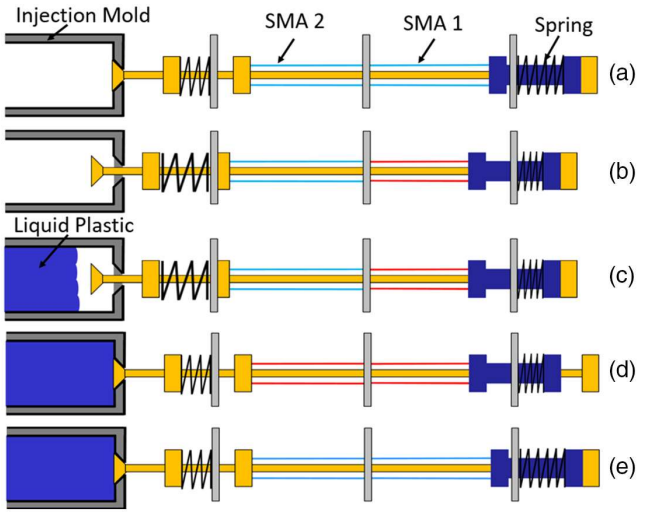

Figure 5. Sketch of the functionality of the actuator using the example of an injection molding process. Reproduced with permission.[32] Copyright 2020, The Authors, published by Front. Robot. AI.

a guiding of the inner parts. The SMA wires are shown in light blue representing the cold state and red representing the hot state with the compression springs shown in black. Figure 5a shows the initial position of the valve before the injection mold process starts. All SMA wires are in the cold state. The normally closed position as initial position is achieved due to the fact, that the force of the SMA1-spring-system is higher than the force of the SMA2-spring-system. Thus, the spring of the SMA1-spring-system always pushes the valve into the closed position. In Figure 5b, the injection mold process has started, the valve opens by activating SMA 1. Through the activation of SMA 1 and the resulting compression of the spring, the spring of the second SMA-spring-system can relax. If the liquid plastic flows in and displaces the air, the air can escape from the cavity through the open valve. If the plastic reaches the valve (Figure 5c), SMA 2 will be activated and closes the valve immediately (Figure 5d). At the same time, SMA 1 can be deactivated. A closed valve allows the plastic to fill out the cavity completely without a back injection. This is possible through the decoupling of the two SMA systems in the mechanical design, which facilitates the fast-closing movement independently of the cooling behavior of the opening actuator. The timing to close the valve by activating SMA 2 can be determined by additional sensors or can be time controlled, based on the start of the injection mold process using a flow simulation. As soon as the cavity has been filled completely with plastic, SMA 2 can be deactivated as well, and the valve restores its initial position (Figure 5e). The process can start again after the ejection of the injection molded part.

4. Electronic Concept

The developed electronics allows for an accurate control of the actuator and the communication between the actuator and an injection mold machine. After a trigger signal is detected, the electronics activates the two SMA wires inside the actuator in a specific order to open and close the valve. For the activation, two voltage controlled current sources are used. The current amplitude and activation time of each SMA wire are microcontroller controlled and programmable via universal serial bus (USB). **Figure 6** shows the complete circuit board.

Additionally, for future research, the electronic contains two differential amplifiers for measuring the voltage of the SMA wires, thus allowing to exploit the self-sensing effect of SMA wires for condition monitoring or control purposes.[38–41]

After completing the circuit board, a validation is performed. The whole period of activation is time dependent, started by a trigger signal. First, SMA 1 is activated for a specific time, which is programmable via USB. After SMA 1 turns off, SMA 2 turns on for a specific time, which is also programmable via USB. The activation times and current amplitudes of SMA 1 and SMA 2 are independently programmable. An example of resulting activation periods of the two SMA wires is shown in **Figure 7**. The black and blue curves indicate the current signal for the two different SMA wires. In the shown period of activation, SMA 1 (valve opening) is activated with a current amplitude of 300 mA for 1 s, while SMA 2 (valve closing) is activated with 400 for 100 ms. This means that the valve is open for 1 s and closes in 100 ms, for which the higher current amplitude of SMA 2 is necessary.

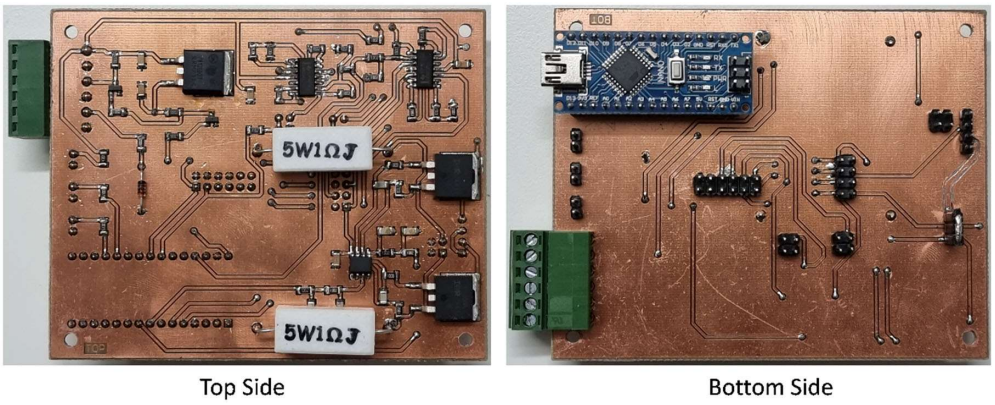

Figure 6. Complete circuit board for activation of the two SMA wires inside the actuator.

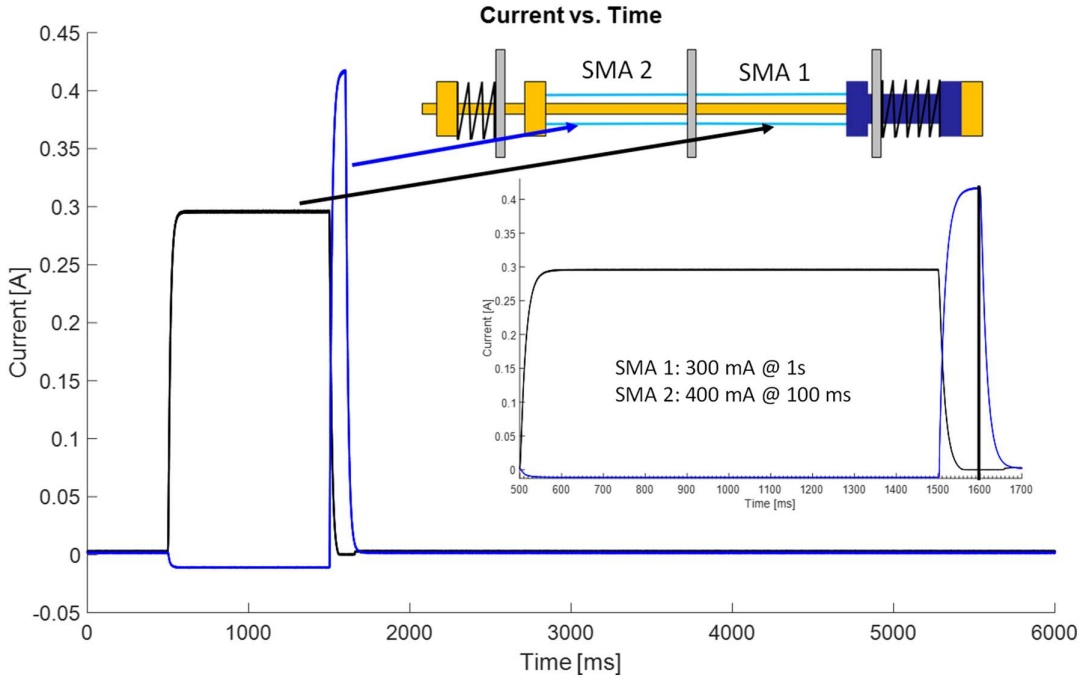

Figure 7. Circuit board validation, example of SMA driving signal.[31]

5. Proof-of-Concept Mechanism: Design, Assembly and Validation of Prototype I

As a first step, a proof-of-concept prototype is designed and assembled to validate the presented decoupled actuator mechanism in combination with the developed electronics. In addition, the significantly decreased installation space using SMA wires as actuator elements is demonstrated. In this regard, a total maximum outer diameter of 10 mm and a total maximum length of 150 mm are the selected design specifications. For the actuator, a total stroke of $\Delta l = 1$ mmis considered, this allows for a fast venting of the cavity through a proper opening of an air exhaust duct. A means of choice to increase the lifetime of SMA wires is reducing their actuation strain, therefore the actuator design limits the maximum strain to $\varepsilon = 2\%$. With this design parameter, the austenitic (contracted) length $l_0$of the SMA wires can be calculated as follows.

$$l_0 = \frac{\Delta l}{\varepsilon} \tag{1}$$

As a result, an austenitic length $l_0 = 50\,\text{mm}$ is calculated. Arranging the SMA wires in a U-shape simplifies the electrical connection as well as enables generating higher forces than using only one wire. Furthermore, the SMA wires have a radial 90° offset and are nested within each other to keep the needed construction space as compact as possible. **Figure 8** shows the wire arrangement inside the prototype.

The design considers using commercially available springs as biasing elements with a stiffness of $k = 0.9\,\text{N mm}^{-1}$ and an outer diameter of $De = 2.9\,\text{mm}$. The SMA wire diameter must be adjusted according to the spring. For the calculation, the

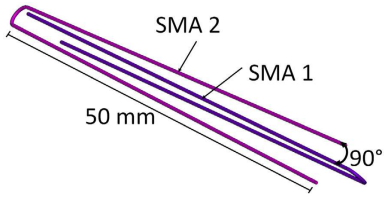

Figure 8. Wire arrangement inside the proof-of-concept prototype.[31]

maximum force of SMA1-spring-system is essential and set to $F_{\text{max1}} = 2.7$ N. The U-shape of the SMA wire results in doubling the provided SMA force. Also, to increase the lifetime it is beneficial to reduce the mechanical stress of the wires in actuation. Therefore, a maximum stress $\sigma_{\text{max1}} = 300\,\text{MPa}$ is chosen. These conditions allow to calculate a wire diameter d as follows.

$$d = \sqrt{\frac{2F}{\pi\sigma}} \tag{2}$$

As a result, an SMA wire diameter of $d = 76\,\mu\text{m}$ is chosen.

To facilitate the assembly, the valve design is divided in two halves. In one halve, the complete internal structure can be installed and adjusted, the second halve functions as a top cover. **Figure 9** shows one half-shell with the internal structure and SMA wires. The half-shell (grey) has an outer diameter of 6 mm and an inner diameter of 3.1 mm. The thickest parts of the internal structure have a diameter of 3 mm. To attach the valve mechanism to the actuator, an M2 thread is attached to the tip of the actuator (orange).

The complete actuator design provides for the two half-shells to be pushed into a housing (**Figure 10**). This keeps the half-

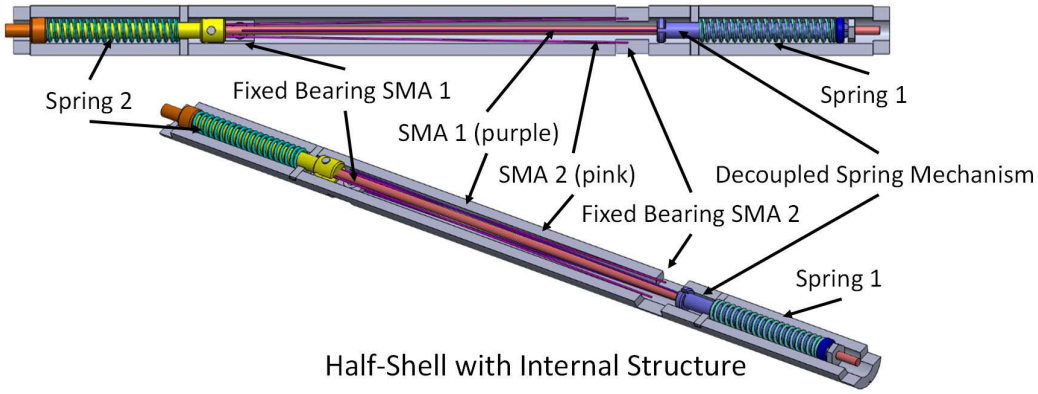

Figure 9. Computer-aided design (CAD) design of the half shell with internal structure.[31]

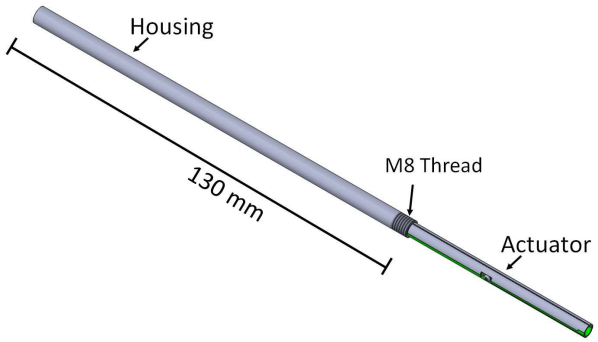

Figure 10. Two half-shells (actuator) pushed together in the housing.[31]

shells together on the one hand and protecting the inner structure from external influences on the other hand. The housing is 130 mm in total length and has a diameter of 8 mm. The previously mentioned requirements for the dimensions of the actuator are thereby fulfilled. For the electrical connection of the actuator, there is a connector inside the housing. To screw on a plug, the prototype has an M8 thread on the outside of the housing.

After designing the mechanics, the parts are manufactured. The half-shells are manufactured using wire eroding and are made of stainless steel. The inner parts are produced via a lathe and a milling machine and are made of brass. The fixed bearings for the wires and the springs, which are sliding surfaces at the same time, are produced by injection molding, using a high temperature-resistant plastic. To avoid short circuits from the wires to the other metal parts, the wires are covered in Teflon tubes. For the electrical connection of the SMA wires inside the prototype, enameled copper wires are used. During the assembly, first, the inner parts are positioned in one half-shell. Then the SMA wires are attached to the inner parts and the corresponding fixed bearings. **Figure 11** shows the assembly with the inner parts and the SMA wires before the two half-shells are put together.

As a last step during the assembly of the prototype, the half-shells are inserted into the housing (**Figure 12**, upper part) and the electrical connection is attached. The finished prototype is shown in Figure 12, lower part.

To proof the concept of the decoupled mechanism inside the prototype, an experimental test rig is built, measuring the stroke of the actuator, the current trough the SMA wires and the voltage drop over the SMA wires. To simulate the usage in high ambient temperatures as needed in injection molding processes, the test rig allows validating the prototype in a climate chamber. The data is being acquired using an NI cRIO 9074 and LabVIEW. The cRIO is connected to a displacement sensor RC171 from PHILTEC to measure the stroke of the actuator. For the voltage and current measurement, the cRIO is connected to the developed circuit board with integrated measurement points to measure voltage and current of the SMA wires. Additionally, a trigger signal for the developed electronics to activate the actuator is generated from the cRIO. **Figure 13** shows the test rig in a block diagram including the actuator inside the climatic chamber.

To validate the actuator performance in combination with the developed electronics, a first experiment is performed. In theory, the actuator should be in the initial position, which is the rearmost position of possible movement. Due to the activation of the

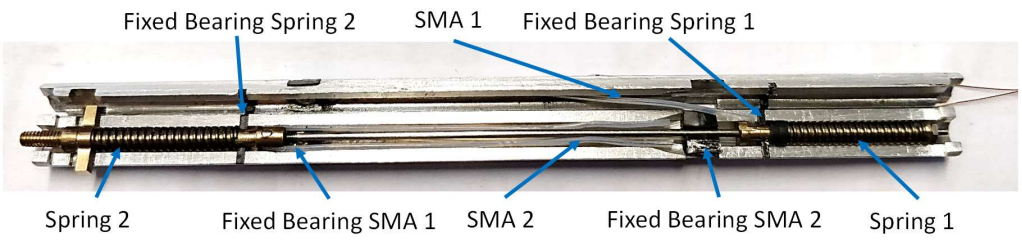

Figure 11. Half-shells with integrated inner parts and SMA wires.[31]

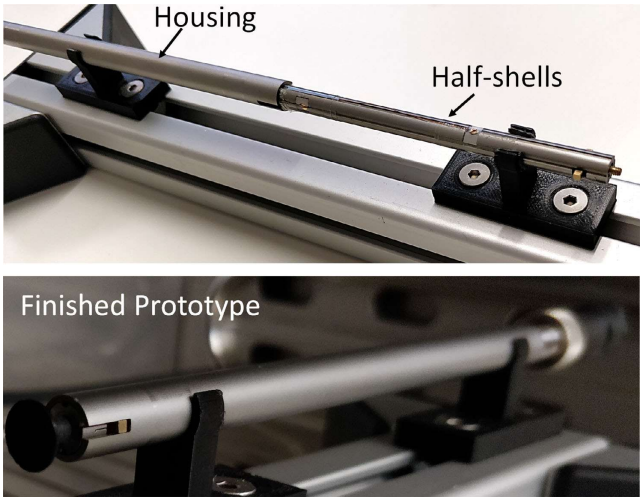

Figure 12. Half-shells inserting into housing (upper part), finished prototype with attached electrical plug (lower part).[31]

SMA wires, the actuator should do a movement of 1 mm in both directions. In the experiment, SMA 1 is activated for 1 s, which leads to the opening of the valve. After this one second, SMA 1 will be deactivated and SMA 2 will be activated at the same time for 100 ms, leading to the closing of the valve. The results of the experiment are shown in **Figure 14**. The current signals generated from the developed electronics are shown in the upper part of Figure 14. The black signal represents the current through SMA 1. A current amplitude of 300 mA and a duration of 1 s is predefined by programming the electronics and confirmed by the measurement. The blue signal represents the current through SMA 2, the amplitude and duration are also predefined with a value of 400 mA and 100 ms. The mechanical output, as reaction of the activation of the two SMA wires, is shown in the lower part of Figure 14. The current starts flowing through the corresponding wire at 500 and 1500 ms. It can be observed that the stroke response is delayed compared to the current, because of the heating process of the SMA wires. The closing movement is done in 100 ms, starting at 1500 ms. The measurement shows that the actuator does not reach the required stroke of 1 mm and that the actuator is not at the rearmost position in the initial position. This is indicated by the larger closing movement compared to the opening movement. As a comparison, consider the stroke at 600 and 1500 ms.

A further experiment highlights the decoupled active closing behavior of the actuator in comparison to a passive closing. Active closing describes the closing movement due to the activation of SMA 2, passive closing means the closing movement due deactivation of SMA 1 and the resulting decompression of spring 1. **Figure 15** displays the results, showing the active closing in black, where a fast decrease of stroke at 1500 ms can be observed. In contrast, the blue curve represents the passive closing, which remains at maximum stroke for a longer period of time and shows a slow decrease of stroke. In both cases, SMA 1 is activated with a 300 mA pulse for 1 s. In addition, the experiment shows that the spring of the closing system is too weak to do a complete passive closing movement.

To validate the actuator performance at a high ambient temperature, the actuator is activated at 65 °C ambient temperature in a climate chamber. **Figure 16** compares the results of the high-temperature and the low-temperature measurements. At each temperature, the actuator is activated 3 times. It can be seen that the performance at 65 °C is much worse than at 25 °C. The initial starting point is shifted 50 µm toward opening of the valve and the opening movement is only 50 µm. The closing movement is about 250 µm and does not reach the end position. At 1800 ms, a slow cooling behavior of SMA 2 can be seen and the actuator is back in its initial position after ≈3 s of cooling time.

The reason for this poor performance is the transformation temperature of the SMA wires. In high ambient temperature, both wires are partially transformed to austenite, which in summary leads to the different initial point and the weaker performance in movement. To improve the high ambient temperature performance, the transformation temperature can be increased by the pre-stress of the SMA wires. For this reason, a second prototype is built. The next chapter explains the development of a high ambient temperature optimized prototype, which finally will show the same performance at 65 and at 25 °C.

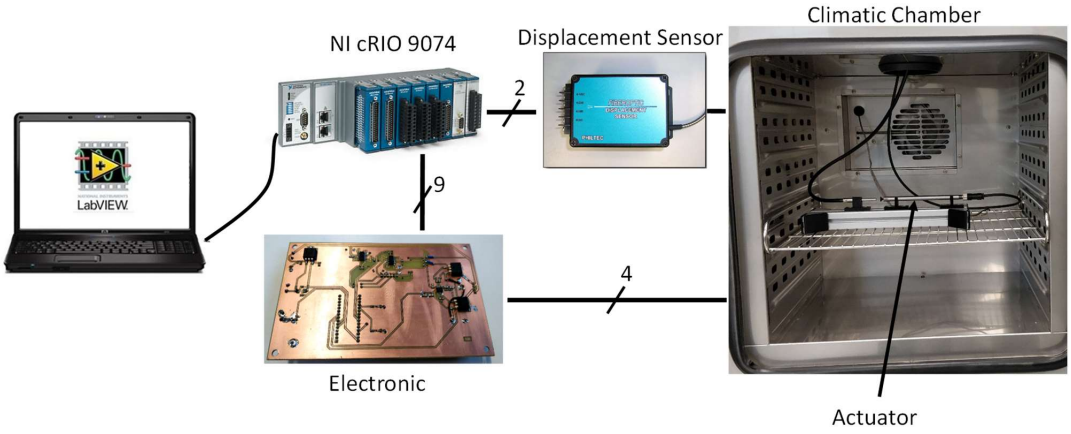

Figure 13. Measurement setup for the validation of the actuator in high ambient temperature environments.[31]

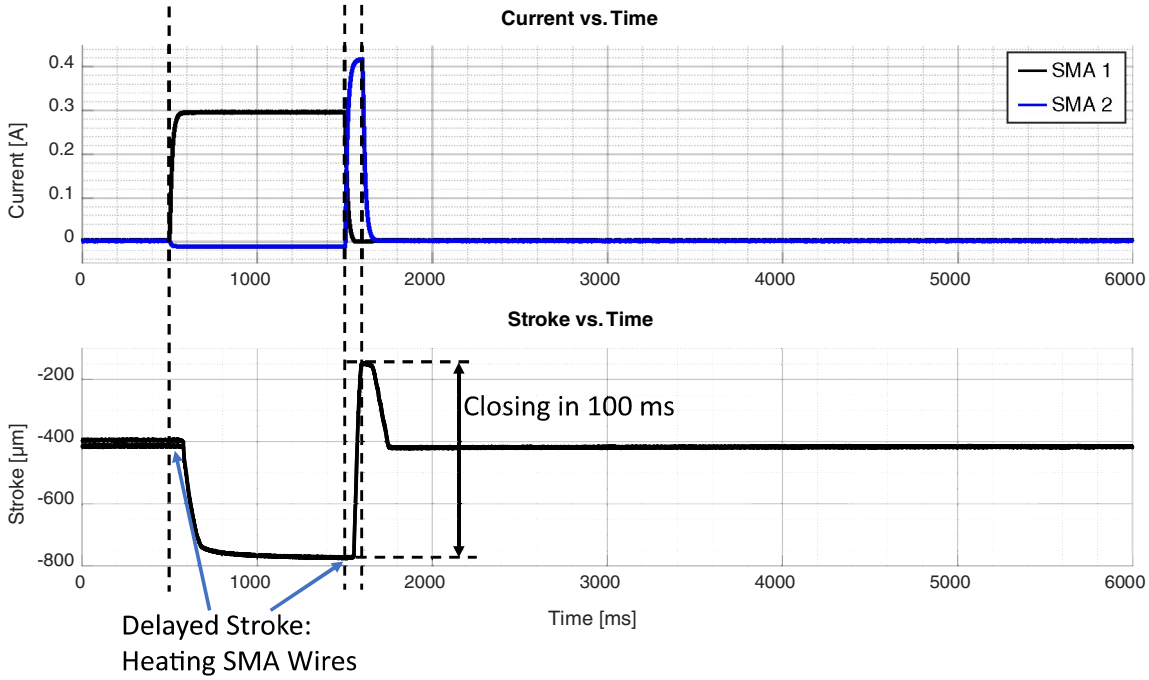

Figure 14. Experiment result of activation SMA 1 for 1 s and SMA 2 for 100 ms.[31]

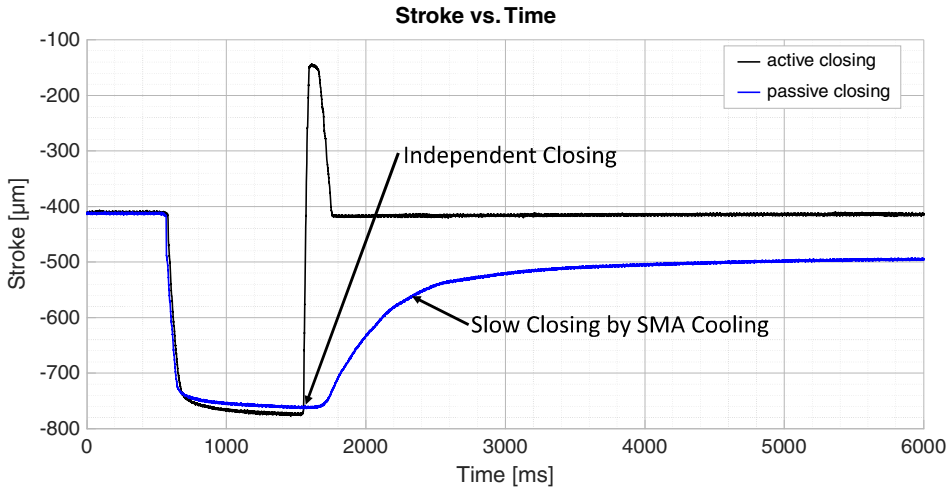

Figure 15. Experimental result of an active closing versus a passive closing movement.[31]

6. Prototype II: High Ambient Temperature Optimization

The first prototype was able to demonstrate the general functionality of the developed SMA mechanism. In this chapter, the optimization for the use of the actuator in increased ambient temperatures is shown.

The first step in the new design process is the adaption of the two SMA-wire-spring-systems. For this, a simulation tool based on a polycrystalline SMA model[41] was developed, allowing for predicting the behavior of an SMA-wire-spring-system in high ambient temperatures. **Figure 17** shows the resulting plot of the simulation tool for the SMA-wire-spring-system, which opens the valve. The hysteresis curve of the SMA wire at ambient temperature is shown in blue, in this case 65 °C. Red indicates the SMA hysteresis after heating and the yellow straight shows the characteristic curve of the mechanical bias spring. The result shows the behavior of two wires, mechanically parallel with a diameter of 150 µm and a spring with a stiffness of 6.68 N mm^{-1} at 65 °C ambient temperature. Two equilibrium points are marking the initial position of the system (blue curve) and the position when the SMA wires are heated (red curve).

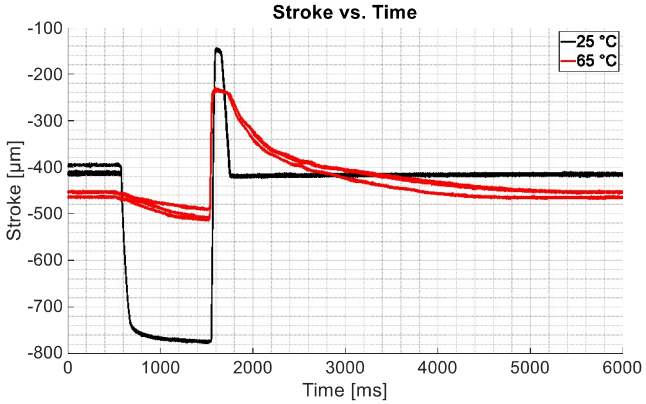

Figure 16. Actuator performance at 25 and 65 °C ambient temperature.[31]

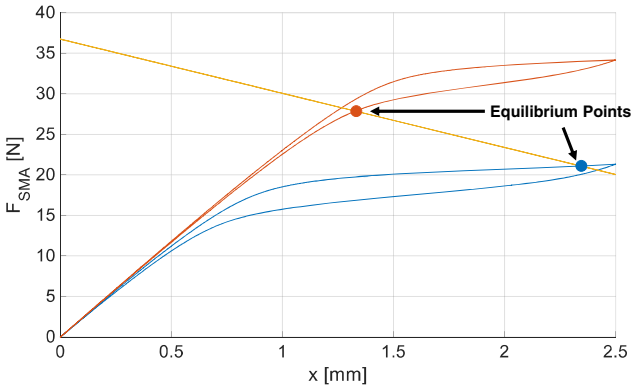

Figure 17. Simulation result for a SMA-spring-system at 65 °C ambient temperature.

The difference of position of both equilibrium points defines the stroke of the actuator system and amounts to 1 mm. The resulting stress for each SMA wire is 597 MPa in the initial state and 788 MPa when heated. To guarantee that the opening SMA-wire-spring-system can do a passive closing, the system is designed to generate approximately double the force in comparison to the closing SMA-wire-spring-system. In the closing SMA-wire-spring-system, SMA wires with a diameter of 100 µm are used. The maximum force of the closing mechanism is 10.3 N, which is equivalent to a stress of 651 MPa per wire.

The final temperature optimized prototype including the electronic box is shown in **Figure 18**. The housing of the prototype is adapted for the usage in an injection molding tool. Before this, a validation of the actuator is done and shown in **Figure 19**. The upper part of Figure 19 shows the current signals generated from the developed electronics. The current signals of the two wires at an ambient temperature of 25 °C are shown in black, pink describes the current signals of both SMA wires at an ambient temperature of 65 °C. Because of the higher ambient temperature, there is less energy needed to heat the wire to its transformation temperature. Therefore, a lower current is required at higher ambient temperatures, which is consequently shown in the two current signals. The lower part of Figure 19 shows the resulting stroke due to the activation of the wires at different ambient temperatures. Blue indicates the stroke at 25 °C ambient

Figure 18. Final temperature optimized prototype with electronic box.

temperature and red shows the stroke at 65 °C. The measurement shows a nearly complete identical behavior at both temperatures. The initial position of the actuator is in the fully closed position and the required maximum stroke of 1 mm can be considered as sufficiently achieved with a generated stroke of more than 950 µm (Figure 19 at 1500 ms). The fast-closing movement reaches the initial position in 100 ms. After the fast closing, the actuator bounces back in a middle position at 2000 ms. The reason for this is that both SMA wires are deactivated at this time. The resulting middle position is a product of the cooling behavior of the used SMA wires and both springs. One possibility to avoid this bouncing behavior is to keep the SMA 2 activated until SMA 1, which is responsible for opening the valve, has cooled down. After SMA 1 has cooled down, the spring 1 keeps the actuator in the initial position and SMA 2 can cool down as well. However, the systematically conditioned side-effect of the middle position shows that passive closing is ensured by spring 1. Also, it is shown that the passive closing takes more time at higher ambient temperatures because of the slower cooling behavior of the SMA wires. The measurement shows some ripples in the movement, which indicates friction in the prototype.

After the validation with the conclusion that the final prototype functions are given as desired, the prototype is subjected to a field test and is built into an injection molding tool. **Figure 20** shows the prototype in the injection molding tool. In advance, flow simulation is used to determine the point at which air entrapment would occur in the cavity, and the prototype is positioned at this position. The shown injection molding tool including the prototype is used to perform trial injection molds. A trial injection mold with an inactive prototype is performed to validate the flow simulation and to make sure that the prototype is located in the right position in the cavity. On the left in **Figure 21**, the result of the trial injection mold with inactive prototype is shown. Predicted correctly, a casting failure due to the trapped air is the result. In a next step, a trial injection mold with the active prototype is conducted. The result is shown on the right-hand side of Figure 21. Since the air can escape, the trial results in a successful cast without any trapped air.

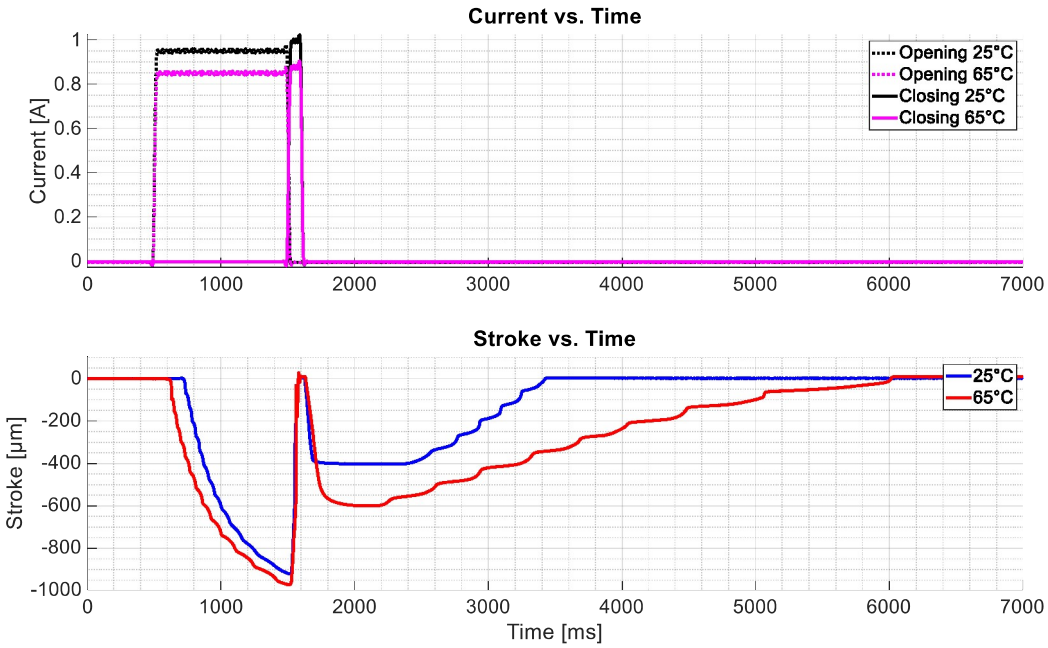

Figure 19. Validation result of the final prototype at different ambient temperatures.

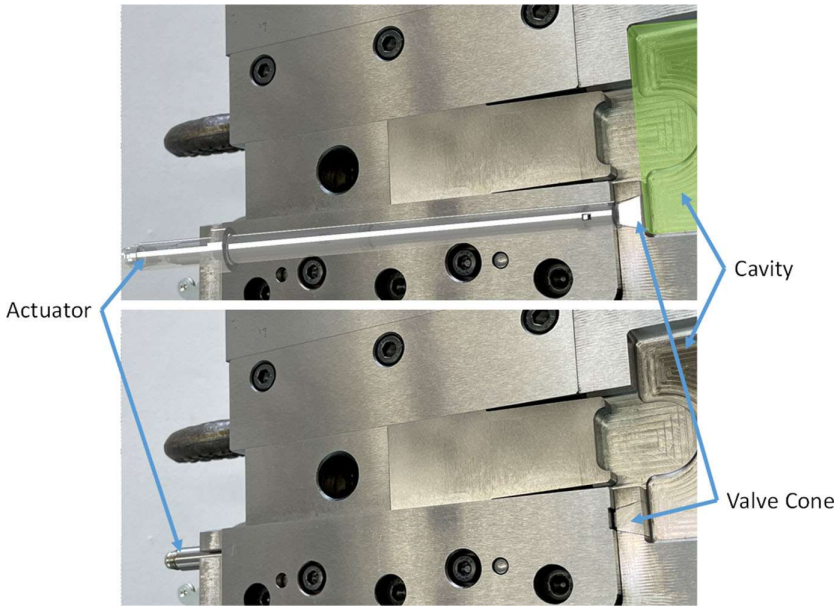

Figure 20. Final prototype built in an injection molding tool.

7. Conclusion and Outlook

This article has presented the development and the validation results of a novel decoupled antagonistic SMA actuator. The actuator is optimized for the usage in high ambient temperature, which is validated via test rig and experimentally confirmed by the trial inserts as an active injection mold venting valve. The motivation for the necessity of venting injection molds has been described. Then, the operating principle of the decoupled antagonistic SMA actuator is presented. To guarantee the correct activation of the SMA wires, an electronics concept is developed. This ensures the opening and fast closing of the valve at defined times in an injection mold process. The circuit board consists of two programmable current sources, which allow to predefine the current amplitude and activation time of each SMA wire. The first developed prototype serves as the proof-of-concept for the novel actuator concept. The design and assembly process for the first prototype is described as well as the assembled test rig. Experiments at different ambient temperatures show that the actuator concept works correctly, with the

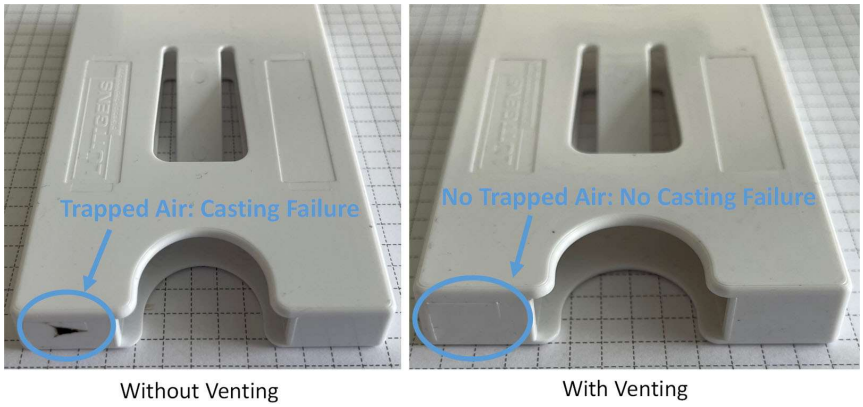

Figure 21. Results of the injection molding process—without activation of the prototype (left), with activation of the prototype (right).

restriction of a decrease in performance at elevated ambient temperatures. For this reason, a second prototype is built with an optimized design. For the design, a simulation tool that allows the prediction of the SMA-system behavior at high ambient temperatures is used. The validation results of the final prototype are shown with the conclusion that the actuator works independently of the ambient temperature. In a final experiment, a test injection mold including the developed actuator as a venting valve is conducted. This field test confirms the test rig experiments and shows the potential of active venting valves avoiding miscasts due to trapped air.

In future steps, the long-life ability of the actuator will be under investigation. These life-cycle tests are carried out in a test rig as well as in an injection molding process. Also, an improvement of the gliding surfaces inside the final prototype will be necessary to avoid the shown ripples in the movement which suggest friction in the bearings.

Acknowledgements

Funded by the Federal Ministry of Education and Research (BMBF) as part of the "KMU-NetC" Program. In addition, the authors would like to thank our project partners Dietrich Lüttgens GmbH & Co.KG and Kunststoff-Institut für die mittelständische Wirtschaft NRW GmbH (K.I.M.W.) for the consistently good cooperation, the production of components, the experiments carried out and the provision of images.

Open Access funding enabled and organized by Projekt DEAL.

Conflict of Interest

The authors declare no conflict of interest.

Data Availability Statement

The data that support the findings of this study are available from the corresponding author upon reasonable request.

Keywords

antagonistic actuator system, high temperature, injection molding, miniaturized actuator system, shape memory alloys, valve

Received: February 10, 2022
Published online:

[1] M. Sreekumar, T. Nagarajan, M. Singaperumal, M. Zoppi, R. Molfino, *Ind. Rob.* **2007**, *34* 285.
[2] P. Motzki, S. Seelecke, *Reference Module in Materials Science and Materials Engineering*, Elsevier Amsterdam, **2019**.
[3] W. Wang, S.-H. Ahn, *Soft Robot.* **2017**, *4* 379.
[4] D. Stoeckel, *Shape Memory Actuators for Automotive Applications*, Materials & Design, **1990**, *11*, No. 6.
[5] Actuator Solutions GmbH and A. S. GmbH, *Actuator Solutions SMA Products*, the company Actuator solutions GmbH, Gunzenhausen, **2018.**
[6] R. Pecora, I. Dimino, *Shape Memory Alloy Engineering: For Aerospace, Structural and Biomedical Applications*, Butterworth-Heinemann, Oxford, **2014**.
[7] D. J. Hartl, D. C. Lagoudas, *Proc. Inst. Mech. Eng., Part G* **2007**, *221*, 535.
[8] C. S. Loh, H. Yokoi, T. Arai, in *2005 IEEE Engineering in Medicine and Biology 27th Annual Conf.*, **2005**, pp. 6900–6903, https://doi.org/10.1109/IEMBS.2005.1616092.
[9] M. Leester-Schädel, B. Hoxhold, C. Lesche, S. Demming, S. Büttgenbach, *Microsyst. Technol.* **2008**, *14*, 697.
[10] A. T. Tung, B. H. Park, G. Niemeyer, D. H. Liang, *IEEE/ASME Trans. Mechatron.* **2007**, *12*, 439.
[11] J. B. Gault, S. D. Bowers, J. S. Campbell, A. E. Hillyerd, Y. Aldehayyat, K. Aagaard, E. P. Witt, *Locking Mechanism*, **2019**.
[12] Cambridge Mechatronics Ltd., CML OIS actuator, [Online], https://www.cambridgemechatronics.com/en/cml-technology/actuators/ (accessed: April 2020.)
[13] D. Clausi, H. Gradin, S. Braun, J. Peirs, D. Reynaerts, G. Stemme, W. van der Wijngaart, in *2011 IEEE 24th Inter. Conf. on Micro Electro Mechanical Systems*, January **2011**, pp. 1281–1284, https://doi.org/10.1109/MEMSYS.2011.5734667.
[14] R. Velázquez, E. Pissaloux, J. Szewczyk, M. Hafez, in *Proc. - IEEE Inter. Conf. on Robotics and Automation*, Vol. *2005*, **2005**, pp. 1344–1349, https://doi.org/10.1109/ROBOT.2005.1570302.
[15] D. Reynaerts, H. Van Brussel, *Mechatronics* **1998**, *8*, 635.
[16] C. C. Lan, J. H. Wang, C. H. Fan, *Sens. Actuators, A* **2009**, *153*, 258.
[17] J. Mohd Jani, M. Leary, A. Subic, M. A. Gibson, *Mater. Des.* **2014**, *56*, 1078.
[18] P. Motzki, *Efficient SMA Actuation — Design and Control Concepts*, VDI-Expertenforum: Smart Materials, Renningen, **2020**, https://doi.org/10.3390/IeCAT2020-08520.

[19] P. Motzki, T. Gorges, M. Kappel, M. Schmidt, G. Rizzello, S. Seelecke, *Smart Mater. Struct.* **2018**, *27*, 075047.
[20] D. C. Lagoudas, *Shape Memory Alloys: Modeling and Engineering Applications*, Springer, New York **2008**.
[21] H. Funakubo, *Shape Memory Alloys*, vol. *1*, no. D., Gordon and Breach Science Publ., Amsterdam, **1987**.
[22] Dynalloy, *Technical Characteristics of Actuator Wires*, Dynalloy Inc, pp. 1–12.
[23] S. A. E. S. Getters, *SmartFlex Brochure*, Italy, **2017.**
[24] S. Langbein, A. Czechowicz, *Konstruktionspraxis Formgedächtnistechnik*, Vol. *1*, Springer Fachmedien, Wiesbaden **2013**.
[25] P. Motzki, F. Khelfa, L. Zimmer, M. Schmidt, S. Seelecke, *IEEE/ASME Trans. Mechatron.* **2019**, *24*, 293.
[26] J. Luntz, B. Barnes, D. Brei, P. W. Alexander, A. Browne, N. L. Johnson, in *Proc. Volume 7290, Industrial and Commercial Applications of Smart Structures Technologies 2009*, SMA wire actuator modular design framework, **2009**, https://doi.org/10.1117/12.816752.
[27] S. Jung, J. Bae, I. Moon, in *Control. Autom. Syst. (ICCAS), 2011 11th Int. Conf.*, **2011**.
[28] H. Janocha, *Unkonventionelle Aktoren - Eine Einführung*, Oldenburg Verlag, München **2010**.
[29] S. Akbari, A. H. Sakhaei, S. Panjwani, K. Kowsari, A. Serjourei, Q. Ge, *Sens. Actuators, A* **2019**, *290*, 177.
[30] D. O. Kazmer, *Injection Mold Design Engineering*, 2nd ed., München, Carl Hanser Verlag GmbH Co KG **2016**.
[31] R. Britz, S. Seelecke, G. Rizzello, P. Motzki, in *ASME 2020 Conf. on Smart Materials, Adaptive Structures and Intelligent Systems, SMASIS 2020*, **2020**, pp. 1–6, https://urldefense.com/v3/__https://doi.org/10.1115/SMASIS2020-2214__;!!N11eV2iwtfs!q6l0zt0g1ElQpQqwLfa3HMDce-KAIQrEUrO-S8OAAobqNshr_vz1Iwr3qMRF_AoRS7NgOvsE1Eb8_NKCI578LODlMbDl8TqOiQ$.
[32] F. Simone, G. Rizzello, S. Seelecke, P. Motzki, *Front. Robot. AI* **2020**, *7*, https://doi.org/10.3389/frobt.2020.608841.
[33] R. Featherstone, Y. H. Teh, *Springer Tracts Adv. Robot.* **2006**, 67 https://doi.org/10.1007/11552246_7.
[34] J. H. Mabe, F. T. Calkins, M. B. Alkislar, in *Proc. Volume 6930, Industrial and Commercial Applications of Smart Structures Technologies 2008*, Variable area jet nozzle using shape memory alloy actuators in an antagonistic design, **2008**, https://doi.org/10.1117/12.776816.
[35] A. Ianagui, E. A. Tannuri, *Mechatronics* **2015**, *30*, 126.
[36] M. Kohl, B. Krevet, E. Just, *Sens. Actuators, A* **2002**, *97–98*, 646.
[37] R. Britz, P. Motzki, S. Seelecke, *Thermal Actuator Arrangement Having Improved Reset Time*, **2019**.
[38] C. C. Lan, C. M. Lin, C. H. Fan, *IEEE/ASME Trans. Mechatronics* **2011**, *16*, 141.
[39] S. K. Chaitanya, K. Dhanalakshmi, *Demonstration of Self-Sensing in Shape Memory Alloy Actuated Gripper*, in IEEE International Symposium on Intelligent Control-Proceedings, **2013**, https://doi.org/10.1109/ISIC.2013.6658620.
[40] T. R. Lambert, A. Gurley, D. Beale, *Smart Mater. Struct.* **2017**, *26* 35004.
[41] G. Rizzello, M. A. Mandolino, M. Schmidt, D. Naso, S. Seelecke, *Smart Mater. Struct.* **2019**, *28*, 025020.

3.3 High-Power Shape Memory Alloy Catapult Actuator for High-Speed and High-Force Applications

Philipp Molitor[2], Rouven Britz[1], Paul Motzki[1,2]

[1] Lehrstuhl für Intelligente Materialsysteme, Fachrichtung Systems Engineering, Fachrichtung Materialwissenschaft und Werkstofftechnik, Universität des Saarlandes, Saarbrücken

[2] AG Intelligente Materialsysteme, Zentrum für Mechatronik und Automatisierungstechnik, ZeMA gGmbH, Saarbrücken

Veröffentlicht in IEEE Access.
DOI: 10.1109/ACCESS.2022.3202210

IEEE Access
Multidisciplinary ⋮ Rapid Review ⋮ Open Access Journal

Received 10 August 2022, accepted 14 August 2022, date of publication 26 August 2022, date of current version 8 September 2022.

Digital Object Identifier 10.1109/ACCESS.2022.3202210

RESEARCH ARTICLE

High-Power Shape Memory Alloy Catapult Actuator for High-Speed and High-Force Applications

PHILIPP MOLITOR[1,2], ROUVEN BRITZ[2], AND PAUL MOTZKI[1,2]

[1]Intelligent Material Systems Laboratory, Center for Mechatronics and Automation Technology (ZeMA gGmbH), 66121 Saarbrücken, Germany
[2]Intelligent Material Systems Laboratory, Department of Systems Engineering, Department of Materials Science and Engineering, Saarland University, 66123 Saarbrücken, Germany

Corresponding author: Philipp Molitor (philipp.molitor@imsl.uni-saarland.de)

ABSTRACT Nickel-Titanium (NiTi) based shape memory alloy (SMA) wires are already often used in industrial actuator applications. Their high energy density allows the building of light-weight actuator systems with high forces using small installation spaces. Combined with the biocompatibility of NiTi, a huge field of applications can be covered by SMA actuated systems. In systems like emergency brakes or switch disconnectors, which require high forces as well as high actuation speed, the high-power capability of NiTi actuators is exploited. The presented work details the development and characterization of a giant power catapult demonstrator, that combines the high-speed and high-force capability of SMA wires. To illustrate the vast force, speed, and power potential of SMA wires, a bowling ball is launched from its resting position vertically into the air using SMA wires. For demonstration purposes, a target altitude for the bowling ball of 500 mm is chosen. With the height and the overall accelerated mass given, an actuation force $F \cong 920$ N is needed. The instantaneous energy release from the designed power source results in the targeted flight height and an overall peak power of $P \cong 0.5$ MW.

INDEX TERMS Keywords actuator, catapult, high-force, high-speed, high-power, high-performance, NiTi, Nitinol, shape memory alloy, SMA.

I. INTRODUCTION

Shape memory alloys (SMA) are well known for their superelasticity as well as their actuation capabilities and are widely used in biomedical applications and specific actuator products [1], [2], [3], [4]. The high energy density of Nickel-Titanium (NiTi) based SMAs [5], [6], [7] allows for the development of high force industrial actuator applications and robotic structures [8], [9], [10], [11], [12]. The notion Nitinol, as a common name for the alloy, is an acronym for the two given components and the place of its discovery. The discovery of the shape memory effect of a binary nickel and titanium alloy is attributed to William J. Buehler and Frederick Wang in 1959 over the course of their research at the Naval Ordnance Laboratory. The shape memory effect is based on the property of the alloy to perform a reversible phase transformation. One distinguishes between the monoclinic low-temperature phase martensite and the cubic space centered high-temperature phase austenite [13], [14]. In contrast to plastic deformation in conventional metals, which leads to a displacement of atoms within the crystal lattice, shape memory alloys show a phase shift in the martensite structure without a displacement of atoms. This so called pseudoplastic deformation is reversible and can be revoked [15], [16]. Heating the structure leads to a phase transformation towards austenite, which comes with a change in macroscopic shape. In the case of SMA wires, the temperature induced transformation to the austenite phase results in a contraction of the SMA wire, which is used to perform mechanical work in actuator systems [17].

Current research in the field of SMA actuators has a strong focus on identifying new areas of application like the field of bio-inspired motion [18], [19], soft robotics [20], [21] as well as modeling and control of the oftentimes complex nonlinear material behavior [22], [23].

Based on their performance capabilities, SMA actuator applications can be classified into fast responding systems

The associate editor coordinating the review of this manuscript and approving it for publication was F. R. Islam.

[24], [25], [26], [27], [28] and those that move very high loads [29], [30].

The content of this paper deals with combining both topics in a descriptive way, resulting in a mechatronic system for technology demonstration purposes. Dana, Vollach and Shilo give an overview of these high-rate SMA applications [27], which can be used for the development of quick release mechanisms in safety applications [26] or contactors as prominent practical examples. In both cases, the SMA actuator must provide high forces in the range of several micro- or milliseconds to either pull a safety pin and activate a brake-/blocking mechanism or disconnect/break a high-voltage and high-current electrical circuit.

To demonstrate both, the possible velocity and the potential force in a complete mechatronic technology demonstrator system outside a laboratory, this work aims to accelerate a bowling ball vertically into the air from rest using only SMA wires. To sufficiently demonstrate this dual high-performance effect, a certain flight height of the bowling ball is necessary. This flight height consequently determines the energy required to accelerate the ball, so that it reaches the desired height.

After defining the design and in consideration of the necessary mechanical and electrical parameters, a demonstrator is designed, built, and put into operation.

The remainder of this paper is composed as follows. In section II, an overview of the overall system concept is provided and the mechanical and electronics designs are presented and discussed. Furthermore, the applied SMA wire bundle configuration is introduced and validated. The final demonstrator setup is described in section III, as well as the possible performance of the developed system. Decisively, an outlook is given and concluding thoughts are discussed in section IV.

II. ACTUATOR SYSTEM CONCEPT, DESIGN, AND VALIDATION

The purpose of the presented demonstrator is illustrating the immense power potential of SMA wires respectively the SMA technology. To accomplish that goal, the actuator system is divided into two main systems, i.e., the mechanical guidance framework and the electronical power- and switching system. As mechanical conditions, a desired flight altitude of $h = 500$ mm and an overall mass m to be accelerated of approx. 3 kg are chosen. The needed kinematic momentum for the acceleration of the mass of the moving system is generated from the contraction of the SMA wires whilst their phase transformation from martensite to austenite using an electrical current. During this thermally induced transformation of the crystal lattice, a corresponding strain of 4% of the material is achieved. Regarding the parameters for height, mass and short acceleration travel, a force of $F \cong 920$ N is needed. Due to the high forces, SMA wires with a diameter of $d = 500$ μm are chosen and put in a radial formation of 3 bundles [31] with 4 wires each. To store the necessary electrical activation energy, a circuit board is designed with an array of capacitors and a maximum operation voltage of 450 V. With the chosen high-power switching components, a current flow of over 600 A per bundle and thus a combined system current flow of over 1800 A can be achieved. This high current through each bundle results in an almost immediate transformation of the crystal lattice from martensite to austenite and the corresponding contraction of the SMA wires.

To gain the maximum effect of the demonstrator, a concept was elaborated combining both parts in an efficacious fully integrated mechatronic system.

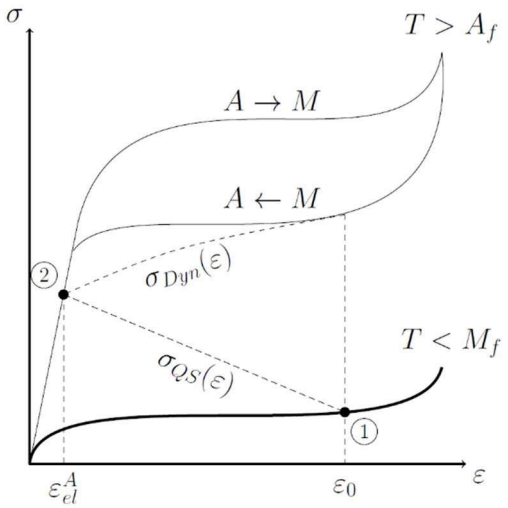

FIGURE 1. Mechanical stress-strain behavior of SMA wires in low temperature (martensitic) and high temperature (austenitic) states [27].

A. BASIC CALCULATIONS FOR DESIGN

As concept base, all needed kinematic parameters have to be evaluated and set. The activation scheme in this demonstrator aims at full SMA wire contraction with maximum velocity and thus generating an acceleration of a mass. Even though the mechanical stress-strain behavior of SMA wires is highly non-linear and hysteretic (Figure 1, [27]), in this specific case the only constraint is to reach the fully austenitic branch (2) from resting position (1) as fast as possible. This means, no further control of the actuator is needed or intended, the only goal is maximum power release upon activation.

Based on energy conservation, with gravity g and the required height of $h_1 = 500$ mm, the necessary velocity v_1 of the launched bowling ball can be calculated as:

$$v_1 = \sqrt{2\,g\,h_1} = 3.13\,\frac{\mathrm{m}}{\mathrm{s}} \tag{1}$$

Furthermore, with the chosen SMA wire length of $l_{martensite} = 400$ mm, the presumed strain of 4% and the resulting wire-length-based acceleration travel of $\Delta x = 16\ mm$, the remaining translatory motion parameters, acceleration time t_1 and the corresponding acceleration a_1,

can be evaluated:

$$t_1 = \frac{2\Delta x}{v_1} = 10.22 \text{ ms} \tag{2}$$

$$a_1 = \frac{v_1}{t_1} = 306.26 \frac{\text{m}}{\text{s}^2} \tag{3}$$

The correlative combined force F can be calculated, considering the kinematic mass $m = 3kg$ and the needed acceleration a_1 from formula (3), as:

$$F = m\, a_1 \cong 920 \text{ N} \tag{4}$$

In perspective of these high forces, SMA wires with a diameter of $d = 500\ \mu$m were picked and put in a 3 by 4 wire radial bundle arrangement (Figure 2).

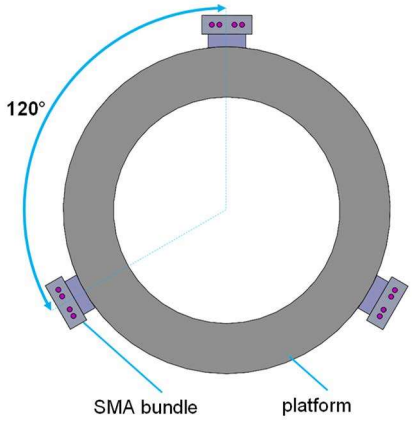

FIGURE 2. Drawing of the radial SMA bundle arrangement used for the bowling ball catapult.

With Equation 4 and the relevant values of the mass of a single wire $m_{SMA} = 0.53$ g, the specific thermal capacity $c = 500$ J/kg K, the specific enthalpy $h = 20$ J/g and the phase transformation temperature rise $\Delta T = 73$ K, the required activation energy W_1 per 4-wire bundle can be calculated.

$$W_1 = 4W_{1,1} = 4m_{SMA}(c\Delta T + h) = 119.12 \text{ J} \tag{5}$$

To deploy the calculated energy in the given time t_1, a dedicated energy source combined with capable control and switching electronics is necessary.

B. MECHANICAL DESIGN

As the SMA wires are exclusively responsible for the demonstrator kinematics, a proper mechanical design is developed to illustrate this matter.

To provide the needed force and power, special SMA wire bundles are designed. The bundle brackets can hold up to 5 wires each. At the moment of launch, every individual SMA wire is providing a maximum peak force of 76.5 N with a corresponding maximum peak mechanical stress of 390 MPa. The wires are set in parallel mechanically and electrically, whereas the clamping stem is also serving as the electrical contact for the SMA wires (Figure 3a). A more detailed view of the clamping bracket is shown in Figure 3b.

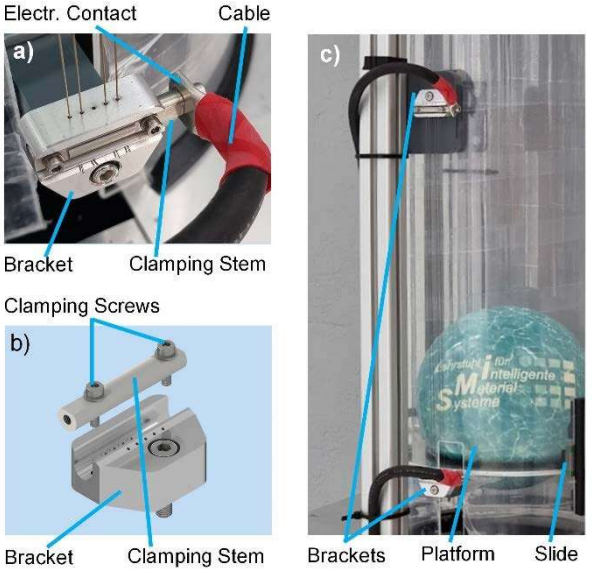

FIGURE 3. a) SMA bundle (bottom bracket) with 2AWG wire attached to the clamping bolt, b) image of the CAD design of the clamping bracket, c) corresponding SMA bundle attachment at top (frame) and bottom (catapult platform).

For the fabrication and assembly of the used SMA bundles, a specific preconditioning routine including a defined biasing mechanism is used, which ensures homogeneous elongation and stress level of $\sigma_1 = 250$ MPa of each wire in a bundle. This guarantees that all SMA wires have the same preconditions before their installation and minimizes individual residual strains.

The bowling ball is set on a brim of aluminum, operating as a catapult platform. One side of the SMA bundles is attached to this brim in a circular arrangement of 120° spacing. Additionally, the platform is mechanically connected to slides guided on linear rails. These rails are connected to a transparent acrylic tube, which has the task of keeping the linear rails in position and guiding the bowling ball on its flight trajectory. To limit the maximum travel of the catapult platform to 16 mm, which is the maximum SMA wire contraction and thus the highest possible acceleration path length, limit stops are attached to the linear rails. This prevents the platform from overshooting and ensures safe separation of the bowling ball from the platform after the acceleration travel, to allow the bowling ball to lift off. The selected position of the end stops was determined, and no variation was made, as the highest possible performance (flight altitude) was aimed for. Therefore, the longest possible acceleration path, i.e., the highest possible active stroke of the SMA bundles used, determines the position of the end stops. A reduction or increase would have no or a negative effect on the performance. For overall sturdiness, the mentioned arrangement is put in a frame of extruded aluminum profiles. The framework is divided into two chambers, the upper one housing the kinematics and the lower the control and power electronics. The other side of the SMA bundles is attached to the upper area of the aluminum frame (Figure 3c).

The platform with the resting bowling ball (Figure 4) is accelerated, as the 3 SMA bundles are activated. As the platform hits the limit stops (Figure 4, dashed lines), the bowling ball leaves the platform, continuing the vertical translatory movement until reaching the turning point at the targeted height. The movement then inverts, leading to the bowling ball landing back on the launching platform. After re-lengthening the SMA wires, the process can be repeated.

The evaluation of the electronic parameters, as well as the design of the control and power electronics, is described in the following section C.

C. CONTROL AND POWER ELECTRONICS

To supply the needed energy in the time t_1 for the SMA wire transformation, a suitable current source is crucial. As commercially available power supply units are either too slow or too expensive, a custom power supply was designed. In Figure 5, a block diagram is shown, which illustrates the interconnection of the core components. For safety reasons, an array of electrolytical capacitors was picked as energy storage.

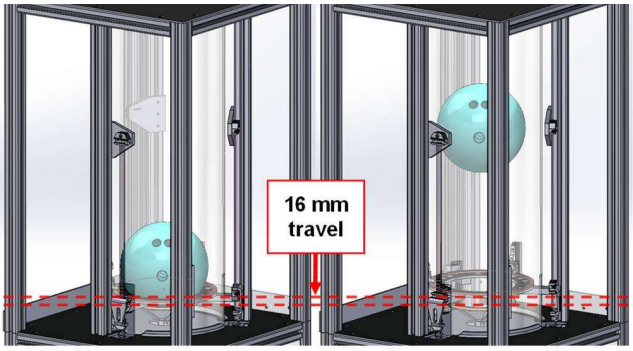

FIGURE 4. Illustration of the bowling ball in its starting position and when reaching the turning point after the lift-off subsequential of the 16 mm acceleration travel.

With an electrical resistance $R_B = 0.45\ \Omega$ per 4-wire SMA bundle, an assumed remaining charge of 0.7% of a discharged capacitor and being $\tau_1 = R_B \cdot C_B$, the relevant capacity can be calculated as:

$$U_C = U_1 e^{\frac{-t_1}{\tau_1}} = U_1 \cdot 0.007 \tag{6}$$

$$C_B = -\frac{t_1}{R_B\, ln\,(0.007)} = 4.6\ \text{mF} \tag{7}$$

Regarding the needed activation energy of $W_1 = 119,12$ J per bundle, the corresponding minimum charging voltage U_1 and the resulting electric current I_1 for a single bundle can be calculated:

$$U_1 = \sqrt{\frac{W_1}{0.5 C_B}} = 227.6\ \text{V} \tag{8}$$

$$I_1 = \frac{U_C}{R_B} = 505.8\ \text{A} \tag{9}$$

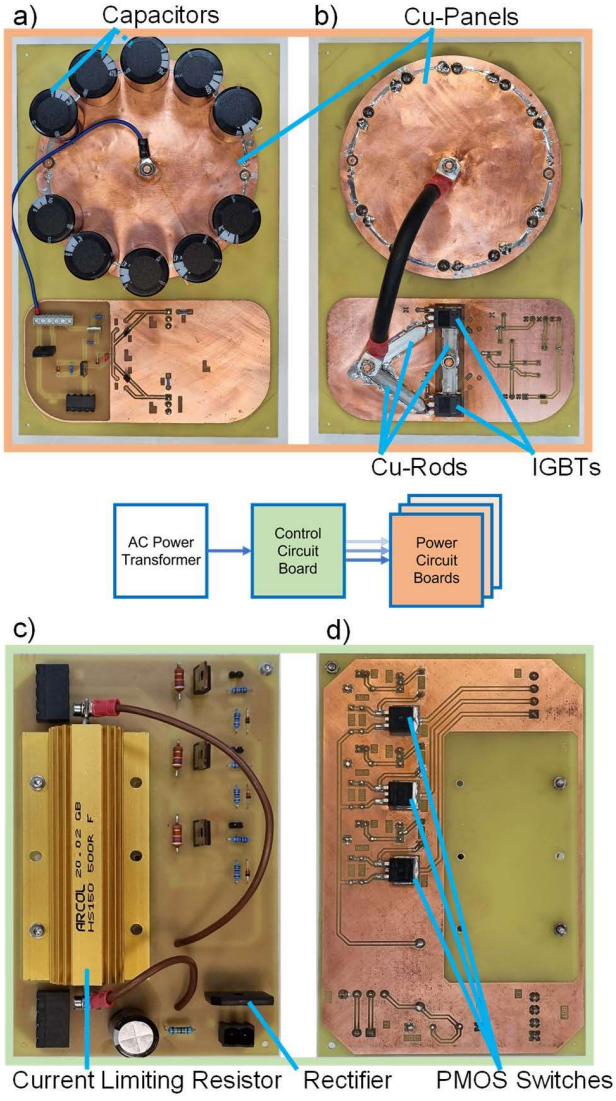

FIGURE 5. Block diagram of the charging circuit with a) power circuit board (top side), with 10/12 connected capacitors and secondary components, b) power circuit board (bottom side), with additionally applied copper sheets and rods leading the current flow from the capacitors through the IGBTs to the SMA wires c) control circuit board (top side), with limiting resistor, full-wave rectifier and secondary components, d) control circuit board (bottom side), with 3 high-power PMOS switches.

To provide the calculated capacity, the circuit board is designed to house up to twelve parallel connected 460 μF capacitors (Figure 5a), which allows an additional buffer of 20% to the needed ten capacitors.

As main switching component, two parallel connected insulated-gate bipolar transistors (IGBT) are used, which allow a maximum current flow of 960 A (Figure 5b). To enable a high-current flow, extra copper plates and rods were made and applied to the circuit board (Figure 5b). Additionally, the circuit board is equipped with all necessary state-of-the-art safety and regulation components like a blocking diode and discharge power resistor, to ensure the proper behavior.

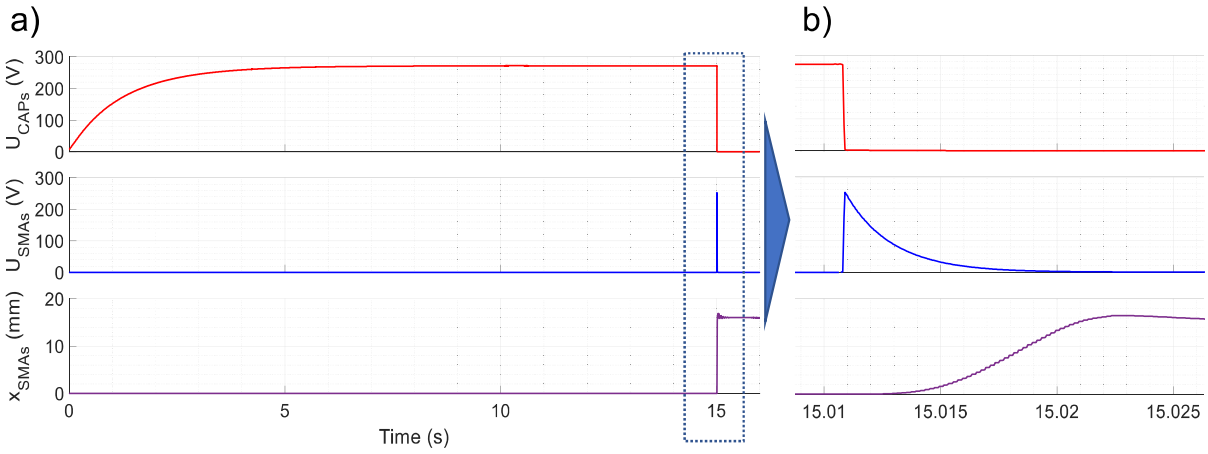

FIGURE 6. Illustration of the charging voltage of the capacitors (top), the voltage drop over the SMA wires (mid) and the resulting strain, respective travel of the SMA wires (bottom) as an a) exemplary sequence of events, b) detailed view at the moment of release.

For charging the capacitor array, the control circuit board is connected to an adjustable AC transformer combined with a full-wave rectifier (Figure 5c), which allows a charging voltage U_1 up to 350 VDC.

Each bundle is served by a dedicated capacitor-based power supply, which all are preconnected to the central control circuit board. On the control board, the charging and discharging of the capacitors is managed sequentially with 3 high-voltage p-channel MOSFETs (Figure 5d), combined with current limiting resistors (Figure 5c) for the charging process. The 3 power circuit boards as well as the control circuit board are connected to a microcontroller, which controls all the relevant sequences of the launching procedure.

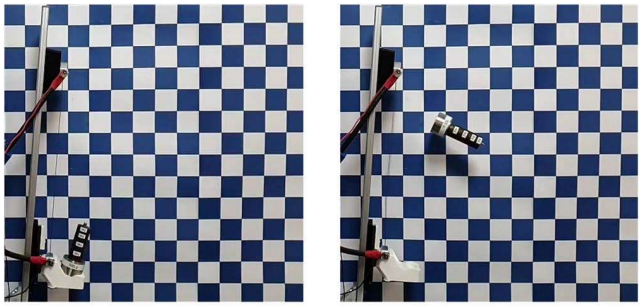

FIGURE 7. Display of the validation setup with relative overall accelerated mass in its starting position (left) and reaching its peak altitude (right).

D. SMA BUNDLE VALIDATION

To verify the functionality of the charging electronics as well as the capacitor based high-current power circuit boards, all parts are tested in a measurement setup linked to several sensors, e.g., *LEM HASS500* current sensor and a *Keyence LK-G87* laser triangulation sensor. To approach the full potential of the setup, the power circuit board is equipped in steps with 5, 8 and finally 10 capacitors. Corresponding to the number of capacitors, 2, 3 or 4 SMA wires are put in the bundles and activated by discharging the capacitors via the SMA wires.

During the charging and discharging process, the voltage of the capacitors, the voltage at the SMA wires, the current flow through the SMA wires, the contraction time, as well as the contraction travel are measured. Figure 6a shows the exemplary sequence of events from charging the capacitors until the instant of the momentary energy release, with the capacitor charging voltage at the top, the measured voltage at the SMA wires in the middle and the performed travel at the bottom. A more detailed view of this measurement is shown in Figure 6b. Additionally, a portion of the overall accelerated kinematic mass is put on a linear slide with a launch pad, attached to one side of the SMA bundle, in relation to the used count of SMA wires and capacitors. As the capacitors are discharged, the proportional weight is accelerated and launched equally to the bowling ball into midair (Figure 7). As the height of the launched weight reached is also measured, the charging voltage of the capacitors can be compared to the theoretical value of $U_1 = 230$ V and later adjusted to reach the aimed flight height. Regarding the measuring results of the validation process it is shown, that with the designed electronics an almost instantaneous discharge via the SMA wires is possible (Figure 8, center diagram) leading to the targeted 16 mm travel (Figure 8, bottom diagram). Furthermore, with an adjusted charging voltage of $U_2 = 280$ V (Figure 8, center diagram) all relative combinations of SMA wire and capacitor count and their corresponding weight the resulting performance can be measured. A maximum current flow of up to $I_2 = 560$ A (Figure 8, top diagram) can be monitored, leading to a discharge time of $t_2 \leq 11$ ms (Figure 8, bottom diagram). The travel exceeding the 16 mm mark, can be explained by the not completely stiff carrier, leading to the overshooting as shown in Figure 8. These experiments are repeated with every power circuit board, until all three needed circuit boards are validated and equipped with ten 460 μF capacitors, providing the needed capacity of 4.6 mF each.

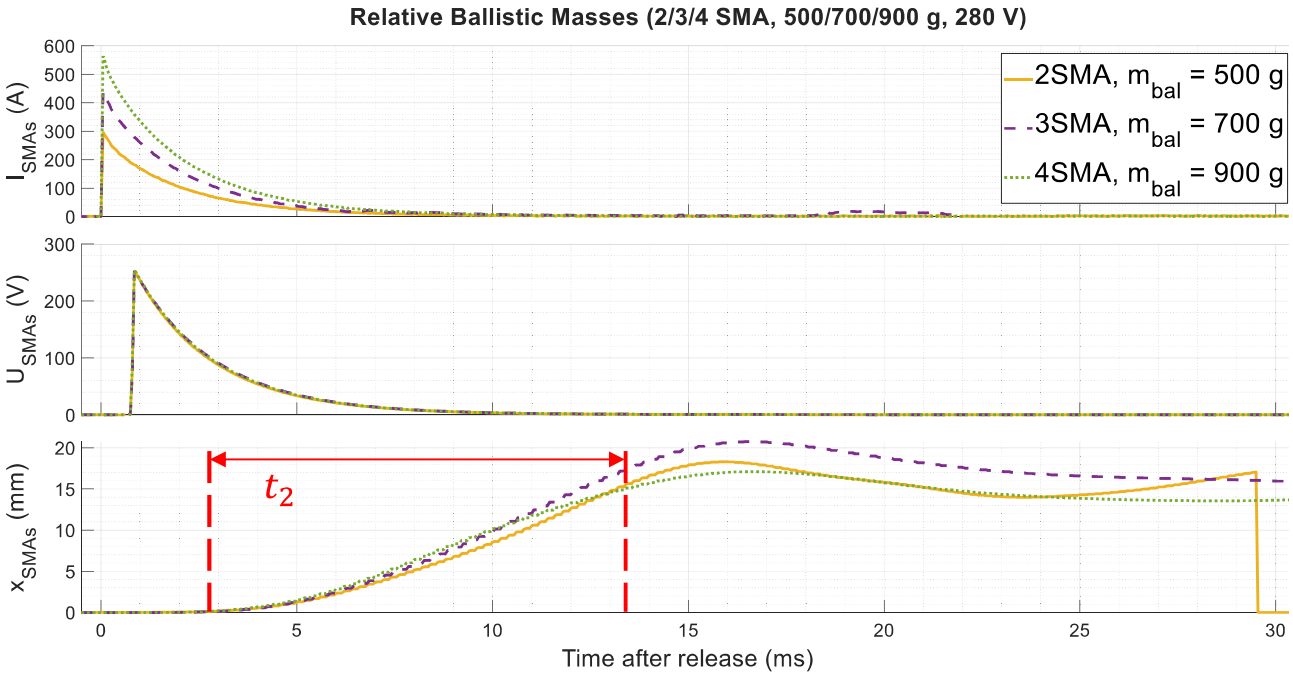

FIGURE 8. Representation of the current flow via the SMA wires (top), the voltage drop over the SMA wires (mid) and the resulting acceleration travel of the SMA wires (bottom) for the combined sequence of events with 2, 3 and 4 SMA wires attached with corresponding charging voltage and the proportional weight lifted. The red marker highlights the acceleration times $t2 \leq 11$ ms of each setup.

Subsequently, all electronics and mechanical components are assembled, combined, and put into operation, which is described in the following section III.

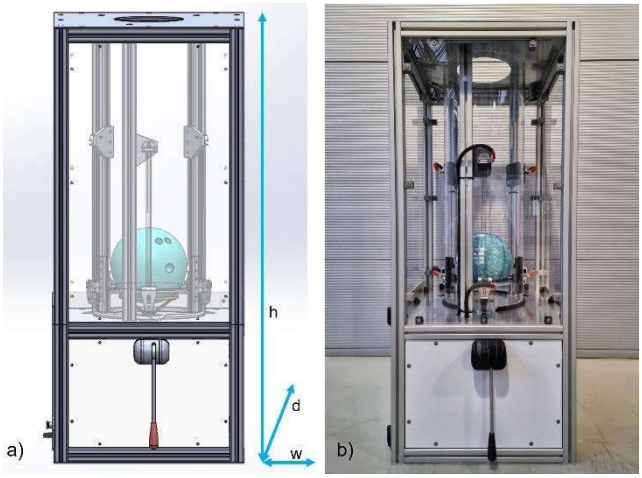

FIGURE 9. a) Image of the CAD assembly, b) Final fully assembled and enclosed demonstrator (height $h = 1260$ mm, width $w = 545$ mm, depth $d = 545$ mm) with top kinematic chamber and bottom electronics chamber.

III. FINAL SETUP AND PERFORMANCE

To examine the combined potential of the three power circuit boards and to compare the reached height of the bowling ball with the calculated height, all components are assembled. As mentioned above, the upper chamber of the aluminum framework serves as sturdy and reliable structure for the mechanical components (Figure 9). Apart from that, the bottom chamber contains all the electronics, such as the power circuit boards, the control circuit board, the microcontroller and necessary secondary components. The chambers are locked up with acrylic and aluminum composite panels (Figure 9) to ensure safe operation and handling. As the aimed current flow and voltage represent a high risk for human health, all the electronic connections are precisely built and thoroughly checked. Consequently, the whole setup is put into operation by applying stepwise rising charging voltages to the capacitors. The following discharge of the capacitors via the SMAs and the resulting movement is monitored and then compared to the expected behavior. Since the observed behavior matched the predictions, the charge voltage is incrementally increased until the target voltage of $U_2 = 280$ V.

The bowling ball is then placed on top of its launching platform and a square patterned sheet is applied at the back side of the demonstrator. Considering the square edge length of 5 cm, the travelled height of the bowling ball can be easily determined.

The first set of attempts is performed with a charging voltage of $U_2 = 280$ V, leading to a travel height of $h_2 = 41$ cm (Figure 10a, dotted red lines), a measured overall system activation energy $W_2 = 435$ J and a combined overall system power $P_2 = 0.43$ MW (Figure 10b). The sequence is repeated five times with always comparable results. Although the reached height presented itself very impressive, it minimally

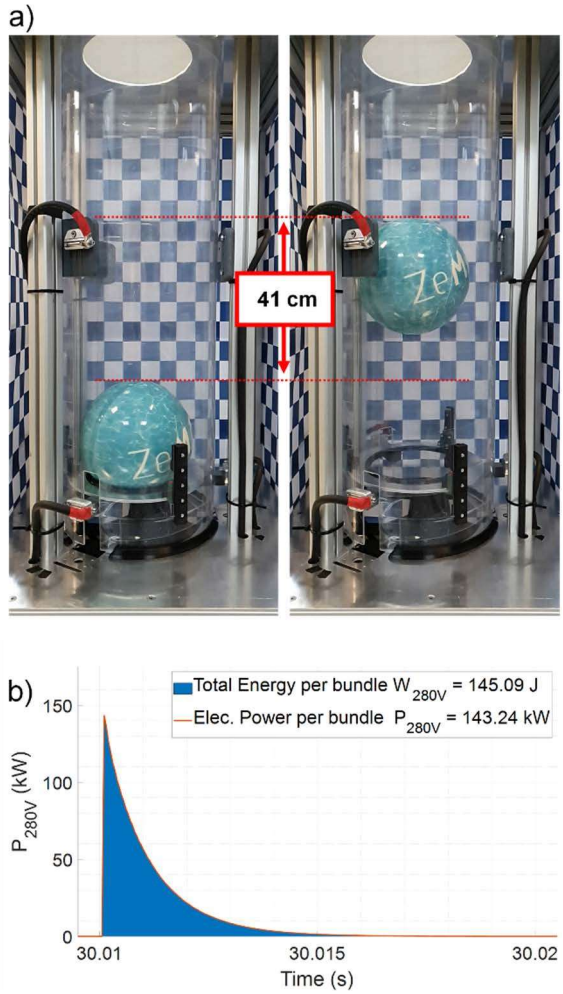

FIGURE 10. a) Comparison of start and end position (red dotted lines) with a charging voltage of 280 V leading to a travelled height of 41 cm, b) Corresponding overall peak power of 429.6 kW (3.143.2 kW) with a charging voltage of 280 V.

undercut the targeted height. The explanation for the measured activation energy W being higher than the calculated theoretical value W_1 is, that the primary calculation was made in an ideal state without consideration of any influences of friction and tensions. Another influence on performance is the inertia of the mass to be accelerated.

At the moment of launch, this results in an increased stress level, which then causes a higher actual transformation temperature. This leads to higher temperature values in Equation (4) and thus higher energy needed. To get closer to the targeted flight height, the charging voltage is further increased.

The next set of attempts is made with an increased charging voltage $U_3 = 300$ V, which is just below the technical limits of the voltage supplying transformer. The following discharge of the capacitors via the SMA wires leads to a travel height of the bowling ball of $h_3 = 45$ cm (Figure 11a, dotted red lines), a measured overall system activation energy $W_3 = 495$ J and a combined overall system power $P_3 = 0.49$ MW (Figure 11b).

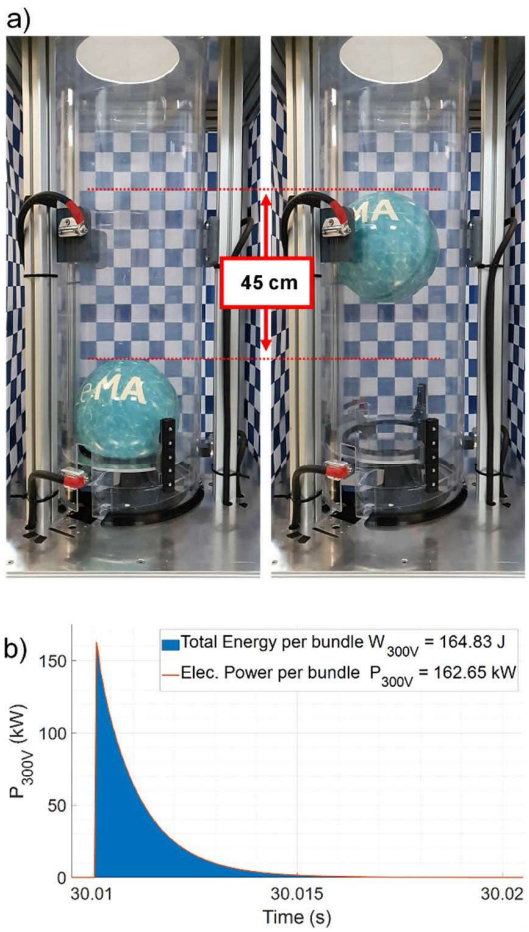

FIGURE 11. a) Comparison of start and end position (red dotted lines) with a charging voltage of 300 V leading to a travelled height of 45 cm, b) Corresponding overall peak power of 488.1 kW (3.162.7 kW) with a charging voltage of 300 V.

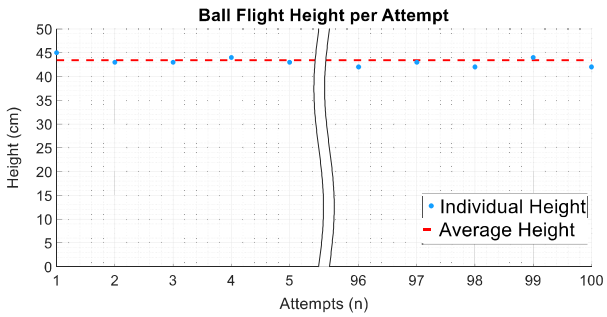

FIGURE 12. Flight heights of the first and last five attempts (solid blue) and the so calculated average flight height (dashed red).

IV. CONCLUSION AND OUTLOOK

In this article, a vivid SMA catapult demonstrator that displays the enormous power potential of SMA technology has been presented. In addition to the development and design of the mechanical structure and actuator components, which successfully launch a bowling ball to the height of about 450 mm, a high-power circuit board is developed, that can deliver a current flow of up to 700 A per board. With a series of fundamental experiments, the reliable functionality and repeatability of the circuit boards is validated. Furthermore, it is shown that the launching sequence can be repeated

without any loss of efficiency being displayed in the constant travelled height of the bowling ball over 100 times (Figure 12). The deviation around the average height value of $h_{avg} = 43.4$ cm can be explained with different ambient temperatures and the resolution of the measuring scale.

The high-speed actuation with the preeminent overall power potential of about 0.5 MW shown by the built demonstrator allows for the option to expand the SMA technology in new areas of application, e.g., load-break switches. The combined high-speed and high-power actuations are a result of the excellent specific energy density of 81.4 kJ/kg and specific power density of 82.2 W/kg of the SMA technology that would hard to be met with competing actuator technologies.

In the next steps, lifetime cycle tests will be conducted in a statistical setup to observe and estimate life cycle times of the used NiTi SMA wires under theses extreme mechanical, thermal and electrical conditions. In addition, the development of a model to predict the behavior of SMA wires in such extreme and highly dynamic conditions will be helpful for the design of commercial applications in the future, as well as further systematic experiments with different loading conditions. Applications that can already be implemented are release mechanisms such as airbag release triggers, load break switches and payload release actuators for space applications.

REFERENCES

[1] R. Pecora and I. Dimino, "SMA for aeronautics," in *Shape Memory Alloy Engineering: For Aerospace, Structural and Biomedical Applications*. Amsterdam, The Netherlands: Elsevier, 2015, pp. 275–304.
[2] M. Kohl, *Shape Memory Microactuators*. Berlin, Germany: Springer, 2004.
[3] T. Duerig, D. Stoeckel, and D. Johnson, "SMA: Smart materials for medical applications," *Proc. SPIE*, vol. 4763, Mar. 2003, Art. no. 508666.
[4] H. Funakubo, *Shape Memory Alloys*, vol. 1. Amsterdam, The Netherlands: Gordon and Breach Science Publication, 1987.
[5] D. Reynaerts and H. Van Brussel, "Design aspects of shape memory actuators," *Mechatronics*, vol. 8, no. 6, pp. 635–656, 1998.
[6] S. J. Furst, "Design, fabrication, and control methods for exploiting the multifunctional sensing and actuation capabilities of shape memory alloy wires," Ph.D. dissertation, Saarland Univ., Saarbrücken, Germany, 2012, doi: 10.22028/D291-22852.
[7] H. Janocha, *Adaptronics and Smart Structures*. Berlin, Germany: Springer-Verlag, 2007.
[8] M. Dolce and D. Cardone, "Mechanical behaviour of shape memory alloys for seismic applications 1. Martensite and austenite NiTi bars subjected to torsion," *Int. J. Mech. Sci.*, vol. 43, no. 11, pp. 2631–2656, 2001.
[9] J. M. Jani, M. Leary, A. Subic, and M. A. Gibson, "A review of shape memory alloy research, applications and opportunities," *Mater. Des.*, vol. 56, pp. 1078–1113, Apr. 2014.
[10] P. Motzki and S. Seelecke, "Industrial applications for shape memory alloys," in *Encyclopedia of Smart Materials*, vol. 4. Amsterdam, The Netherlands: Elsevier, 2022, pp. 254–266.
[11] P. Motzki, F. Khelfa, M. Schmidt, S. Seelecke, and L. Zimmer, "Design and validation of a reconfigurable robotic end-effector based on shape memory alloys," *IEEE/ASME Trans. Mechatronics*, vol. 24, no. 1, pp. 293–303, Feb. 2019, doi: 10.1109/TMECH.2019.2891348.
[12] J. Jeong, K. Hyeon, J. Han, C. H. Park, S.-Y. Ahn, S.-K. Bok, and K.-U. Kyung, "Wrist assisting soft wearable robot with stretchable coolant vessel integrated SMA muscle," *IEEE/ASME Trans. Mechatronics*, vol. 27, no. 2, pp. 1046–1058, Apr. 2022, doi: 10.1109/TMECH.2021.3078472.
[13] W. J. Buehler, J. V. Gilfrich, and R. C. Wiley, "Effect of low-temperature phase changes on the mechanical properties of alloys near composition TiNi," *J. Appl. Phys.*, vol. 34, no. 5, p. 1475, 1963.
[14] F. E. Wang, W. J. Buehler, and S. J. Pickart, "Crystal structure and a unique 'martensitic' transition of TiNi," *J. Appl. Phys.*, vol. 36, no. 10, p. 3232, 1965.
[15] S. Langbein and A. Czechowicz, *Konstruktionspraxis Formgedächtnistechnik*. Bochum, Germany: Springer Vieweg, 2013.
[16] M. Bäker, *Funktionswerkstoffe*. Braunschweig, Germany: Springer Vieweg, 2014.
[17] D. C. Lagoudas, *Shape Memory Alloys*. Boston, MA, USA: Springer, 2008.
[18] H. Jeon, Q. N. Le, S. Jeong, S. Jang, H. Jung, H. Chang, H. J. Pandya, and Y. Kim, "Towards a snake-like flexible robot with variable stiffness using an SMA spring-based friction change mechanism," *IEEE Robot. Autom. Lett.*, vol. 7, no. 3, pp. 6582–6589, Jul. 2022, doi: 10.1109/LRA.2022.3174363.
[19] X.-T. Nguyen, A. A. Calderon, A. Rigo, J. Z. Ge, and N. O. Perez-Arancibia, "SMALLBug: A 30-mg crawling robot driven by a high-frequency flexible SMA microactuator," *IEEE Robot. Autom. Lett.*, vol. 5, no. 4, pp. 6796–6803, Oct. 2020, doi: 10.1109/LRA.2020.3015457.
[20] H. Yang, M. Xu, W. Li, and S. Zhang, "Design and implementation of a soft robotic arm driven by SMA coils," *IEEE Trans. Ind. Electron.*, vol. 66, no. 8, pp. 6108–6116, Aug. 2019, doi: 10.1109/TIE.2018.2872005.
[21] J. Jeong, K. Hyeon, S.-Y. Jang, C. Chung, S. Hussain, S.-Y. Ahn, S.-K. Bok, and K.-U. Kyung, "Soft wearable robot with shape memory alloy (SMA)-based artificial muscle for assisting with elbow flexion and forearm supination/pronation," *IEEE Robot. Autom. Lett.*, vol. 7, no. 3, pp. 6028–6035, Jul. 2022, doi: 10.1109/LRA.2022.3161700.
[22] X. Liu, H. Liu, and J. Tan, "Actuation frequency modeling and prediction for shape memory alloy actuators," *IEEE/ASME Trans. Mechatronics*, vol. 26, no. 3, pp. 1536–1546, Jun. 2021, doi: 10.1109/TMECH.2020.3023097.
[23] H. Jin, Y. Ouyang, H. Chen, J. Kong, W. Li, and S. Zhang, "Modeling and motion control of a soft SMA planar actuator," *IEEE/ASME Trans. Mechatronics*, vol. 27, no. 2, pp. 916–927, Apr. 2022, doi: 10.1109/TMECH.2021.3074971.
[24] P. Motzki, T. Gorges, M. Kappel, M. Schmidt, G. Rizzello, and S. Seelecke, "High-speed and high-efficiency shape memory alloy actuation," *Smart Mater. Struct.*, vol. 27, no. 7, pp. 87–100, 2018.
[25] J. Qiu, J. Tani, D. Osanai, Y. Urushiyama, and D. Lewinnek, "High-speed response of SMA actuators," *Int. J. Appl. Electromagn. Mech.*, vol. 12, nos. 1–2, pp. 87–100, Feb. 2001.
[26] Y. Malka and D. Shilo, "A fast and powerful release mechanism based on pulse heating of shape memory wires," *Smart Mater. Struct.*, vol. 26, no. 9, Sep. 2017, Art. no. 095061.
[27] A. Dana, S. Vollach, and D. Shilo, "Use the force: Review of high-rate actuation of shape memory alloys," *Actuators*, vol. 10, no. 7, p. 140, Jun. 2021.
[28] S. Vollach and D. Shilo, "The mechanical response of shape memory alloys under a rapid heating pulse," *Exp. Mech.*, vol. 50, no. 6, pp. 803–811, Jul. 2010.
[29] V. Brailovski, P. Terriault, T. Georges, and D. Coutu, "SMA actuators for morphing wings," *Phys. Proc.*, vol. 10, pp. 197–203, Jan. 2010.
[30] H. Abuzied, A. Abbas, M. Awad, and H. Senbel, "Usage of shape memory alloy actuators for large force active disassembly applications," *Heliyon*, vol. 6, no. 8, Aug. 2020, Art. no. e04611.
[31] R. Britz and P. Motzki, "Analysis and evaluation of bundled SMA actuator wires," *Sens. Actuators A, Phys.*, vol. 333, Jan. 2022, Art. no. 113233.

PHILIPP MOLITOR received the master's degree in mechatronics and sensor technologies from the Saarland University of Applied Sciences, in 2021. He is currently pursuing the Ph.D. degree in systems engineering with Saarland University, Saarbrücken, Germany. His current research interests include shape memory wires as actuator-sensor systems in high-power applications and elastocaloric cooling systems.

ROUVEN BRITZ received the master's degree in mechatronics from Saarland University, Saarbrücken, Germany, in 2016, where he is currently pursuing the Ph.D. degree in systems engineering. His current research interests include shape memory alloy wires in actuator-sensor systems in industrial and high-power applications.

PAUL MOTZKI received the Ph.D. degree in mechatronics and systems engineering from Saarland University, Saarbrücken, Germany, in 2018. Since 2022, he has been a Professor with the Department of Systems Engineering, Saarland University, in cooperation with the Center for Mechatronics and Automation Technology (ZeMA gGmbH), Saarbrücken, after leading the Research Division "Smart Material Systems," ZeMA, since 2016. His research interests include the development of smart material-based artificial muscles and multifunctional actuator-sensor systems, in particular shape memory alloys, and electroactive polymers.

4 AUSBLICK

Diese Arbeit beschäftigt sich mit FGL-Drähten in Hochleistungsanwendungen und zeigt Grundlagenversuche im Bereich der FGL-Bündel zur Erzeugung hoher Kräfte sowie die Entwicklung eines anwendungsnahen Prototyps im Bereich der schnellen Aktivierung von FGL-Drähten. Um das volle Potential von beiden Hochleistungsbereichen aufzuzeigen, wird zusätzlich der Aufbau eines Technologiedemonstrators gezeigt, der beide Bereiche vereint.
In den Grundlagenversuchen zum Verhalten von FGL-Bündeln wird zwar die Zukunftsträchtigkeit dieser deutlich, um diese jedoch tatsächlich sicher in eine praktische Anwendung zu bringen, sind weitere Untersuchungen notwendig. Der wohl entscheidendste Faktor ist hier das postulierte verbesserte Oberflächen-Volumen-Verhältnis, das zu der gewünschten Dynamikverbesserung führen soll. Um dies zu validieren und Aussagen im Vergleich zu entsprechenden FGL-Halbzeugen zu treffen, sind in der Zukunft entsprechende Versuche notwendig. Faktoren wie der Abstand zwischen den Drähten, die verwendete Drahtdicke und -anzahl sind dabei zu beachten. Unterschiedliche Kühlmethoden zur weiteren Leistungssteigerung wie Luftströmungen oder eine Einbettung der Drähte in Polymere sind ebenfalls denkbar und erfordern weitere Experimente. Auch das Verhalten bei zyklischen Aktivierungen und die Lebensdauer sind zukünftig zu untersuchende Größen. Letzteres ist besonders interessant, da zwar, durch den Aufbau der Bündel, eine Redundanz beim Reißen einzelner Drähte vorhanden und ein Komplettausfall des Bündels somit nahezu ausgeschlossen ist, die dadurch entstehende Mehrbelastung der verbleibenden Drähte jedoch nicht zu vernachlässigen ist. Für den Einsatz in Anwendungen sind zudem noch Herstellungsverfahren und die Befestigung der Drähte entscheidende Punkte. Der durch die Bündelung entstehende niedrige elektrische Widerstand muss ebenfalls für die Entwicklung anwendungsnaher Ansteuerelektroniken berücksichtigt werden.
Bei dem entwickelten Aktor und den sich darin befindenden schnell aktivierten FGL-Drähten liegt in der Zukunft ein ähnlicher Schwerpunkt wie bei den

Grundlagenversuchen der FGL-Bündel. Auch hier sind weitere Untersuchungen nötig, die auf die Lebensdauer der Drähte abzielen. Bisher gibt es keine Untersuchungen darüber, wie sich der zur schnellen Aktvierung benötigte hohe Stromfluss durch die Drähte auf deren Lebensdauer auswirkt. Den Einfluss der, durch den Einsatz in erhöhten Umgebungstemperaturen bedingten erhöhten Drahtspannungen auf die Lebensdauer sollte ebenfalls zukünftig untersucht werden. Weitere Schritte, den Prototyp zu einem Produkt weiterzuentwickeln, sind neben der Verbesserung interner Reibeffekte ein maschinengerechteres Design im Hinblick auf Fertigung und Zusammenbau der Aktoren. Die Elektronik kann dahingehend weiterentwickelt werden, dass eine Schaltüberwachung bzw. Zustandsüberwachung mittels der „self-sensing“ Eigenschaft der FGL-Drähte möglich ist.

Durch die nötigen Untersuchungen in Bezug auf die Lebensdauer in den einzelnen Gebieten der Hochleistungsanwendungen ist diese auch in der Kombination der beiden Gebiete in dem entwickelten Demonstrator ein wegweisender Faktor für zukünftige Arbeiten. Die Identifizierung von Anwendungsfällen mit einmaliger oder geringer Anzahl an Aktivierungen und die anschließende Entwicklung von Prototypen sind unabhängig von den Lebensdauerversuchen möglich und sinnvoll, um andere konstruktive Aufgabenstellung, beispielsweise die Miniaturisierung einzelner Komponenten, im Vorfeld zu lösen.

LITERATURVERZEICHNIS

[1] G. B. KAUFFMAN and I. MAYO, “The Story of Nitinol: The Serendipitous Discovery of the Memory Metal and Its Applications,” *Chem. Educ.*, vol. 2, no. 2, pp. 1–21, 1997, doi: 10.1007/s00897970111a.

[2] H. Funakubo, *Shape Memory Alloys*, vol. 1, no. D. Amsterdam: Gordon and Breach Science Publ., 1987.

[3] W. J. Buehler, J. V. Gilfrich, and R. C. Wiley, “Effect of Low-Temperature Phase Changes on the Mechanical Properties of Alloys near Composition TiNi,” *J. Appl. Phys.*, vol. 34, no. 5, pp. 1475–1477, 1963, doi: 10.1063/1.1729603.

[4] B. Senf *et al.*, “Sensing and Actuating Functions by Shape Memory Alloy Wires Integrated into Fiber Reinforced Plastics,” 2017, doi: 10.1016/j.procir.2017.03.291.

[5] G. Rizzello and P. Motzki, “Chapter 6 - Smart materials for mini-actuators,” L. B. T.-E. Manfredi, Ed. Academic Press, 2022, pp. 117–163.

[6] D. C. Lagoudas, *Shape Memory Alloys: Modeling and Engineering Applications*. New York: Springer, 2008.

[7] J. Mohd Jani, M. Leary, A. Subic, and M. A. Gibson, “A review of shape memory alloy research, applications and opportunities,” *Mater. Des.*, vol. 56, 2014, doi: 10.1016/j.matdes.2013.11.084.

[8] M. H. Wu, “INDUSTRIAL APPLICATIONS FOR SHAPE MEMORY ALLOYS,” in *International Conference on Shape Memory and Superelastic Technolgies*, 2000, vol. 182, pp. 171–182.

[9] M. Dolce and D. Cardone, “Mechanical behaviour of shape memory alloys for seismic applications 2. Austenite NiTi wires subjected to tension,” *Int. J. Mech. Sci.*, vol. 43, no. 11, pp. 2657–2677, 2001, doi: 10.1016/S0020-7403(01)00050-9.

[10] P. Motzki, F. Khelfa, L. Zimmer, M. Schmidt, and S. Seelecke, “Design and Validation of a Reconfigurable Robotic End-effector Based on Shape Memory Alloys,” *IEEE/ASME Trans. Mechatronics*, vol. 24, no. 1, pp. 293–303, 2019, doi: 10.1109/TMECH.2019.2891348.

[11] P. Motzki and S. Seelecke, “Industrial Applications for Shape Memory Alloys,” in *Encyclopedia of Smart Materials*, A.-G. Olabi, Ed. Elsevier, 2022, pp. 254–266.

[12] T. Duerig, D. Stoeckel, and D. Johnson, “SMA - Smart Materials for Medical Applications,” in *SPIE, Smart Materials, Structures, and Systems*, 2003, vol. 4763, pp. 7–15, doi: 10.1117/12.508666.

[13] J. H. Crews, “Development of a Shape Memory Alloy Actuated Robotic Catheter for Endocardial Ablation: Modeling, Design Optimization, and Control,” 2011, [Online]. Available: http://gradworks.umi.com/34/63/3463761.html.

[14] L. Zimmer *et al.*, “An SMA-Based Multifunctional Implant for Improved Bone Fracture Healing,” in *Smart Materials, Adaptive Structures and Intelligent Systems*, 2021, vol. 85499, p. V001T05A001.

[15] B. Ganse *et al.*, “Concepts and clinical aspects of active implants for the treatment of bone fractures,” *Acta Biomater.*, vol. 146, pp. 1–9, 2022, doi: 10.1016/j.actbio.2022.05.001.

[16] N. B. Morgan, “Medical shape memory alloy applications - The market and its products,” *Mater. Sci. Eng. A*, vol. 378, no. 1-2 SPEC. ISS., pp. 16–23, Jul. 2004, doi: 10.1016/j.msea.2003.10.326.

[17] M. Es-Souni, M. Es-Souni, and H. Fischer-Brandies, “Assessing the biocompatibility of NiTi shape memory alloys used for medical applications,” *Anal. Bioanal. Chem.*, vol. 381, no. 3, pp. 557–567, 2005, doi: 10.1007/s00216-004-2888-3.

[18] R. Pfeifer, C. W. Müller, C. Hurschler, S. Kaierle, V. Wesling, and H. Haferkamp, “Adaptable orthopedic shape memory implants,” in *Procedia CIRP*, Jan. 2013, vol. 5, pp. 253–258, doi: 10.1016/j.procir.2013.01.050.

[19] B. Kim, S. Lee, J. H. Park, and J.-O. Park, “Design and fabrication of a locomotive mechanism for capsule-type endoscopes using shape memory alloys (SMAs),” *IEEE/ASME Trans. Mechatronics*, vol. 10, no. 1, pp. 77–86, 2005, doi: 10.1109/TMECH.2004.842222.

[20] C. S. Loh, H. Yokoi, and T. Arai, “New Shape Memory Alloy Actuator: Design and Application in the Prosthetic Hand,” in *2005 IEEE Engineering in Medicine and Biology 27th Annual Conference*, 2005, pp. 6900–6903, doi: 10.1109/IEMBS.2005.1616092.

[21] M. Sreekumar, T. Nagarajan, M. Singaperumal, M. Zoppi, and R. Molfino, “Critical review of current trends in shape memory alloy actuators for intelligent robots,” *Ind. Rob.*, vol. 34, no. 4, pp. 285–294, 2007, doi: 10.1108/01439910710749609.

[22] H. Yang, M. Xu, W. Li, and S. Zhang, “Design and Implementation of a Soft Robotic Arm Driven by SMA Coils,” *IEEE Trans. Ind. Electron.*, vol. 66, no. 8, pp. 6108–6116, 2019, doi: 10.1109/TIE.2018.2872005.

[23] M. Mandolino, R. Britz, Y. Goergen, G. Rizzello, and P. Motzki, “Development of an SMA driven articulation and autofocus mechanism for endoscope applications,” in *ACTUATOR 2022; International Conference and Exhibition on New Actuator Systems and Applications*, 2022, pp. 1–4.

[24] M. A. Mandolino, Y. Goergen, P. Motzki, and G. Rizzello, “Design and Characterization of a Fully Integrated Continuum Robot Actuated by Shape Memory Alloy Wires,” in *2022 IEEE 17th International Conference on Advanced Motion Control (AMC)*, 2022, pp. 6–11, doi: 10.1109/AMC51637.2022.9729267.

[25] F. Simone, G. Rizzello, S. Seelecke, and P. Motzki, “A Soft Five-Fingered Hand Actuated by Shape Memory Alloy Wires : Design , Manufacturing , and Evaluation,” *Front. Robot. AI*, vol. 7, no. 608841, 2020, doi: 10.3389/frobt.2020.608841.

[26] D. Stoeckel, “Shape Memory Actuators for Automotive Applications,” 1990.

[27] F. Butero, “Shape memory actuators for automotive applications,” *Adv. Mater. Process.*, vol. 166, no. 3, pp. 37–40, 2008, doi: 10.1016/b978-0-7506-1009-4.50028-7.

[28] E. Zimmerman, V. Muntean, T. Melz, B. Seipel, and T. Koch, “Novel pre-crash-actuator-system based on SMA for enhancing side impact safety,” 2009, doi: 10.1007/978-3-642-00745-3_4.

[29] E. Williams and M. H. Elahinia, “An Automotive SMA Mirror Actuator: Modeling, Design, and Experimental Evaluation,” *J. Intell. Mater. Syst. Struct.*, vol. 19, no. 12, pp. 1425–1434, 2008, doi: 10.1177/1045389X07087328.

[30] D. J. Hartl and D. C. Lagoudas, “Aerospace applications of shape memory alloys,” *Proc. Inst. Mech. Eng. Part G J. Aerosp. Eng.*, vol. 221, no. 4, pp. 535–552, Apr. 2007, doi: 10.1243/09544100JAERO211.

[31] R. Pecora and I. Dimino, “SMA for Aeronautics,” in *Shape Memory Alloy Engineering: For Aerospace, Structural and Biomedical Applications*, 2014.

[32] V. Shankar, G. N. Dayananda, P. Senthil Kumar, M. Subba Rao, and R. Balasubramaniam, “Development of electronic actuation system for shape-memory-alloy-based aerospace structures,” in *SPIE, Smart Materials, Structures, and Systems*, 2003, vol. 5062, pp. 914–921, doi: 10.1117/12.514740.

[33] V. Brailovski, P. Terriault, T. Georges, and D. Coutu, “SMA actuators for morphing wings,” *Phys. Procedia*, vol. 10, pp. 197–203, 2010, doi: 10.1016/j.phpro.2010.11.098.

[34] D. Reynaerts and H. Van Brussel, “Design aspect of shape memory actuators,” *Mechatronics*, vol. 8, pp. 635–656, 1998, doi: 10.1016/S0957-4158(98)00023-3.

[35] H. Janocha, *Adaptronics and Smart Structures*, 2. Berlin Heidelberg: Springer Verlag, 2007.

[36] H. Janocha, *Unkonventionelle Aktoren - Eine Einführung*, 2. München: Oldenburg Verlag, 2013.

[37] H. Abuzied, A. Abbas, M. Awad, and H. Senbel, “Usage of shape memory alloy actuators for large force active disassembly applications,” *Heliyon*, vol. 6, no. 8, p. e04611, 2020, doi: 10.1016/j.heliyon.2020.e04611.

[38] S. Shabalovskaya and J. Van Humbeeck, *Biocompatibility of Nitinol for biomedical applications*. Woodhead Publishing Limited, 2008.

[39] N. Lewis, A. York, and S. Seelecke, “Experimental characterization of self-sensing SMA actuators under controlled convective cooling,” *Smart Mater. Struct.*, vol. 22, no. 9, 2013, doi: 10.1088/0964-1726/22/9/094012.

[40] H. Li, C. X. Mao, and J. P. Ou, “Strain self-sensing property and strain rate dependent constitutive model of austenitic shape memory alloy: Experiment and theory,” *J. Mater. Civ. Eng.*, 2005, doi: 10.1061/(ASCE)0899-1561(2005)17:6(676).

[41] F. Simone, G. Rizzello, and S. Seelecke, “Metal muscles and nerves - A self-sensing SMA-actuated hand concept,” *Smart Mater. Struct.*, vol. 26, no. 9, 2017, doi: 10.1088/1361-665X/aa7ad5.

[42] A. Gurley, T. R. Lambert, D. Beale, and R. Broughton, “Dual measurement self-sensing technique of NiTi actuators for use in robust control,” *Smart Mater. Struct.*, vol. 26, no. 10, p. 105050, 2017, [Online]. Available: http://stacks.iop.org/0964-1726/26/i=10/a=105050.

[43] S. K. Chaitanya. and K. Dhanalakshmi, “Demonstration of self-sensing in Shape Memory Alloy actuated gripper,” 2013, doi: 10.1109/ISIC.2013.6658620.

[44] J. Prechtl, S. Seelecke, P. Motzki, and G. Rizzello, “Self-Sensing Control of Antagonistic SMA Actuators Based on Resistance-Displacement Hysteresis Compensation,” 2020.

[45] P. Motzki, J. Kunze, A. York, and S. Seelecke, “Energy-efficient SMA Vacuum Gripper System,” *Actuator 16 - 15th Int. Conf. New Actuators*, no. June, pp. 526–529, 2016, doi: 10.13140/RG.2.2.25486.97609.

[46] D. Scholtes, S. Seelecke, and P. Motzki, “Development of a Bistable SMA Actuated Industrial Gripper Based on a Compliant Design,” 2021.

[47] L. Zimmer, S. Seelecke, and P. Motzki, “Development of an SMA based End-effector Prototype for Material Handling in Manufacturing Processes,” 2021.

[48] P. Motzki and S. Seelecke, “Bistabile Aktorvorrichtung mit einem Formgedächtniselement.” 2016, [Online]. Available: https://depatisnet.dpma.de/DepatisNet/depatisnet?action=bibdat&docid=DE102016108627A1.

[49] P. Motzki, “Efficient SMA Actuation — Design and Control Concepts,” 2020, doi: 10.3390/IeCAT2020-08520.

[50] T. Gorges, P. Molitor, R. Britz, and P. Motzki, “Development of Rotatory Decoupled Antagonistic SMA Actuators,” in *ACTUATOR 2022; International Conference and Exhibition on New Actuator Systems and Applications*, 2022, pp. 1–4.

[51] D. Scholtes, Y. Goergen, R. Britz, and P. Motzki, “Development of a Lightweight, Compact and Energy Efficient Pinch Valve Driven by Shape Memory Alloy Wires,” in *ACTUATOR 2022; International Conference and Exhibition on New Actuator Systems and Applications*, 2022, pp. 1–4.

[52] P. Motzki and S. Seelecke, “BISTABLE ACTUATOR DEVICE HAVING A SHAPE MEMORY ELEMENT,” WO 2017/194591 A1, 2016.

[53] R. Britz, P. Motzki, and S. Seelecke, “Scalable Bi-Directional SMA-Based Rotational Actuator,” *Actuators*, vol. 8, no. 3, p. 60, 2019, doi: 10.3390/act8030060.

[54] SAES Group, “SmartFlex Springs and Wires.”, URL: https://www.saesgetters.com/sites/default/files/SMARTFLEX%20SPRINGS%20AND%20WIRES.pdf, Letzter Zugriff: 25.10.2022.

[55] Dynalloy, “Technical Characteristics of Actuator Wires,” *Dynalloy Inc*, pp. 1–12, URL: https://www.dynalloy.com/pdfs/TCF1140.pdf, Letzter Zugriff: 25.10.2022.

[56] M. J. Mosley, C. Mavroidis, and C. Pfeiffer, “Design and Dynamics of a Shape Memory Alloy,” *Engineer*, pp. 1–14.

[57] F. Simone, G. Rizzello, P. Motzki, and S. Seelecke, “Design of a dexterous Finger actuated by SMA bundle wires,” in *Dritte Transdisziplinäre Konferenz - Technische Unterstützungssysteme, die die Menschen wirklich wollen*, 2018, pp. 355–362, doi: http://d-nb.info/1182269923.

[58] S.-M. Kirsch *et al.*, “SMA Antagonistic-Micro-Wire Bundle - First Measurement Results,” 2020.

[59] D. Bevilacqua, G. Soleti, D. Naso, G. Rizzello, and P. Motzki, “Bio-Inspired Flapping Wing Antagonist Actuation with SMA Wires,” in *ACTUATOR 2022; International Conference and Exhibition on New Actuator Systems and Applications*, 2022, pp. 1–4.

[60] S. Vollach, R. Caciularu, and D. Shilo, “Equilibrium stress during the response of shape memory alloys to an abrupt heat pulse,” *Scr. Mater.*, vol. 141, pp. 50–53, 2017, doi: 10.1016/J.SCRIPTAMAT.2017.07.016.

[61] S. Vollach and D. Shilo, “The mechanical response of shape memory alloys under a rapid heating pulse,” *Exp. Mech.*, vol. 50, no. 6, pp. 803–811, 2010, doi: 10.1007/s11340-009-9320-z.

[62] S. Vollach, D. Shilo, and H. Shlagman, “Mechanical Response of Shape Memory Alloys Under a Rapid Heating Pulse - Part II,” *Exp. Mech.*, vol. 56, no. 8, pp. 1465–1475, 2016, doi: 10.1007/s11340-016-0172-z.

[63] A. Dana, S. Vollach, and D. Shilo, “Use the force: review of high-rate actuation of shape memory alloys,” *Actuators*, vol. 10, no. 7, Jul. 2021, doi: 10.3390/ACT10070140.

[64] T. Gorges and P. Motzki, “Efficient Shape Memory Alloy Activation with Alternating Current and Real-time Energy Measurement,” *IEEE/ASME Trans. Mechatronics*, 2021.

[65] P. Motzki, “Advanced Design and Control Concepts for Actuators Based on Shape Memory Alloy Wires,” Saarland University, 2018.

[66] P. Motzki, T. Gorges, M. Kappel, M. Schmidt, G. Rizzello, and S. Seelecke, “High-Speed and High-Efficiency Shape Memory Alloy Actuation,” *Smart Mater. Struct.*, vol. 27, no. 7, p. 075047, Jun. 2018, doi: 10.1088/1361-665X/aac9e1.

[67] R. Britz and P. Motzki, “Analysis and evaluation of bundled SMA actuator wires,” *Sensors Actuators A Phys.*, no. 1-2 SPEC. ISS, p. 113233, Nov. 2021, doi: 10.1016/J.SNA.2021.113233.

[68] R. Britz *et al.*, “SMA wire bundles - Mechanical and electrical concepts,” in *ACTUATOR 2018 - 16th International Conference and Exhibition on New Actuators and Drive Systems, Conference Proceedings*, 2018, pp. 514–517.

[69] R. Britz, G. Rizzello, and P. Motzki, “High-Speed Antagonistic Shape Memory Actuator for High Ambient Temperatures,” *Adv. Eng. Mater.*, vol. n/a, no. n/a, Apr. 2022, doi: https://doi.org/10.1002/adem.202200205.

[70] R. Britz, S. Seelecke, G. Rizzello, and P. Motzki, “Decoupled Antagonistic SMA Actuator for Valve Applications,” 2020, doi: 10.1115/SMASIS20-2214.

[71] R. Britz, P. Motzki, and S. Seelecke, “THERMAL ACTUATOR ARRANGEMENT HAVING IMPROVED RESET TIME.” 2019.

[72] B. Reedlunn, S. Daly, and J. Shaw, “Superelastic shape memory alloy cables: Part I – Isothermal tension experiments,” *Int. J. Solids Struct.*, vol. 50, no. 20–21, pp. 3009–3026, Oct. 2013, doi: 10.1016/J.IJSOLSTR.2013.03.013.

[73] B. Mas, D. Biggs, I. Vieito, A. Cladera, J. Shaw, and F. Martínez-Abella, “Superelastic shape memory alloy cables for reinforced concrete applications,” *Constr. Build. Mater.*, vol. 148, pp. 307–320, Sep. 2017, doi: 10.1016/J.CONBUILDMAT.2017.05.041.

[74] B. Reedlunn, S. Daly, and J. Shaw, “Superelastic shape memory alloy cables: Part II – Subcomponent isothermal responses,” *Int. J. Solids Struct.*, vol. 50, no. 20–21, pp. 3027–3044, Oct. 2013, doi: 10.1016/J.IJSOLSTR.2013.03.015.

[75] S. Vahidi, J. Arghavani, E. Choi, and A. Ostadrahimi, “Mechanical response of single and double-helix SMA wire ropes,” *Mech. Adv. Mater. Struct.*, vol. 0, no. 0, pp. 1–14, 2021, doi: 10.1080/15376494.2021.1955313.

[76] M. Branciforte, F. La Rosa, G. Muscato, and A. Fonti, “Experimental setup to analyze the relation between resistance and length on SMA wires,” *Proc. 2012 1st Int. Conf. Innov. Eng. Syst. ICIES 2012*, pp. 81–85, 2012, doi: 10.1109/ICIES.2012.6530849.

[77] D. O. Kazmer, *Injection Mold Design Engineering*, 2nd ed. Carl Hanser Verlag GmbH Co KG, 2016.

ANHANG

Beitragsberichte

Formgedächtnislegierungsdrähte in Hochleistungsanwendungen

Erläuterung der Beiträge der Autoren zur Veröffentlichung:

Analysis and Evaluation of Bundled SMA Actuator Wires

Rouven Britz war für die Planung, Durchführung und Auswertung der Experimente verantwortlich. Er schrieb die Veröffentlichung und erstellte die Bilder.

Paul Motzki war in beratender Funktion während und nach den Experimenten tätig. Er las die Veröffentlichung Korrektur.

Ort, Datum	Rouven Britz
Ort, Datum	Paul Motzki

Formgedächtnislegierungsdrähte in Hochleistungsanwendungen

Erläuterung der Beiträge der Autoren zur Veröffentlichung:

High-Speed Antagonistic Shape Memory Actuator for High Ambient Temperatures

Rouven Britz war für die Entwicklung des Aktors zuständig. Dies umfasst Konzept, Design, Konstruktion, Aufbau und Validierung der gezeigten Prototypen. Außerdem war er für die Koordination der bei Projektpartnern stattfindenden Feldversuche verantwortlich. Er schrieb die Veröffentlichung und erstellte die Bilder.

Gianluca Rizzello war für die Entwicklung des verwendeten Simulationstool und das sich dahinter befindende FGL-Model verantwortlich.

Paul Motzki war in beratender Funktion während der gesamten Projektlaufzeit tätig. Er las die Veröffentlichung Korrektur.

Ort, Datum	Rouven Britz
Ort, Datum	Gianluca Rizzello
Ort, Datum	Paul Motzki

Formgedächtnislegierungsdrähte in Hochleistungsanwendungen

Erläuterung der Beiträge der Autoren zur Veröffentlichung:

High-Power Shape Memory Alloy Catapult Actuator for High-Speed and High-Force Applications

Philipp Molitor entwickelte den Demonstrator im Rahmen seiner Masterarbeit. Er war für das Konzept, Design, Konstruktion, Aufbau und Validierung des gezeigten Demonstrators zuständig. Er schrieb die Veröffentlichung und erstellte die Bilder.

Rouven Britz war Betreuer der Masterarbeit und leitete die Entwicklung des Demonstrators. Er war in fachlich technisch beratender Funktion tätig und leistete praktische Unterstützungsarbeit während der gesamten Entwicklung. Er gab Hilfestellung bei dem Schreiben der Veröffentlichung und las diese Korrektur.

Paul Motzki war in beratender Funktion während der Entwicklung tätig. Er las die Veröffentlichung Korrektur.

Ort, Datum	Philipp Molitor
Ort, Datum	Rouven Britz
Ort, Datum	Paul Motzki

EIGENE PUBLIKATIONEN

Peer-reviewed Journalpublikationen

R. Britz, P. Motzki, S. Seelecke; *Scalable Bi-Directional SMA-Based Rotational Actuator; in actuators;* 2019; DOI: 10.3390/act8030060.

R. Britz, P. Motzki; *Analysis and evaluation of bundled SMA actuator wires*; in Sensors and Actuators A: Physical; 2022; DOI: 10.1016/j.sna.2021.113233.

R. Britz, G. Rizzello, P. Motzki; *High-Speed Antagonistic Shape Memory Actuator for High Ambient Temperatures*; in Advanced Engineering Materials; 2022; DOI: 10.1002/adem.202200205.

Philipp Molitor, **R. Britz**, P. Motzki; *High-Power Shape Memory Alloy Catapult Actuator for High-Speed and High-Force Applications*; in IEEE Access; 2022; DOI: 10.1109/ACCESS.2022.3202210.

Patente

UNIVERSITÄT DES SAARLANDES & ZeMA gGmbH; *Thermische Aktoranordnung mit verbesserter Rückstellzeit*; Erfinder: **R. Britz**, S. Seelecke, P. Motzki; Anmeldung: 18.09.2019; Patentschrift: DE 10 2019 125 143.

UNIVERSITÄT DES SAARLANDES & ZeMA gGmbH; *Thermal actuator arrangement having improved reset time*; Erfinder: **R. Britz**, S. Seelecke, P. Motzki; Anmeldung: 18.09.2019; Patentschrift: WO 2021/052933.

UNIVERSITÄT DES SAARLANDES & ZeMA gGmbH; *Verstellbarer Steifigkeitsaktor zum variablen einstellen einer Steifigkeit*; Erfinder: **R. Britz**, L. Zimmer, P. Motzki, S. Seelecke; Anmeldung: 13.09.2021; Patentschrift: DE 10 2021 123 651.

UNIVERSITÄT DES SAARLANDES & ZeMA gGmbH; *Implantat zur Fixierung und Genesungsunterstützung von Knochenbrüchen*; Erfinder: **R. Britz**, L. Zimmer, P. Motzki, S. Seelecke, T. Pohlemann; Anmeldung: 13.09.2021; Patentschrift: DE 10 2021 123 656.

MATELIGENT GMBH; *Thermoelastischer Stellgeber in kompakter Aufbauweise*; Erfinder: L. Zimmer, **R. Britz**, Y. Goergen, D. Scholtes, P. Motzki, S. Seelecke, J. Preetz; Anmeldung: 25.05.2022; Patentschrift: PCT/EP2022/064242.

Peer-reviewed Konferenzbeiträge

P. Motzki, **R. Britz**, S. Seelecke; *Modular SMA-Based Bi-directional Rotational Actuator*; in Conference Proceedings: ASME 2016 Conference on Smart Materials, Adaptive Structures, and Intelligent Systems; 2016; DOI: 10.1115/SMASIS2016-9017.

R. Britz, P. Motzki, S. Seelecke; *Skalierbarer Rotationsaktor auf Basis von Formgedächtnislegieurungsdrähten*; in Tagungsband Fachtagung Mechatronik 2017; 2017; ISBN: 978-3-00-055832-0.

R. Britz, F. Welsch, S.-M. Kirsch, F. Simone, M. Schmidt, P. Motzki, S. Seelecke; *SMA Wire Bundles – Mechanical and Electrical Concepts*; in Conference Proceedings: ACTUATOR 2018 - 16th International Conference on New Actuators; 2018; ISBN: 978-3-8007-4675-0.

Y. Goergen, R. Chadda, **R. Britz**, D. Scholtes, N. Koev, P. Motzki, R. Werthschützky, M. Kupnik, S. Seelecke; *Shape Memory Alloys in Continuum and Soft Robotic Applications*; in Conference Proceedings: ASME 2019 Conference on Smart Materials, Adaptive Structures, and Intelligent Systems; 2019; DOI: 10.1115/SMASIS2019-5610.

R. Britz, S. Seelecke, G. Rizzello, P. Motzki; *Decoupled Antagonistic SMA Actuator for Valve Applications*; in Conference Proceedings: ASME 2020 Conference on Smart Materials, Adaptive Structures, and Intelligent System; 2020; DOI:10.1115/SMASIS2020-2214.

L. Zimmer, **R. Britz**, Y. Goergen, G. Rizzello, T. Pohlemann, M. Orth, B. Ganse, S. Seelecke, P. Motzki; *AN SMA-BASED MULTIFUNCTIONAL IMPLANT FOR IMPROVED BONE FRACTURE HEALING*; in Conference Proceedings: ASME 2021 Conference on Smart Materials, Adaptive Structures, and Intelligent Systems; 2021; DOI: 10.1115/SMASIS2021-67261.

M. Mandolino, **R. Britz**, Y. Goergen, G. Rizzello, P. Motzki; *Development of an SMA driven articulation and autofocus mechanism for endoscope applications*; in Conference Proceedings: ACTUATOR 2022 International Conference and Exhibition on New Actuator Systems and Applications; 2022; ISBN: 978-3-8007-5894-4.

P. Molitor, **R. Britz**, P. Motzki; *High-Power and High-Speed SMA Bowling Ball Demonstrator*; in Conference Proceedings: ACTUATOR 2022 International Conference and Exhibition on New Actuator Systems and Applications; 2022; ISBN: 978-3-8007-5894-4.

D. Scholtes, Y. Goergen, **R. Britz**, P. Motzki; *Development of a Lightweight, Compact and Energy Efficient Pinch Valve Driven by Shape Memory Alloy Wires*; in Conference Proceedings: ACTUATOR 2022 International Conference and Exhibition on New Actuator Systems and Applications; 2022; ISBN: 978-3-8007-5894-4.

T. Gorges, P. Molitor**, R. Britz**, P. Motzki; *Development of Rotatory Decoupled Antagonistic SMA Actuators*; in Conference Proceedings: ACTUATOR 2022 International Conference and Exhibition on New Actuator Systems and Applications; 2022; ISBN: 978-3-8007-5894-4.

P. Molitor, **R. Britz**, Y. Goergen, P. Motzki; *High-Power SMA Bowling Ball Catapult*; in Conference Proceedings: ASME 2022 Conference on Smart Materials, Adaptive Structures, and Intelligent Systems; 2022; DOI: 10.1115/SMASIS2022-FM1.

T. Gorges, P. Molitor, **R. Britz**, Y. Goergen, P. Motzki; *Control of Rotatory Decoupled Antagonistic SMA Actuators*; in Conference Proceedings: ASME 2022 Conference on Smart Materials, Adaptive Structures, and Intelligent Systems; 2022; DOI: 10.1115/SMASIS2022-FM1.

Y. Goergen, **R. Britz**, M. Mandolino, G. Rizzello, P. Motzki; *A Novel Compact Concept Design of a SMA Based Endoscope*; in Conference Proceedings: ASME 2022 Conference on Smart Materials, Adaptive Structures, and Intelligent Systems; 2022; DOI: 10.1115/SMASIS2022-FM1.

Konferenzvorträge

R. Britz, P. Motzki, S. Seelecke; *Rotationsaktor auf FGL-Basis*; Konferenz: VDI Expertenforum 2016; 2016.

R. Britz, P. Motzki, S. Seelecke; *Entwicklung von neuartigen Formgedächtnis-Aktuatoren für die Anwendung in Spritzgießwerkzeugen*; Konferenz: 3. WerkstoffWoche 2019; 2019.